May 2022

In-Phantom Film Measurements of Two Treatment Planning Systems for Single-Fraction Spine SBRT

Michael J. Taylor
Louisiana State University and Agricultural and Mechanical College

IN-PHANTOM FILM MEASUREMENTS OF TWO TREATMENT PLANNING SYSTEMS FOR SINGLE-FRACTION SPINE SBRT

A Thesis

Submitted to the Graduate Faculty of the
Louisiana State University and
Agricultural and Mechanical College
in partial fulfillment of the
requirements for the degree of
Master of Science

in

The Department of Physics and Astronomy

by
Michael James Taylor
B.S., University of West Florida, 2019
August 2022

Acknowledgments

I would like to thank Dr. Jonas Fontenot for taking the time to serve as my major advisor for this work, providing much-needed guidance, and always pushing me to do my best. I thank Katelynn Fontenot and Liz Buell for their help in scheduling the necessary meetings in the busy clinic. I acknowledge Elekta Ltd. for providing Mary Bird Perkins Cancer Center a research grant to partially fund this project. At Elekta, I also thank Meredith Coyle and Dr. Raine Wang's beam modeling team, as well as the Mary Bird Perkins IT department for their valuable assistance in setting up the Monte Carlo based treatment planning system.

I express gratitude to those who served on my supervisory committee, Dr. Kenneth Matthews, Dr. A. Ravi P. Rau, and Daniel Neck, the latter who was an invaluable help in treatment planning system commissioning and verification. I greatly appreciate Dr. Suchit Patel for his advice and review of the treatment plans, as well as all the physicists, residents, and therapists at Mary Bird Perkins for their availability to answer all of my questions during this project.

I thank my fellow LSU medical physics classmates, Reagan Dugan, Elizabeth Park, and Charles Zimmerman, and Michael McMahon for going on this journey with me through graduate school these past three years. I also thank Andrew McGuffey for being there to bounce ideas about film dosimetry with me. I thank Paige Whittington for all her hard work keeping me informed on the university's administrative and graduation requirements.

Finally, I will be forever grateful to my parents, sisters, and the little congregation at Open Door Tabernacle for their unconditional love, support, and prayers during my time here in Louisiana.

Table of Contents

List of Tables

List of Figures

Abstract

Purpose: Treatment planning accuracy for spine stereotactic body radiation therapy (SBRT) varies depending on the dose calculation algorithm utilized in the treatment planning system (TPS). This project compared the end-to-end accuracy between spine SBRT plans calculated in a convolution-superposition based TPS (TPS_{CS}) and Monte Carlo based TPS (TPS_{MC}) with radiochromic film measurements. The hypothesis was that TPS_{MC} would calculate the dose gradient in the critical region between the vertebral body and the spinal cord more accurately than TPS_{CS}.

Methods: Single-fraction spine SBRT treatments following RTOG 0631 and local institutional guidelines were planned in TPS_{CS} and TPS_{MC} at five vertebral sites in an anthropomorphic phantom. The plans were delivered with a linear accelerator with Gafchromic EBT-XD film inserted at each site. For each plan, the TPS-calculated and film-measured anterior-posterior (AP) dose profiles through isocenter were obtained and 2D gamma pass rate (GPR) was calculated at multiple dose difference/distance-to-agreement criteria.

Results: For each TPS-film AP profile pair, the dose falloff difference and profile shift were measured posterior to the vertebral body. Each sample' normality was confirmed with a Shapiro-Wilk test, equality of variances was determined between the TPS_{CS} and TPS_{MC} samples with Levene's test, then an unpaired t-test was used to detect statistically significant differences between TPS_{CS} and TPS_{MC} ($n = 5$, $\alpha = 0.05$). Across the five treatment sites, the mean dose falloff difference was -0.0 ± 0.8 mm ($+0.7 \pm 7.8\%$) in TPS_{CS} and -0.7 ± 0.5 mm ($-7.8 \pm 6.0\%$) in TPS_{MC}. The mean profile shift was -0.1 ± 0.3 mm in TPS_{CS} and $+0.0 \pm 0.6$ mm in TPS_{MC}. No statistically significant differences were observed in the profile metrics between each TPS. TPS_{CS} yielded consistently higher average GPR across the sites, with statistically significant differences found for all criteria tested except 2%/1mm and 1%/1mm. GPR in the critical region for both TPSs produced very accurate results for all criteria tested except 3%/1mm, 2%/1mm, and 1%/1mm occasionally.

Conclusion: Each TPS provided similar end-to-end accuracy in the critical region. The lower GPR in other areas of the TPS_{MC} plans may be increased by adjusting TPS-specific settings to limit plan complexity.

Chapter 1. Introduction

1.1. Background

Many types of cancer, including those originating in the pelvis, colon, lung, breast, and vertebral bodies commonly metastasize to the extradural region of the spinal cord. This produces symptoms in the patient such as cord compression, vertebral fracture, and most commonly, pain. Radiation therapy is effective at relieving pain quickly and noninvasively, but care must be taken to avoid overdosing the spinal cord. This can cause radiation myelopathy, inducing sensory and motor deficits or even paralysis. Conventional radiation therapy usually involves delivering a fraction of the total radiation dose daily over several weeks, allowing healthy tissue to repair itself. Conversely, stereotactic body radiation therapy (SBRT) involves delivering large doses of radiation in five, three, or sometimes merely one fraction. SBRT is well suited for spinal metastases due to its higher dose conformity, higher dose gradient, and higher biological effective dose compared to conventionally fractionated radiotherapy.[1]

A patient undergoing any type of radiotherapy must first have their treatment simulated on a computed tomography (CT) scan in a treatment planning system (TPS). The intrinsic accuracy of a TPS is influenced by several factors, such as patient anatomy, the dose calculation grid, the optimization methods, and, most notably, the dose calculation algorithm. In spine SBRT treatment planning, the need for accuracy is particularly important in the high-dose gradient regions[2] between the treated vertebral body and the spinal cord and also for the small fields typically utilized to create such dose distributions.[3] Sometimes sub-millimeter accuracy is needed to achieve sufficient target coverage while sparing the spinal cord.

One class of dose calculation algorithms extensively utilized in radiation treatment planning is convolution-superposition (CS) models. In these models, dose in each voxel is calculated deterministically by convolving total energy released per unit mass (terma) with a polyenergetic dose spread kernel, which has been retrospectively calculated using Monte Carlo simulations.[4, 5] The terma and kernel represent the energy deposited by the primary photons and secondary interactions, respectively.[6–8] To decrease calculation time for clinical use, some approximations are employed, such as neglecting interactions when they fall below a threshold terma or occur past a certain distance along the path. Such approximations may lead to inaccuracies in dose calculation due to the neglecting of some scatter radiation.[6]

Alternatives to CS models are Monte Carlo (MC) based algorithms, which record the histories of primary photon interactions and secondary particles per voxel stochastically. Interactions occur based on linear attenuation coefficients and cross sections, i.e., first principles.[6, 9–11] The statistical accuracy of the calculation is dependent on the number of histories,[11] so, for many years, calculation times were too long for daily use in the clinic. However, advances in computing speed have increased this algorithm's clinical feasibility. Previous studies have found that MC-based algorithms generally yield a more accurate calculation than CS-based algorithms near tissue-bone interfaces[1, 3] and in low-density regions.[3, 12] The region between the vertebral body and the spinal cord or cauda equina in spine SBRT plans is an especially crucial tissue-bone interface.

Previous studies have compared CS-based and MC-based TPSs specifically for spinal SBRT treatments.[3, 13–15] These studies found that both dose calculation methods are currently capable of producing clinically acceptable plans. However, end-to-end dosimetric verification with measurements in an anthropomorphic phantom is needed to test the overall accuracy of the

calculated dose distributions in realistic anatomy. For this study's purposes, end-to-end means evaluating the accuracy of the dose distributions after incorporating all treatment steps and accumulating all sources of error, from simulation to delivery.[16–18] Such a process for comparing CS-based and MC-based TPSs with radiochromic film measurements at the spine is lacking within the currently published literature.

1.2. Hypothesis and Specific Aims

The goal of this study was to investigate and compare the end-to-end dosimetric accuracy of a CS-based TPS (TPS_{CS}) and an MC-based TPS (TPS_{MC}) for spine SBRT treatments. It was hypothesized that, for single-fraction spine SBRT treatments, TPS_{MC} would calculate the dose gradient between the vertebral body and the spinal cord more accurately than TPS_{CS} when compared to film measurements in an anthropomorphic phantom. This hypothesis was tested through the following specific aims:

Aim 1: Generate single-fraction spine SBRT treatment plans in TPS_{CS} and TPS_{MC} on an anthropomorphic phantom.

Aim 2: Deliver the SBRT plans to the phantom and measure the resulting dose distribution using radiochromic film.

Aim 3: Analyze the film-measured dose distributions around each treatment target and compare with the TPS-calculated dose planes.

Chapter 2. Methods and Materials

2.1. Phantom

The Alderson RANDO anthropomorphic phantom used in this work (Figure 2.1) is made of soft tissue equivalent material based on the ICRP Standard Man and a natural human skeleton with soft tissue equivalent material injected into any hollow areas of the bone. The phantom also contains lung equivalent material, composed of a less dense soft tissue equivalent foam.[19] The phantom is divided transversely into 36 sections, numbered 0 to 35 in the superior-inferior (SI) direction. Each section is 2.5 cm thick, except for section 35, which mounts to the inferior wooden frame. A plastic ring mounts section 0 to the superior wooden frame. Adjacent sections are held together by pairs of internal plastic rods at a 4-inch (10.16 cm) center-to-center distance from each other in sections 0 to 11. Pairs of plastic rods at a 10.1-inch (25.65 cm) center-to-center distance connect adjacent sections 11 to 35. The latter pairs of rods can be mounted into either wooden frame so that only a portion of the phantom sections may be joined if desired (Figure 2.2). The phantom also contains many removable cylindrical plugs (5 mm diameter) that fill holes designed for radiation measurement devices. For this study, however, they served as fiducials for film registration.

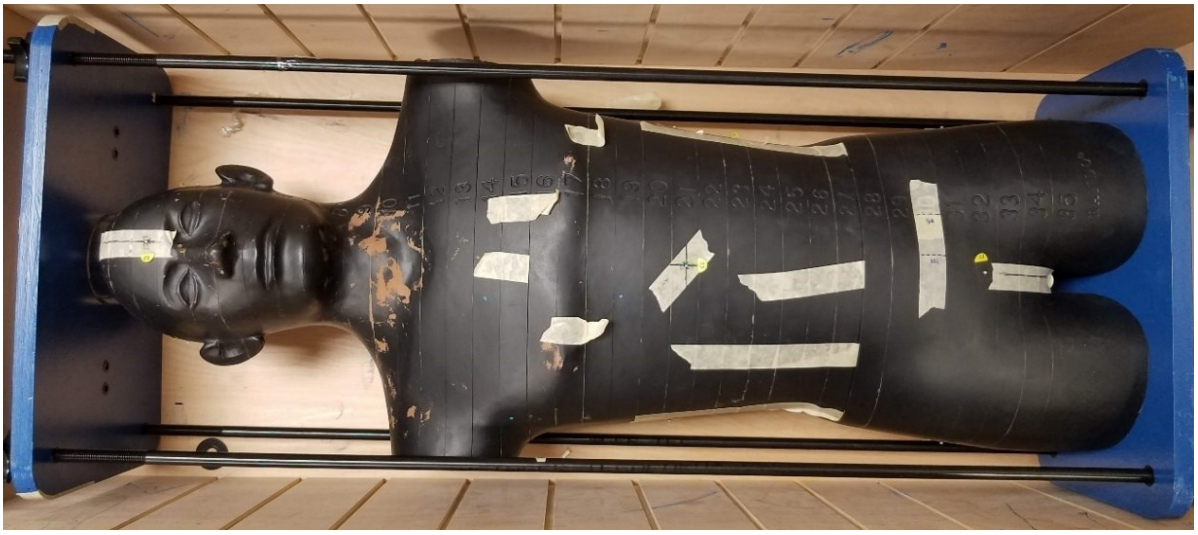

Figure 2.1. Alderson RANDO anthropomorphic phantom fully assembled in its frame.

Five vertebral sites, shown in Figure 2.3, were selected for treatment: C4, T1, T12, L2, and L4, where C stands for cervical vertebra, T for thoracic, and L for lumbar. These sites were chosen to sample different shaped dose distributions and varying nearby organs at risk (OARs). The construction of the phantom also warranted that these vertebrae be chosen since each spanned two sections, split approximately in the middle (Table 2.1), allowing for film dose plane measurements at these sites.

Figure 2.2. Superior phantom frame with internal rod mounting holes and a circular slot for mounting the head ring (Left). Inferior phantom frame with knobs for mounting to the phantom's holes (Right).

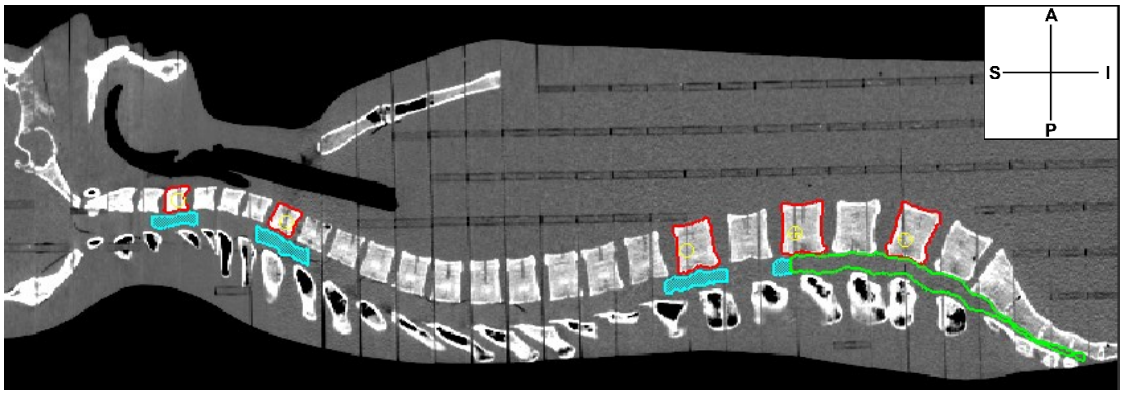

Figure 2.3. Sagittal view of the phantom CT. The five treatment sites, spinal cord portions, and cauda equina are contoured in red, cyan, and green, respectively. In the coordinate axes, 'A' is the anterior direction, 'P' is posterior, 'S' is superior, and 'I' is inferior.

2.2. Treatment Planning

The entire phantom was assembled, and sections 3 to 33 were scanned in a computed tomography (CT) scanner (Lightspeed RT, General Electric Healthcare, Chicago, Illinois) with a 120 kVp x-ray tube energy, 298 mA tube current, 1.25 mm slice thickness, and a 50 cm field of view. The selected tube energy was typical of that used to scan patients at our institution, and the tube current was selected to produce a very high signal to noise ratio. The slice thickness and field of view combination produced a CT voxel size of $0.97 \times 0.97 \times 1.25$ mm^3.

Table 2.1. Phantom sections included at each treatment site.

Treatment Site	Sections Spanning the Treatment Site
C4	7 - 8
T1	10 - 11
T12	21 - 22
L2	24 - 25
L4	27 - 28

At the time of the study, Pinnacle[3] v9.10 (Phillips Medical Systems, Fitchburg, Wisconsin) was the current clinically commissioned system for external beam treatment planning at our institution and will hereupon be referred to as 'TPS_{CS}.' The phantom's CT images were imported into TPS_{CS}. For each treatment site, the entire vertebral body and pedicles were contoured as the clinical target volume (CTV) following international consensus guidelines.[20] No gross tumor volume (GTV) was contoured. Currently, there exists no consensus for planning target volume (PTV) contouring for spine SBRT, so long as the PTV expands at most 3 mm from the CTV. For this project, a board-certified radiation oncologist recommended that the PTV be defined as a 2 mm isotropic expansion of the CTV except where the contour would intersect with the cauda equina or the vertebral foramen area around the spinal cord. Figure 2.4 displays the CTV and PTV contoured on the T12 site.

The phantom contained no mock spinal cord inside the vertebral bodies, so an approximate spinal cord was contoured. RTOG 0631 provides SI limits for contouring the spinal cord at each vertebral site. First, the vertebral foramen was manually contoured from 5 mm above the most superior slice containing the CTV to 5 mm below the most inferior slice containing the CTV.[21] This contour was then contracted 2.5 mm inward transversely (see Figure 2.4) and assigned as the spinal cord. The cauda equina was manually contoured, beginning 6.25 mm inferior from the most superior slice of the L2 CTV, and ending 3.75 mm superior to the fourth sacral bone tip. The cauda equina size varied throughout contour, with a maximum diameter of about 1.8 cm. Points of interest were defined at the approximate centers of four nearby diode plugs in the transverse plane where isocenter was at each TPS_{CS} site (Figure 2.4). These markers served as the registration points for each site.

In addition to the spinal cord and cauda equina, the following mock OARs were contoured inside the phantom per the RTOG 0631 guidelines: esophagus, trachea and larynx, skin, stomach, duodenum, renal hilum/vascular trunk, right and left lungs, and right and left renal cortices. The brachial plexus was also partially contoured adjacent to the C4 and T1 vertebrae, and the sacral plexus was partially contoured adjacent to the L4 vertebra. The remaining OARs were not contoured because either their dose constraints were above the prescription dose, or their locations were far enough from the treatment sites that it was safe to assume they would not exceed their doses limits.[21] An external contour around the entire phantom was also created.

The prescription dose (Rx), target coverage, and hotspot limits also followed RTOG 0631. Rx was a single fraction of 1600 cGy to at least 90% of the PTV volume. Hot spots greater than or equal to 1680 cGy (105% of Rx) were limited to a volume of 2 cc or less outside of the CTV and within 1 cm from the outer edge of the CTV. Hot spots greater than or equal to 1760 cGy (110% of Rx) were kept within the CTV. The dose limits for the cord were no more than 14 Gy to 0.035 cc and no more than 10 Gy to 0.35 cc or 10% of the volume. The dose limits for the cauda equina were no more than 16 Gy to 0.035 cc and no more than 14 Gy to 5 cc.[21] The dose limits for the other OARs contoured are listed in Table 2.2.

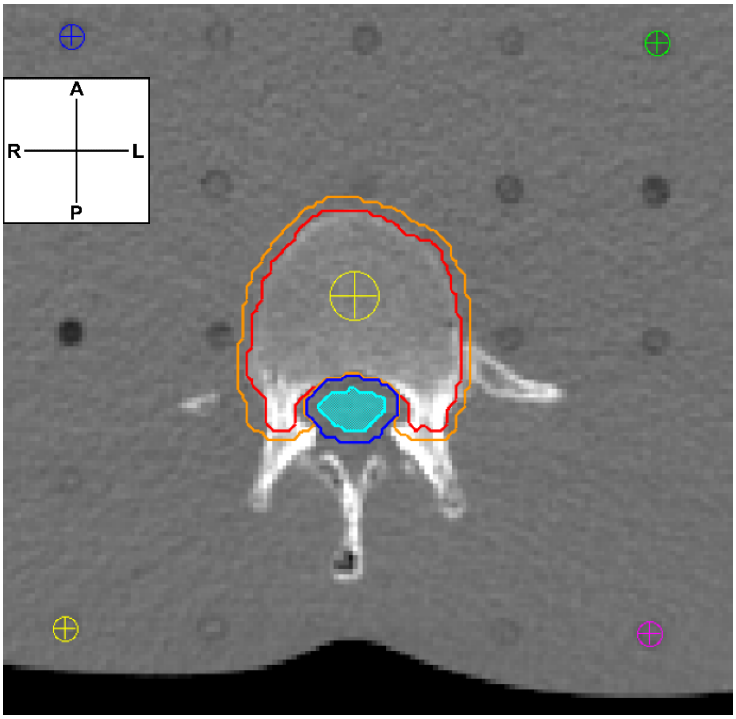

Figure 2.4. Transverse CT view of the T12 vertebral site in TPS_{CS}. The CTV is contoured in red, the PTV in orange, the vertebral foramen in blue, and the spinal cord is shaded in cyan. The yellow point in the vertebral body is the beam isocenter of the plan, and the multicolored points around the site are the TPS registration points. In the coordinate axes, 'A' is the anterior direction, 'P' is posterior, 'R' is patient right, and 'L' is patient left.

Table 2.2. OAR dose-volume constraints for the phantom spine SBRT plans, all of which are designated as serial tissues, except for the lung and renal cortex, which are parallel tissues.

Tissue	Volume	Max Dose to Volume	Endpoint
Spinal Cord	< 0.035 cc < 0.35 cc (or 10%)	1400 cGy 1000 cGy	myelitis
Cauda Equina	< 0.035 cc < 5 cc	1600 cGy 1400 cGy	neuritis
Sacral Plexus	< 0.035 cc < 5 cc	1800 cGy 1440 cGy	neuropathy
Esophagus	< 0.035 cc < 5 cc	1600 cGy 1190 cGy	stenosis / fistula
Ipsilateral Brachial Plexus	< 0.035 cc < 3 cc	1750 cGy 1400 cGy	neuropathy
Trachea & Larynx	< 0.035 cc < 4 cc	2020 cGy 1050 cGy	stenosis / fistula
Skin	< 0.035 cc < 10 cc	2600 cGy 2300 cGy	ulceration
Stomach	< 0.035 cc < 10 cc	1600 cGy 1120 cGy	ulceration / fistula
Duodenum	< 0.035 cc < 5 cc	1600 cGy 1120 cGy	ulceration
Renal Hilum / Vascular Trunk	< 2/3 total volume	1060 cGy	malignant hypertension
Lung (Right & Left)	1000 cc	740 cGy	pneumonitis
Renal Cortex (Right & Left)	200 cc	840 cGy	basic renal function

Source: Ryu S, et al., RTOG 0631, 2014[21]

The beam model in TPS_{CS} was clinically commissioned according to manufacturer guidelines. For each treatment plan designed in TPS_{CS}, two separate VMAT beams were defined, each with an energy of 6 MV FFF (flattening filter free). One arc moved counter-clockwise from 175° (patient right) to 185° (patient left) with a collimator angle of 45°. The other arc moved clockwise from the same angles in the opposite direction with a collimator angle of 320°.[22] The beam isocenter of each treatment site was placed in the approximate transverse center of the vertebral body in the CT slice between the two phantom sections that the vertebra was split at. The dose calculation grid for each treatment site was defined to cover the range of sections listed in Table 2.3 below, covering nearby OARs. All dose grids had a 2 mm resolution and included the frame rods of the phantom. The CT scanner's couch was subtracted, overriding the physical density to match that of air in TPS_{CS}.

Table 2.3. Phantom sections included in each TPS_{CS} dose grid.

Treatment Site	Sections Included in TPS_{CS} Dose Grid
C4	3 - 18
T1	3 - 19
T12	17 - 33
L2	20 - 33
L4	20 - 33

1-cm width rings structures were contoured in TPS_{CS} around the CTV and PTV to aid the inverse optimization (see Appendix A for more details). The final gantry spacing of each plan was set to 2° per segment, resulting in 352 control points (176 per arc) per plan. The multileaf collimator (MLC) movement was constrained to 4.6 mm per degree, the minimum dynamic leaf gap was set to 1 cm, and the opening density matrix was 0.5×0.5 cm^2. The convolution dose iteration was 10 and the stopping tolerance was 1×10^{-5}. The final dose of the plans was calculated using TPS_{CS}'s Adaptive Convolve algorithm, which is a faster variant of its full collapsed-cone convolution-superposition algorithm that reduces the dose grid in low-dose gradient regions.[23] The density/fluence grid was matched to the dose grid.

Monaco v5.51 (Elekta, Stockholm, Sweden) with its X-ray Voxel Monte Carlo (XVMC) dose calculation algorithm was chosen as the MC-based TPS used in this study and will be further referred to as 'TPS_{MC}.' After the five treatment plans were completed in TPS_{CS}, the CT images, contoured structures, and isocenters were imported into TPS_{MC} (Figure 2.5), whose 6 MV FFF beam model was commissioned following the manufacturer guidelines. TPS_{MC} automatically filled any hollow areas of ring-shaped contours imported from TPS_{CS}. This filling of rings took place around the superior and inferior edges of the C4 and T1 vertebrae and throughout the center of the T12, L2, and L4 vertebral bodies. This did not affect the main inverse optimization process since TPS_{MC}'s shrink margin feature was used to assist the inverse optimization, but the contours had to be manually corrected since filling the ring structures changed the dose-volume distribution of them. See Appendix A for more details.

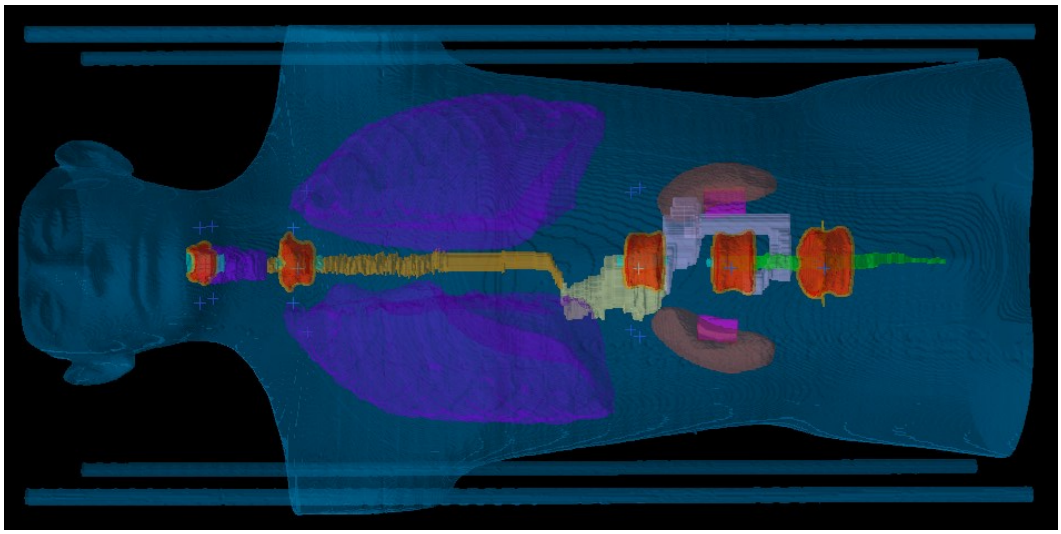

Figure 2.5. 3D reconstruction of the phantom CT in TPS_{MC}, showing the vertebral targets and OARs contoured.

One dual-arc 6 MV FFF beams was defined for each plan in TPS_{MC}. When defining a single dual-arc beam in TPS_{MC}, the beam is optimized around one half of the target during the first arc, and the other half during the second arc.[24] TPS_{MC} is also capable of changing the degree of modulation after a user defined arc increment (20° in this case). For the Agility MLC models (Elekta, Stockholm, Sweden) used in our institution's linear accelerator (linac), TPS_{MC} can utilize the y-axis jaws of the linac to block the width the MLC leaves in 1 mm increments. These advantages negated the need to rotate the collimator between VMAT arcs, which remained at 0° for all beams in TPS_{MC}. A couch structure may be imported into TPS_{MC}, but for this work, the CT couch was covered with a large structure with its electron density overridden to match that of air. This was analogous to the couch subtraction method in TPS_{CS}.

In TPS_{MC}, the 2 mm dose calculation grid contained the entire external contour around the phantom and the four frame rods. The MC dose calculation algorithm's statistical uncertainty was set to 2% per control point. The first stage of the treatment plan calculation was fluence modulation, which used a preliminary pencil beam calculation of dose. The second stage was segmentation, which contained the actual MC dose calculation. The maximum number of control points allowed was set to 350, but TPS_{MC} automatically varies the control point spacing depending on the gantry angle and plan optimization objectives.[24] Each plan in TPS_{MC} ultimately ended up with a different number of control points. The minimum segment width was set to 0.5 cm, the beamlet width was set to 3 mm, and the fluence smoothing was set to medium.[25] Smooth segment optimization (SSO) and high precision leaf positions were enabled, and the speed-to-plan quality was set to 5. Minimum CT number was -200 and target margin was set to 2 mm (Tight).

After all the spine treatment plans were calculated, they were reviewed for clinical efficacy by a board-certified radiation oncologist.

2.3. TPS_{MC} Dose Model Validation

To verify the accuracy of the TPS_{CS} and TPS_{MC} dose models, four IMRT plans from AAPM Task Group Report 119 (TG-119), 'Multitarget,' 'Prostate,' 'Head/Neck,' and 'Cshape (easy version)' were created in each TPS on solid 30-cm×30-cm stacked solid water slabs (The Original

Plastic Water, CIRS, Norfolk, Virginia).[26] The solid water was CT scanned at the same parameters as the spine plans, except the tube current was set to 440 mAs and the slice thickness was 2.5 mm. The contours for the TG-119 validation plans were obtained from the AAPM website.[27] All TG-119 validation plans were calculated with the same TPS parameters as the spine plans. All plans in each TPS were single-arc except for the Head/Neck, which was dual-arc.

With the Versa HD linac (SN 153187, Elekta, Stockholm, Sweden), the dose at various points in the solid water were measured and compared with the calculated dose in the corresponding TPS with a 0.3 cc ion chamber (Model 31011, SN 0058, PTW, Freiburg, Germany) cross-calibrated with a 0.6 cc Farmer chamber (Model 30013, SN 03435, PTW, Freiburg, Germany). The same electrometer (Model 206, SN 11207335, CNMC Company, Inc., Nashville, Tennessee) was used for all measurements. The source-to-surface distance (SSD) remained 92.5 cm throughout all plans, but the dose at different depths were obtained by rearranging the water slabs, changing the anterior-posterior (AP) position of the milled slab holding the ion chamber.

The average measured point dose was based on three reading of the ion chamber, corrected for temperature inside the slab's chamber cavity and for atmospheric pressure. The difference from the planned point dose was calculated, normalized with respect to the prescribed dose per fraction for each plan. Confidence limits (CL) were calculated for the mean dose differences in the high and low dose regions with the following equation:[26]

$$\mathrm{CL_{diff}} = |\text{Dose Difference}| + 1.96\sigma$$

Assuming a normal distribution, this value implies that 95% of measurements in either the high or low dose region should deviate from the planned dose by ± $\mathrm{CL_{diff}}$ most.

Gamma pass rates (GPR) of the TG-119 validation plans measured on a 2D diode array (MapCHECK2, Sun Nuclear Corporation, Melbourne, Florida) were compared with those delivered from the $\mathrm{TPS_{CS}}$ plans. Before delivering the plans to the diode array, it was dose calibrated based on the planned dose calculated in $\mathrm{TPS_{CS}}$ at the center of the array, 100 cm source-to-axis distance (SAD), 10×10 $\mathrm{cm^2}$ field size. Gamma analyses were performed in the software SNC Patient v7.0 (Sun Nuclear Corporation, Melbourne, Florida) at the following dose difference / distance to agreement (ΔD/DTA) criteria: 5%/1mm, 3%/3mm, 3%/2mm, 3%/1mm, 2%/2mm, 2%/1mm, and 1%/1mm. ΔD was set to absolute dose (measured - planned), Van Dyk was turned on, normalized to the maximum planned dose, and measurement uncertainty was applied. A 10% maximum planned dose threshold was applied to each the gamma analysis. CL was also calculated for the mean GPR at each gamma criterion with the following equation:[26]

$$\mathrm{CL_{GPR}} = |100\% - \text{Mean GPR}| + 1.96\sigma$$

Assuming a normal distribution, this value implies that 95% of gamma analyses should yield GPRs greater than or equal to (100% - $\mathrm{CL_{GPR}}$).

TG-119's preliminary plans, 'AP:PA' and 'Bands' were also made in $\mathrm{TPS_{MC}}$ alone, delivered to a 0.007 cc microchamber (Model A16, REF 92726, SN XAA030841, Standard Imaging, Middleton, Wisconsin) in the water slabs and to the diode array. In the 'Bands' plan, the dose difference was, at most, only -1%, with an average difference -0.3% off across all the dose "bands." At 3%/3mm criteria, GPR was 100% for both P1 and P2, and at 2%/2mm criteria, 99.2% and 99.1% for P1 and P2, respectively (data not shown). Because of the close agreement, these measurements were not repeated for $\mathrm{TPS_{CS}}$, as it was previously commissioned for clinical use.

2.4. Film Dosimetry

After the five spine SBRT treatments plans in TPS_{CS} and the five in TPS_{MC} were completed and approved, the plans were sent to our institution's record and verify system (MOSAIQ v2.81, Elekta, Sunnydale, CA) and delivered on the previously mentioned linac, measuring the dose with radiochromic film.

Radiochromic film is a near tissue equivalent passive integrating radiation detector. EBT brand radiochromic film specifically consists of an active layer of pentacosa-10,-12-diynoic acid lithium salt (Li-PCDA) sandwiched between two polyester substrates. The Li-PCDA microcrystals polymerize upon exposure to ionizing radiation, which darkens the film, the intensity of which is dependent on the dose of radiation. Aluminum oxide nanoparticles in the active layer reduce energy dependence. When not in use, the film must be stored in darkness to prevent unwanted polymerization.[28] Properly calibrated, radiochromic film provides high-resolution two-dimensional dose measurements.

Gafchromic EBT-XD film (Lot 11062002, REF 859138, Ashland LLC, Bridgewater, New Jersey) was selected for this study for its high saturation dose (40 Gy) and reduced appearance of lateral response artifacts.[28–30] The calibration for this film batch was performed with 15 5×5 cm^2 square cuts from a single sheet of radiochromic film using the same linac described previously. Each film patch was irradiated separately at the following nominal dose values: 0, 24, 36, 60, 80, 120, 180, 280, 400, 620, 920, 1380, 1600, 2000, 2500 cGy (Figure 2.6).

The linac's 6 MV beam was calibrated to a nominal output of 0.8 cGy per monitor unit (MU) for a 0.6 cc Farmer chamber at 100 cm SAD, a 10 cm depth (the TG-51 measurement depth of the linac[28]), 11 cm of backscatter material, and a 10×10 cm^2 field size. Before irradiation of the calibration films, the linac output for that day was measured by delivering 100 MU of the 6 MV beam to the previously described Farmer chamber at the above conditions. Three output measurements were recorded with an electrometer (Model 206, SN 11401357, CNMC Company, Inc., Nashville, Tennessee), then averaged for that treatment day. All chamber measurements were corrected for temperature inside the slab's chamber cavity and for atmospheric pressure. The calculated measured dose per MU was used to determine the actual dose delivered to each calibration patch.

After the linac output measurement, each calibration film was irradiated perpendicular to the beam axis between solid water slabs at the same conditions described above, but with 10 cm of backscatter material. The flattening filter was included in calibration for a more uniform dose distribution.

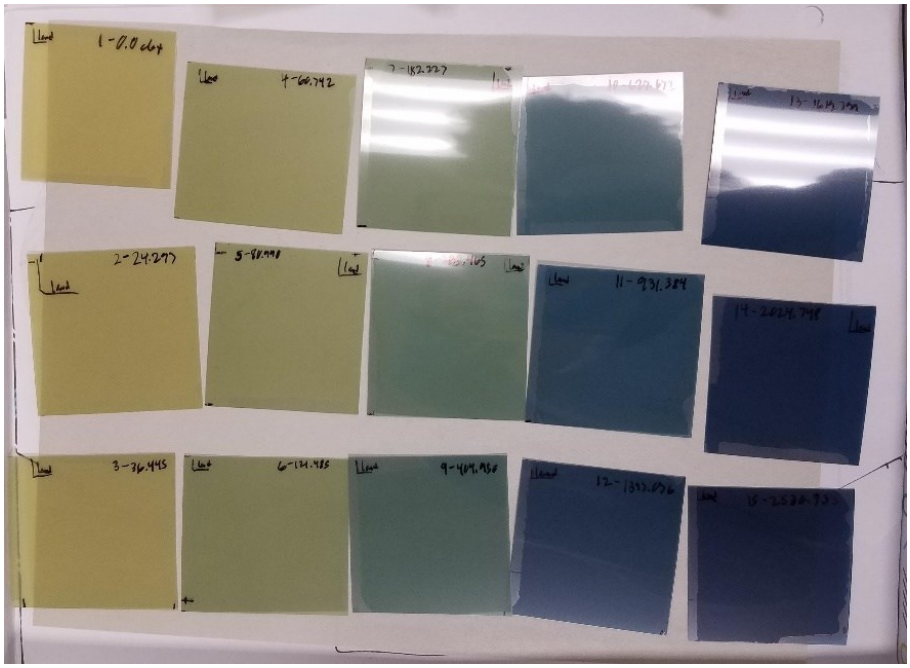

Figure 2.6. The 15 calibration films immediately after irradiation.

Approximately 48 hours after irradiation of the last calibration film, the films were scanned together in a color flatbed scanner (Epson Expression 10000XL, Epson America, Los Alamitos, California). Forty-eight hours was selected as the minimum post-exposure interval since radiochromic film response increases rapidly within the first 24 hours after irradiation but plateaus afterward.[28, 31] The scan was performed with all films in landscape orientation at 150 DPI (0.169 mm pixel size), 48-bit color, 16.5 inches×12.2 inches, and in transmission mode. All image enhancements were disabled.

Before scanning the experimental films, however, five preview warmup scans were performed to reduce film response differences due to temperature changes. A 2 mm glass plate was also placed over the films in the scanner bed (including the scanner's calibration area) to ensure film flatness and avoid the Callier effect.[28] This glass plate was cleaned with isopropyl alcohol then dusted with a microfiber cloth before each scanning session. The scanner bed was dusted as well.

The scanned calibration films were saved as .tiff files and imported into a commercial film analysis software package (RIT113 Classic v6.5, Radiological Imaging Technology, Inc., Colorado Spring, Colorado). Using the software, the pixel values (PVs) of the red, green, and blue (RGB) channels were averaged together and a 5×5-pixel median filter was applied by default to reduce noise. A 3×3 cm^2 region of interest (ROI) was placed over each calibration film in the scan to get a mean PV and standard deviation for each dose. The delivered dose value for each irradiated film patch was entered, forming the calibration curve fitted to a piecewise polynomial.[32] A profile was also placed along each calibration patch to confirm that the variation was below 3%.[28]

On the day of each spine plan delivery, the linac output was measured at the same conditions as before (0.6 cc Farmer chamber, 100 cm SAD, 10 cm depth, 11 cm backscatter material, 10×10 cm^2 field size, temperature, and pressure corrections), this time with a 6 MV FFF beam. The same electrometer was used for all treatment days except for the day of the L4 site treatment when it unavailable. A substitute electrometer (Model 206, SN 10812253, CNMC Company, Inc., Nashville, Tennessee) was used instead. These output measurements were

performed to scale each film's dose values before the analysis and reduce dosimetric effects of daily output variations. Three output measurements were recorded, then averaged for each treatment day.

For each treatment site, an 8-inch×10-inch film sheet was cut in half parallel to the short edge. This half was then cut to the outline of the phantom section of the current treatment site and, if necessary, cut to avoid contact with the pair of internal plastic rods that connect each section. Each film was labeled according to its treatment site (C4, T1, etc.), TPS (TPS_{CS} or TPS_{MC}), and trial (A, B, or C). The left, right, anterior, and posterior directions were labeled as well. The labeled film was taped between the phantom sections of the appropriate treatment site, shown in Table 2.4, then the four registration points were marked with a fine-tipped permanent marker through the film at the center of the diode plugs.

Separating the phantom sections after each treatment sometimes caused the edges of the film to delaminate. Since the registration points of the T12, L2, and L4 sites were placed near the edge of the film, four additional backup registration points were also marked closer to the middle of the film for these treatment sites (Figure 2.7). Ultimately, though, none of these backup registration points were needed during analysis.

Table 2.4. Phantom sections where the film was inserted, and the surrounding sections assembled for each treatment site.

Treatment Site	Sections Adjacent to Film	TPS_{CS} 10 cGy Isodose Limits	Sections Assembled During Treatment
C4	7 - 8	5 - 10	0 - 13
T1	10 - 11	7 - 14	0 - 13
T12	21 - 22	18 - 26	15 - 28
L2	24 - 25	20 - 29	18 - 31
L4	27 - 28	23 - 32	21 - 34

To allow for easier phantom handling, only a portion of the whole phantom was assembled per treatment site (Figure 2.8). The sections of the phantom assembled for each site are also listed in Table 2.4. For treatment sites T12, L2, and L4, 14 phantom sections were assembled, with the film inserted at the transverse isocenter plane of the beam in the middle (7 sections were superior and 7 sections were inferior to the film). This range of phantom sections fully contained 10 cGy isodose volume calculated by TPS_{CS}. The location of the C4 and T1 sites, however, warranted the need for the plastic ring, and thus section 0 of the phantom, to mount the phantom to the superior frame (Figure 2.2). This meant that the films for the C4 and T1 treatments did not have the same number of sections superior and inferior to them. Sections 0 to 13 still contained the full 10 cGy isodose volume for C4 and almost the full 10 cGy isodose volume for T1, however.

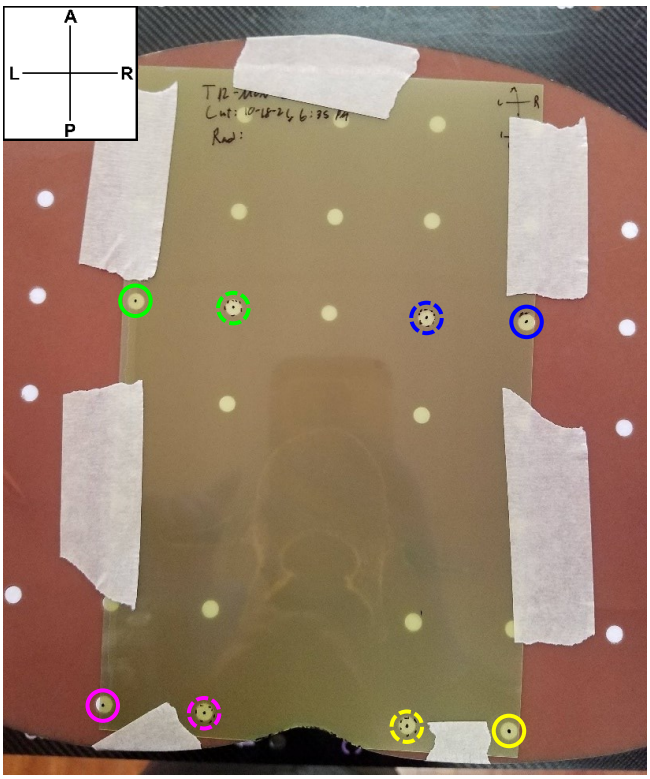

Figure 2.7. Film inserted at the T12 site prior to delivering a plan from TPS_{MC}. The four points marked on the outermost diode plugs (solid circles) were the primary registration points, corresponding with the TPS registration points in Figure 2.4. The inner four marks (dotted circles) were backup registration points in case film delamination occurred. Note that the registration point layout is mirrored compared to that in Figure 2.4 since the left and right directions are flipped from the CT transverse view.

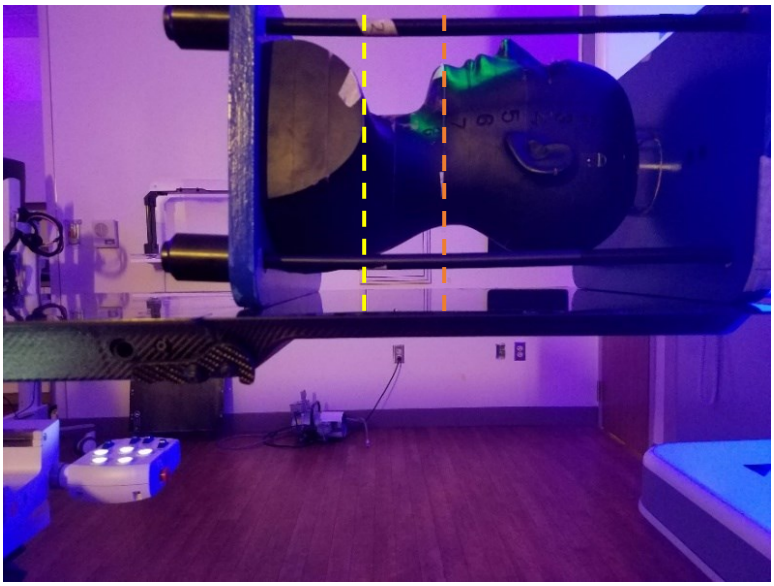

Figure 2.8. The phantom assembled for the C4 and T1 treatment sites. The orange dotted line marks the plane where the C4 film was inserted, and the yellow dotted line marks where the T1 film would be inserted.

After the phantom was assembled with the film securely taped inside, the phantom was laid supine on the treatment couch and the treatment site was aligned by eye to the treatment room lasers. The HexaPOD frame, which enables the HexaPOD couch equipped on the linac to adjust in six degrees of freedom, was mounted on the couch as close to isocenter as possible without covering the path of the primary beam, following the institution's standard operating procedure. A kV cone beam CT (CBCT) image was then performed on the phantom with a small field of view and F1 and S20 filters. After registering the CBCT image to the original planning CT using the Grey Value (T + R) method in the XVI software (Elekta, Stockholm, Sweden), the HexaPOD couch was automatically moved to the corrected position, shifting in the three cardinal directions as well as the pitch, roll, and yaw angular directions. Once the phantom was properly aligned, the treatment plan was delivered (trial A). The film was promptly removed from the phantom, and the time of irradiation was noted on it. The same treatment plan was then delivered to two more films (trials B and C) for that treatment site, following the same setup, imaging, and alignment process.

2.5. Film Analysis

All 30 measurement films (5 plans for each TPS, 3 trials delivered per plan) were digitized with the flatbed scanner. Like the calibration films, 48 hours was the minimum post-exposure time, but none of the measurement films exceeded a 51 hour wait time. The scanner parameters and cleaning process for the glass plate were identical to that of the calibration films. Each measurement film was scanned individually in its landscape orientation, approximately along the lateral central axis of the scanner bed at 150 DPI (0.169 mm pixel size), 48-bit color, 16.5 inches×12.2 inches, transmission mode, with no image enhancements. See Figure 2.9 for an example.

The films scans were saved as .tiff files. Each film scan was opened in the commercial film analysis software as the 'Reference' image with a 5×5-pixel median filter applied. The calibration curve was applied to the image, then the image was scaled by the following factor to reduce the effect of daily linac output variations:

$$\frac{0.8\ \text{cGy/ MU}}{\text{treatment day's output (cGy/MU)}}$$

Each film scan was digitally rotated and mirrored so that the film coordinate system matched that of the TPS dose plane, then the film scan was assigned as the 'Target' image. The corresponding TPS dose plane (exported with 1 mm resolution that was interpolated from the 2 mm dose grid resolution) was then opened as the 'Reference' image.

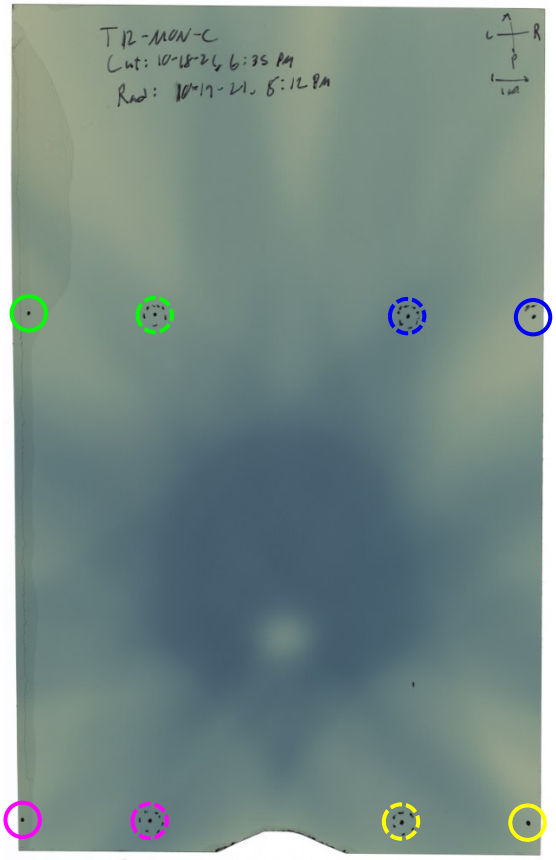

Figure 2.9. TPS_{MC} T12 film scan, trial A. The circled registration points correspond to those marked in Figure 2.7.

Prior to the analysis, a registration template for each vertebral site was defined in the film analysis software. Each registration template was defined using the Right/Left (+x/-x) and Superior/Inferior (+y/-y) coordinates of the registration points in TPS_{CS}. TPS_{CS} displays coordinates relative to the CT image's DICOM origin point, but since each dose plane was exported into the film analysis software with its isocenter at the center of the image, the original coordinates of each registration point had to be shifted relative the distance from the isocenter to the DICOM origin. The appropriate registration template was applied to 'Reference' TPS image, then the corresponding digital registration points were placed manually at the marks on the 'Target' film image. This registration caused the film image's resolution, 0.169 mm, to downscale to that of the TPS image, 1 mm. The software also outputted standard deviations of each film's registration based on a method described by Fitzpatrick et al.[33]

After registration of the TPS and film images, a limited ROI was defined in TPS image. Using the known coordinates from TPS_{CS} of each site's isocenter, the coordinates of various points of interest, such as the edges of the PTV and cord/cauda, were used to locate the same points in the analysis image. This allowed an ROI to be defined in the software, extending vertically 1 cm above each site's anterior PTV edge to 1 cm below the posterior cord/cauda edge. This vertical length ensured an appropriate margin existed for the AP profile analyses. For sites C4 and T1, the ROI extended horizontally 3 cm from the center of the spinal cord/cauda equina in both the left and right directions. For the T12, L2, and L4 sites, it extended 4 cm. These horizontal widths produced sufficient coverage for the gamma analyses. Identical ROI were automatically generated

on the registered film images. For both TPSs and across the multiple trials for each treatment site, the ROI location and size were constant. For example, the C4 and T1 sites had different ROI sizes, but the C4 ROI had the same size and location across all trials for both TPSs, and the T1 ROI had the same size and location across all trials for both TPSs.

In this ROI, the AP dose profiles through isocenter for both the TPS and film images were exported and analyzed in a custom MATLAB script (R2021b, MathWorks, Natick, Massachusetts). The two main metrics used to compare the TPS-calculated and film-measured AP dose profiles were the *dose falloff difference* and *profile shift*.

For each TPS and film profile, two positions, D_{high} and D_{low}, were first determined (see Figure 2.10 for an example). D_{high} is the last position of the 1600 cGy isodose value before the negative slope of the profile begins. D_{low} is the first position on the profile that reaches a threshold dose gradient of -500 cGy/cm after the negative slope begins. The profiles for the L4 TPS_{MC} plans, however, did not reliably reach this dose gradient, so a threshold value of -200 cGy/cm was used instead.

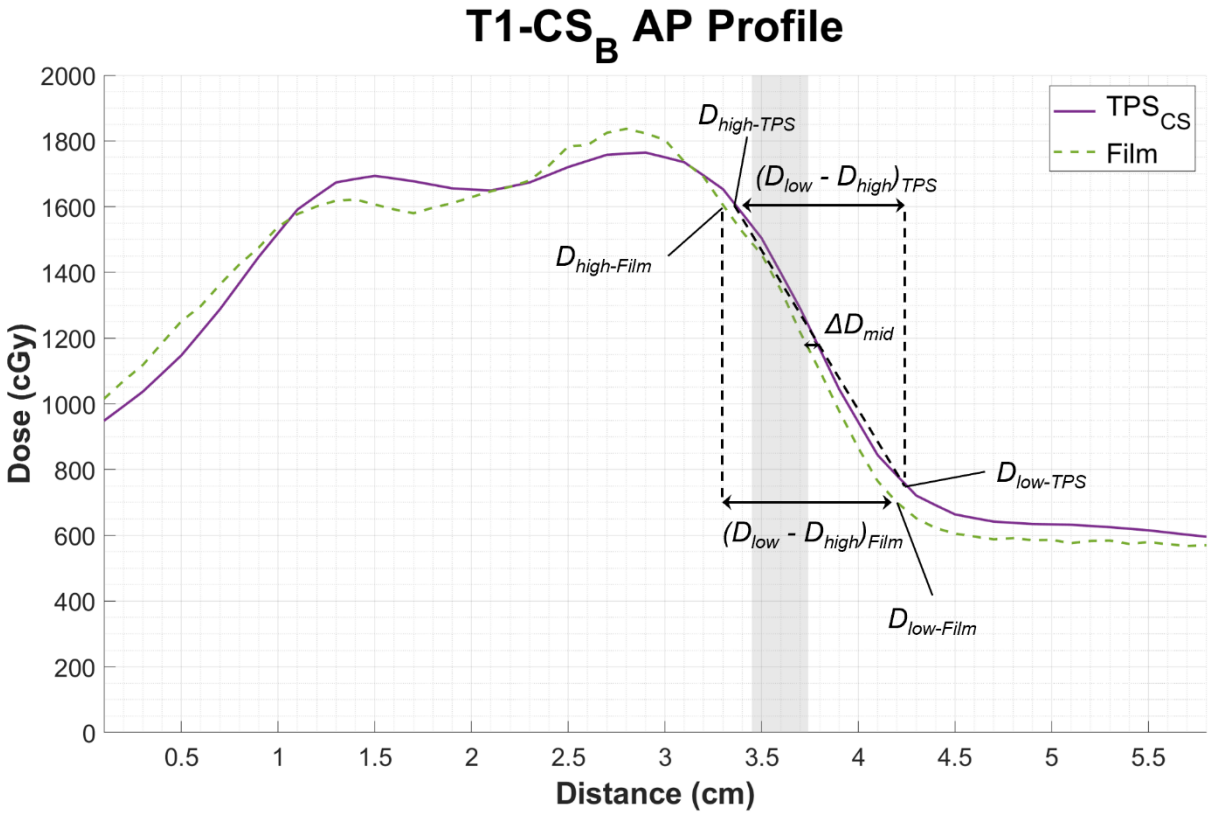

Figure 2.10. TPS_{CS}-calculated and film-measured dose profiles for the T1 site, Trial B. The shaded region represents the area between the posterior PTV edge and the anterior cord edge. D_{high} is the last profile position of the 1600 cGy isodose value, and D_{low} is the first profile position that reaches -500 cGy/cm. The *dose falloff difference* is the positive distance (mm) measured between D_{high} and D_{low} on the TPS profile subtracted from the same distance measured on the film profile. The *profile shift*, ΔD_{mid}, is the TPS profile's D_{high} and D_{low} midpoint position (mm) subtracted from the position that matches the same dose value on the film profile.

The dose falloff difference was defined as the positive distance (mm) measured between D_{high} and D_{low} on the TPS profile subtracted from the same distance measured on the film profile (Figure 2.10). In addition, the dose falloff percent difference was calculated by normalizing the dose falloff difference by the current TPS profile's dose falloff as in the below equation:

$$\frac{(\text{Dose falloff}_{\text{Film}} - \text{Dose falloff}_{\text{TPS}})}{\text{Dose falloff}_{\text{TPS}}} \times 100\%$$

A positive dose falloff difference indicates the film profile has a more gradual dose slope relative to the TPS profile. A negative dose falloff difference indicates the film had a sharper slope. A difference of zero would be ideal.

The profile shift, ΔD_{mid}, was defined as the TPS profile's D_{high} and D_{low} midpoint position (mm) subtracted from the position that matches the same dose value on the film profile (Figure 2.10). A positive profile shift indicates the film profile was shifted posterior to the TPS profile, and a negative profile shift indicates an anterior shift. A shift of zero would be ideal.

It was assumed that the average dose falloff difference and average profile shift across each site's three trials were sampled from normally distributed populations of equal variance. Normality was confirmed with a Shapiro-Wilks test run on each TPS sample using the shapiro.test[34] function in a custom R v4.0.1 (R Foundation, Vienna, Austria) script. A Shapiro-Wilk p-value greater than an α value of 0.05 would indicate that each sample comes from a normally distributed population. Equal variances were confirmed between the TPS_{CS} and TPS_{MC} samples with the vartestn function in MATLAB, with the test type set to 'LeveneAbsolute.' A Levene p-value greater than the same α value would indicate that the two TPS samples come from populations of equal variance. A two-tailed, unpaired, equal variance t-test was then performed on each TPS sample of metrics using MATLAB's ttest2 function.[35] A T-test p-value less than α would indicate a statistically significant difference exists between the two samples.

The film analysis software performed 2D gamma analysis[36] on the three trials for each treatment site at the same ΔD/DTA criteria as the TG-119 validation plans: 5%/1mm, 3%/3mm, 3%/2mm, 3%/1mm, 2%/2mm, 2%/1mm, and 1%/1mm. All the ΔD refer to the percentage of global maximum planned dose. A 10% maximum planned dose threshold was applied as well, but such low dose values ultimately did not appear in the ROI. The three GPRs for each site were then averaged.

With the previously described code, using an α of 0.05 throughout, the Shapiro-Wilk test was performed on each ΔD/DTA criteria sample of GPR to confirm the samples came from normally distributed populations. Levene's test was performed between the TPS_{CS} and TPS_{MC} average GPRs for each criterion to determine whether there were equal variances between the two TPS samples. If variances were equal, an unpaired equal variance t-test was then performed on the samples. If unequal, an unpaired unequal variance t-test was used.

Chapter 3. Results

3.1. Treatment Planning Results

Table 3.1 displays the TPS_{CS} and TPS_{MC} spine planning results for each treatment target. The TPS_{MC} plans always had a lower overall maximum dose. While all plans in TPS_{CS} had their global maximum dose points inside the CTV, per the advice of the approving radiation oncologist, all plans except for L4 in TPS_{MC} had the maximum dose point fall within 2 mm outside of the CTV (within the PTV). For most spine plans, TPS_{MC} generated around twice as many MUs than TPS_{CS}, which resulted in much longer beam-on times during each treatment. The number of control points per plan were similar between TPS_{CS} and TPS_{MC}. The one exception was the T12 plans, which had 99 fewer control points in TPS_{MC} than TPS_{CS}. Though the PTV coverage of the TPS_{MC} sites were initially higher than shown in Table 3.1, the coverage had to be lowered to a set value in order to limit dose hotspots greater than 1680 cGy (105% Rx), which were larger in TPS_{MC} than in TPS_{CS} for all sites except C4 and L4. Despite this, the TPS_{MC} plans consistently yielded higher PTV coverage than the TPS_{CS} plans, albeit at worse Paddick conformity indices.[37]

Table 3.2 shows the planning results for the spinal cord and cauda equina. The TPS_{MC} plans spared the spinal cord more than those in TPS_{CS} after fewer optimizations. The L4 plan in TPS_{MC} also spared the cauda equina more than the L4 plan in TPS_{CS}.

The calculated transverse dose planes at each treatment site's isocenter are displayed in Figure 3.1 through Figure 3.5. The isocenter inside the vertebral body as well as the four registration points for each site are displayed on the TPS_{CS} dose maps. The CTV is contoured in red, the PTV in orange, the spinal cord in cyan, and the cauda equina in green. As a whole, TPS_{CS} produced colder dose plans than TPS_{MC}.

Table 3.1. Planning results of the target volume coverage in TPS_{CS} and TPS_{MC}. All dose values are based on a 0.001 cc volume. The record and verify system rounded the MUs to the nearest 0.1 MU and defined one additional control point per arc in the TPS_{MC} plans.

Site	TPS	Max Dose (cGy)	Total MU	Total Control Points	105% Isodose Volume Outside CTV (cc)	Max Dose Outside CTV, PTV (cGy)	CTV, PTV Rx Coverage (%)	Conformity Index
C4	TPS_{CS}	1770.1	3300.0	352	1.339	1747.2, 1682.0	94.51, 94.32	0.83
	TPS_{MC}	1757.0	5073.9	339	0.862	1757.0, 1737.5	96.37, 95.00	0.73
T1	TPS_{CS}	1783.3	4174.0	352	0.570	1747.1, 1647.0	97.61, 91.38	0.93
	TPS_{MC}	1740.0	8754.8	345	1.576	1740.0, 1738.4	96.56, 93.01	0.75
T12	TPS_{CS}	1779.8	4194.0	352	1.122	1739.6, 1675.5	95.77, 93.25	0.91
	TPS_{MC}	1738.0	8547.7	253	1.813	1738.0, 1727.0	95.02, 94.30	0.77
L2	TPS_{CS}	1782.5	3800.0	352	0.556	1748.1, 1647.3	99.62, 92.18	0.95
	TPS_{MC}	1740.0	7423.6	374	1.269	1740.0, 1704.3	99.72, 97.75	0.83
L4	TPS_{CS}	1751.2	3469.0	352	1.056	1713.2, 1661.8	99.89, 93.15	0.96
	TPS_{MC}	1734.0	7581.8	387	0.571	1721.5, 1699.5	98.04, 95.24	0.79

Table 3.2. Planning results for the spinal cord and cauda equina in TPS_{CS} and TPS_{MC}. All dose values are based on a 0.001 cc volume.

Site	TPS	Spinal Cord Volume Receiving 10 Gy (%, cc)	Max Cord Dose (cGy)	Cauda Equina Volume Receiving 14 Gy (cc)	Max Cauda Dose (cGy)
C4	TPS_{CS}	7.78, 0.172	1364.2	-	-
	TPS_{MC}	3.09, 0.065	1157.4	-	-
T1	TPS_{CS}	6.19, 0.156	1284.6	-	-
	TPS_{MC}	4.81, 0.121	1259.0	-	-
T12	TPS_{CS}	7.86, 0.219	1244.6	-	-
	TPS_{MC}	4.30, 0.121	1192.5	-	-
L2	TPS_{CS}	8.18, 0.060	1218.0	0.076	1506.5
	TPS_{MC}	5.37, 0.039	1186.0	0.485	1515.5
L4	TPS_{CS}	-	-	1.013	1571.5
	TPS_{MC}	-	-	0.645	1552.0

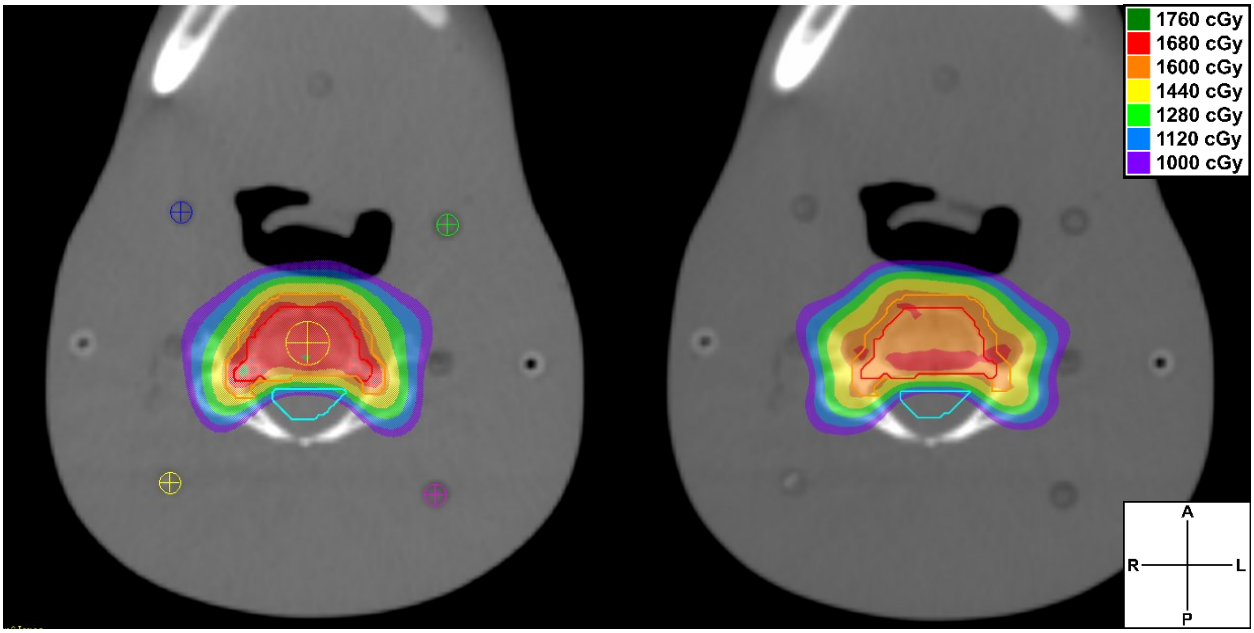

Figure 3.1. Calculated transverse dose distribution at the C4 site in TPS_{CS} (Left) and TPS_{MC} (Right).

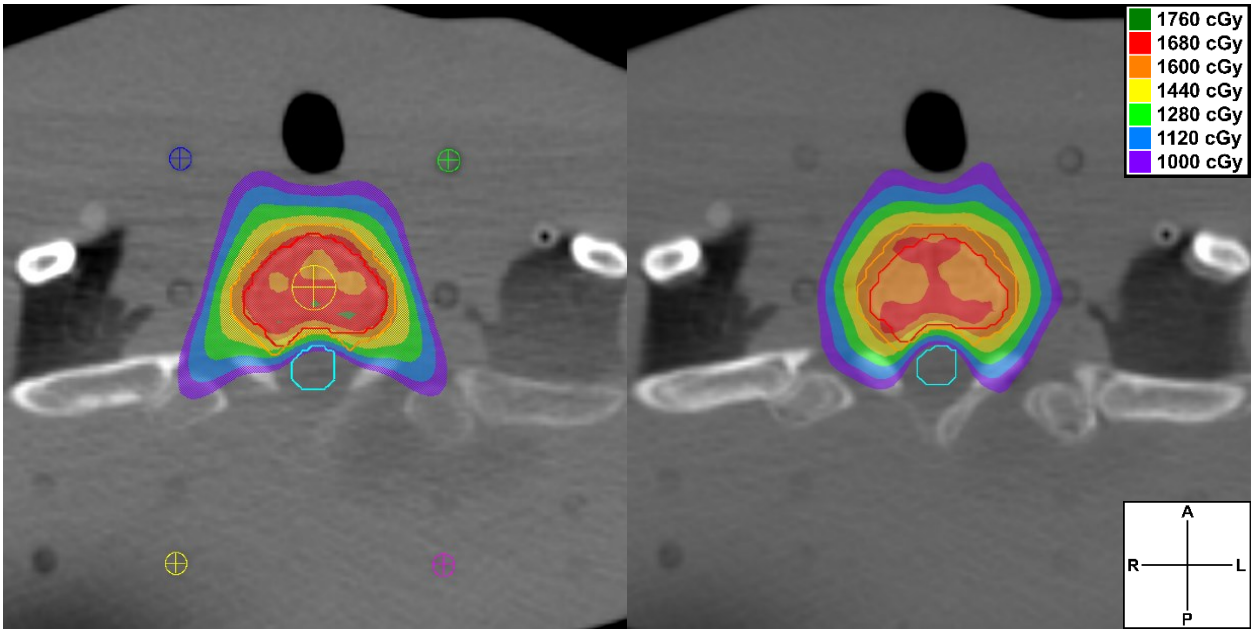

Figure 3.2. Calculated transverse dose distribution at the T1 site in TPS_{CS} (Left) and TPS_{MC} (Right).

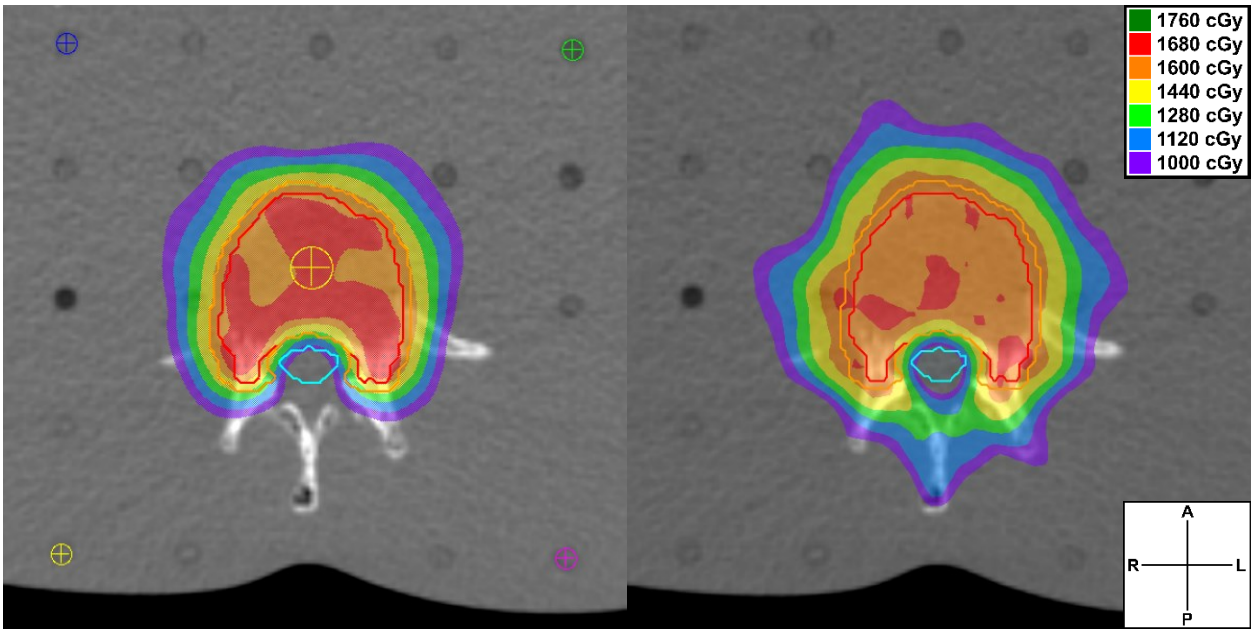

Figure 3.3. Calculated transverse dose distribution at the T12 site in TPS_{CS} (Left) and TPS_{MC} (Right).

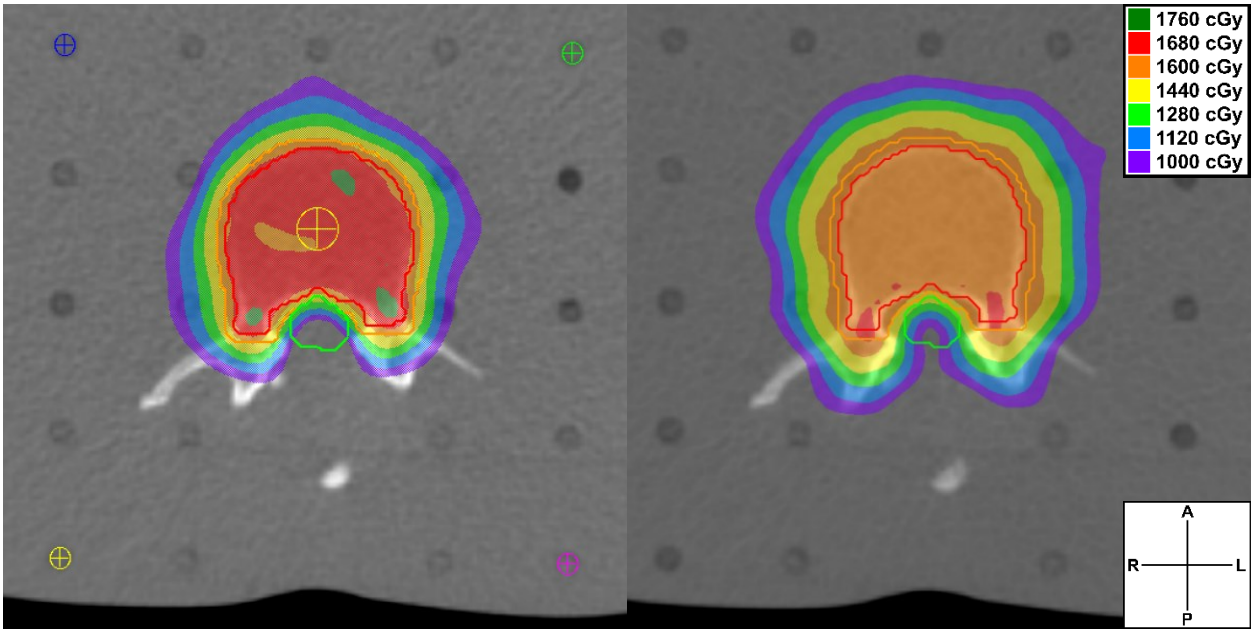

Figure 3.4. Calculated transverse dose distribution at the L2 site in TPS_{CS} (Left) and TPS_{MC} (Right).

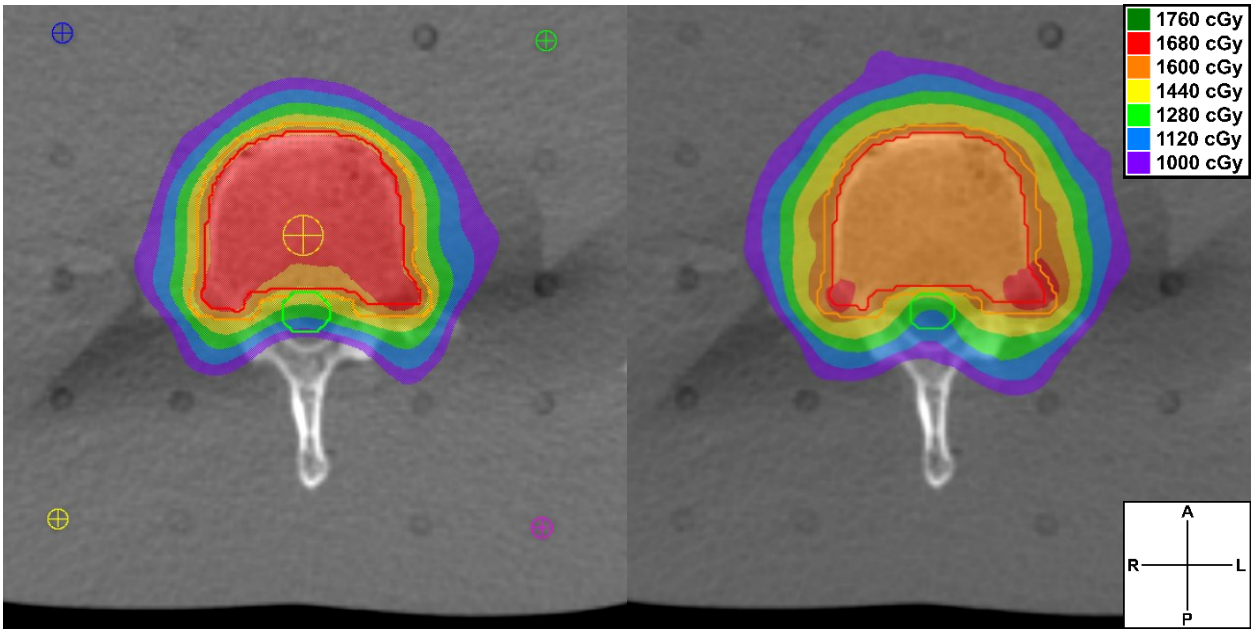

Figure 3.5. Calculated transverse dose distribution at the L4 site in TPS_{CS} (Left) and TPS_{MC} (Right).

3.2. Validation Plan Results

Table 3.3 displays the total MU and total number of control points generated in the TG-119 validation plans. As in spine plans, TPS_{MC} generated more MUs than TPS_{CS}, except at the Cshape site. The number of controls points between each TPS were similar except for at the Head/Neck site, with TPS_{MC} generating 76 fewer than TPS_{CS}.

Table 3.3. Total MUs delivered and total number of control points created for each TG-119 site and TPS. The record and verify system rounded the MUs to the nearest 0.1 MU and defined one additional control point per arc in the TPS_{MC} plans.

TG-119 Site	TPS	Total MU	Total Number of Control Points
Multitarget	TPS_{CS}	359.0	176
	TPS_{MC}	850.1	194
Prostate	TPS_{CS}	307.0	176
	TPS_{MC}	517.3	181
Head/Neck	TPS_{CS}	1118.0	352
	TPS_{MC}	1336.9	276
Cshape	TPS_{CS}	1056.0	176
	TPS_{MC}	1058.7	177

The point doses of the validation plans delivered to solid water slabs are displayed in Table 3.4 through Table 3.7. All high-dose points were more accurate in TPS_{MC} than in TPS_{CS}. All low-dose points, except for the head/neck isocenter, were more accurate in TPS_{CS} than in TPS_{MC}. The average low-dose points across the four plans had similar accuracy between both TPSs, though TPS_{MC} had a lower σ. In both TPSs, the validation plan's high dose and low dose point measurements, averaged across the four plans, were not as accurate as the institutional averages from the published task group report, -0.2% and +0.3% dose differences, respectively. The point

with the highest difference was in the high dose region of the Cshape plan (for 6.7% TPS_{CS} and 4.6% for TPS_{MC}).

The validation plans delivered to the diode array yielded GPRs displayed in Figure 3.6 and Figure 3.7 as well as Table 3.8 and Table 3.9. The gamma analyses showed that, at 2%/2mm criteria, the most common area of failure was inside the targets. For the multitarget plan, the GPRs of TPS_{CS} were comparable to TPS_{MC} for all criteria except 1%/1mm. For the prostate, both planning systems yielded similar GPR for all criteria except 3%/1mm, 2%/1mm, and 1%/1mm, where TPS_{MC} GPR was higher. For the head/neck site, TPS_{CS} GPRs were consistently higher than TPS_{MC} GPRs for all criteria except 5%/1mm. For the Cshape plan, TPS_{MC} always outperformed TPS_{CS}. Overall, averaging the GPR across all four sites for each gamma criteria yielded very similar GPRs for all criteria except for 3%/1mm, 2%/1mm, and 1%/1mm, with TPS_{MC} having higher GPRs for these. In summary, at 1mm DTA (excluding 5%/1mm), TPS_{MC} tended to have higher GPRs than TPS_{CS}.

The average 3%/3mm GPR across the TG-119 sites for TPS_{CS} and TPS_{MC} was 99.6% and 99.5%, respectively. These both exceeded the published TG-119 institutional average, 97.9%. The average 2%/2mm GPR across the TG-119 sites for TPS_{CS} and TPS_{MC} was also very high, 97.4% and 97.5%, respectively.

Table 3.4. Point dose measurements for the TPS_{CS} validation plans in solid water slabs. The isocenter planned doses are based on mean dose to a contoured ion chamber volume (0.081 cc). The other planned doses are based on the absolute point dose.

TPS_{CS} TG-119 Site	Prescribed Dose (cGy per fraction)	Measurement Point (Dose Region)	Planned Dose (cGy)	Mean Measured Dose ± σ (cGy)	Dose Difference (%)
Multitarget	200	Isocenter (High)	209.04	213.77 ± 0.00	+2.4
		4 cm Superior (Low)	132.01	136.17 ± 0.23	+2.1
		4 cm Inferior (Low)	64.58	62.49 ± 0.09	-1.0
Prostate	180	Isocenter (High)	194.60	199.57 ± 0.00	+2.8
		2.5 cm Posterior (Low)	147.98	149.46 ± 0.09	+0.8
Head/Neck	200	Isocenter (High)	220.88	231.34 ± 0.35	+5.2
		4.0 cm Posterior (Low)	123.14	132.64 ± 0.30	+4.7
Cshape (easy)	200	Isocenter (Low)	62.52	62.59 ± 0.09	+0.0
		2.5 cm Anterior (High)	218.56	232.05 ± 0.30	+6.7

Table 3.5. Mean dose difference ± σ, and CL_{diff} for the high and low dose points for the TPS_{CS} validation plans.

	Mean Dose Difference ± σ (%)	CL_{diff} (%)
High Dose Regions	+4.3 ± 2.1	8.3
Low Dose Regions	+1.3 ± 2.2	5.7

Table 3.6. Point dose measurements for the TPS_{MC} validation plans in solid water slabs. The isocenter planned doses are based on mean dose to a contoured ion chamber volume (0.067 cc). The other planned doses are based on the mean dose to the points, which had a custom-sized volume of 0.007 cc.

TPS_{MC} TG-119 Site	Prescribed Dose (cGy per fraction)	Measurement Point (Dose Region)	Planned Dose (cGy)	Mean Measured Dose ± σ (cGy)	Dose Difference (%)
Multitarget	200	Isocenter (High)	208.20	211.80 ± 0.00	+1.8
		4 cm Superior (Low)	130.76	137.88 ± 0.46	+3.6
		4 cm Inferior (Low)	88.89	92.25 ± 0.23	+1.7
Prostate	180	Isocenter (High)	193.24	196.90 ± 0.00	+2.0
		2.5 cm Posterior (Low)	127.58	130.02 ± 0.17	+1.4
Head/Neck	200	Isocenter (High)	211.66	220.31 ± 0.31	+4.3
		4.0 cm Posterior (Low)	112.70	109.33 ± 0.23	-1.7
Cshape (easy)	200	Isocenter (Low)	48.42	50.06 ± 0.17	+0.8
		2.5 cm Anterior (High)	206.18	215.43 ± 0.30	+4.6

Table 3.7. Mean dose difference ± σ, and CL_{diff} for the high and low dose points for the TPS_{MC} validation plans.

	Mean Dose Difference ± σ (%)	CL_{diff} (%)
High Dose Regions	+3.2 ± 1.5	6.1
Low Dose Regions	+1.1 ± 1.9	4.8

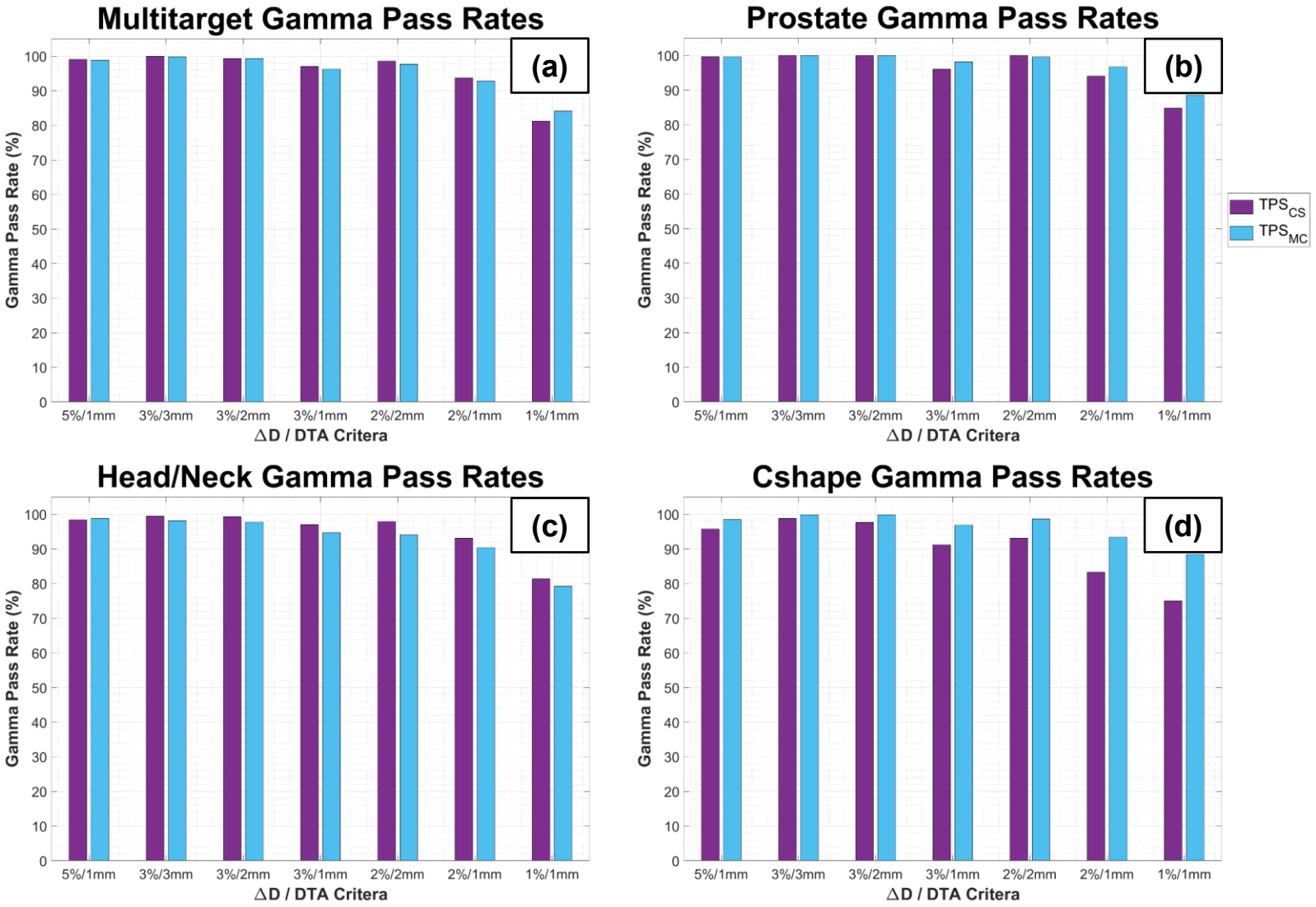

Figure 3.6. GPR for each TPS at multiple ΔD/DTA criteria for each TG-119 treatment site: (a) Multitarget, (b) Prostate, (c) Head/Neck, and (d) Cshape.

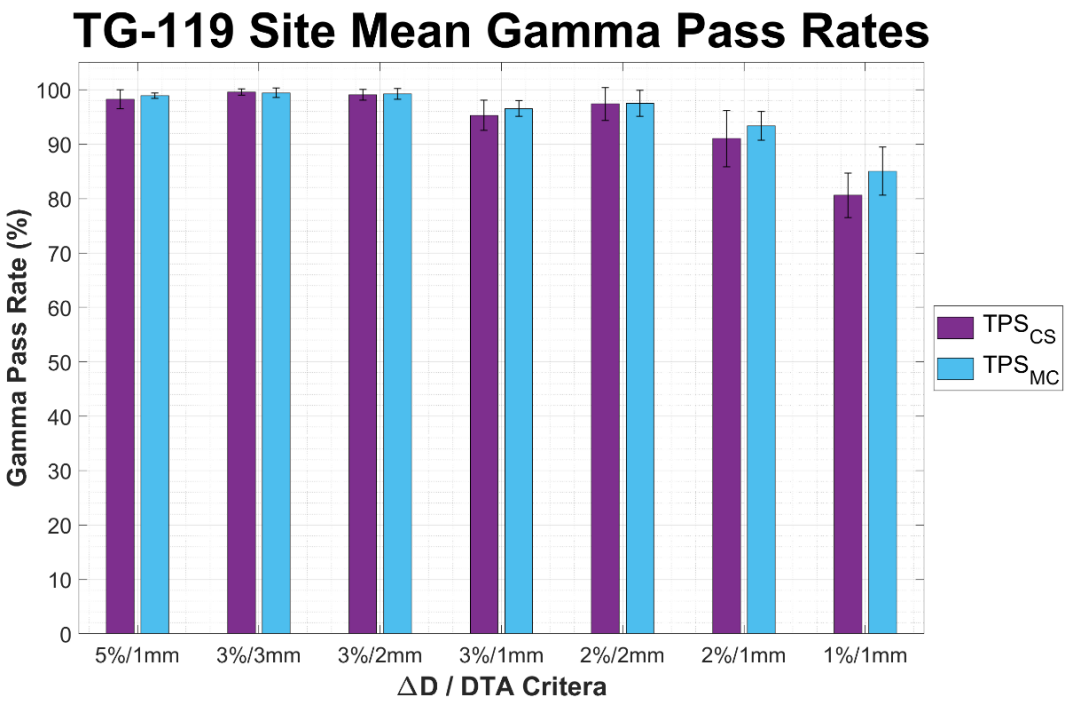

Figure 3.7. Mean GPR across all TG-119 treatment sites for each TPS at multiple ΔD/DTA criteria. The error bars extend plus and minus one sample σ of the mean.

Table 3.8. GPR at multiple ΔD/DTA criteria for the TPS_{CS} validation plans.

ΔD/DTA Criteria	Multitarget GPR (%)	Prostate GPR (%)	Head/Neck GPR (%)	Cshape (easy) GPR (%)	Mean GPR ± σ across sites (%)	CL_{GPR} (%)
5%/1mm	99.1	99.7	98.4	95.8	98.25 ± 1.72	5.1
3%/3mm	100.0	100.0	99.5	98.8	99.58 ± 0.57	1.5
3%/2mm	99.3	100.0	99.3	97.7	99.08 ± 0.97	2.8
3%/1mm	97.0	96.0	97.0	91.2	95.30 ± 2.77	10.1
2%/2mm	98.6	100.0	97.9	93.1	97.40 ± 3.00	8.5
2%/1mm	93.7	94.0	93.1	83.3	91.03 ± 5.16	19.1
1%/1mm	81.2	84.8	81.4	75.0	80.60 ± 4.08	27.4

Table 3.9. GPR at multiple ΔD/DTA criteria for the TPS_{MC} validation plans.

ΔD/DTA Criteria	Multitarget GPR (%)	Prostate GPR (%)	Head/Neck GPR (%)	Cshape (easy) GPR (%)	Mean GPR ± σ across sites (%)	CL_{GPR} (%)
5%/1mm	98.8	99.6	98.8	98.5	98.93 ± 0.47	2.0
3%/3mm	99.8	100.0	98.2	99.8	99.45 ± 0.84	2.2
3%/2mm	99.3	100.0	97.8	99.8	99.23 ± 0.99	2.7
3%/1mm	96.3	98.2	94.7	96.9	96.53 ± 1.45	6.3
2%/2mm	97.7	99.6	94.1	98.7	97.53 ± 2.41	7.2
2%/1mm	92.8	96.8	90.4	93.4	93.35 ± 2.64	11.8
1%/1mm	84.1	88.5	79.2	88.4	85.05 ± 4.41	23.6

3.3. Film Calibration Curve

On the day of calibration film irradiation, the linac output was 0.8099 cGy/MU at the calibration conditions. This value was multiplied by the MU delivered per calibration patch to obtain the actual calibration dose values listed in Table 3.10.

Figure 3.8 displays the calibration curve for the film batch. Each point represents the mean of the red, green, and blue channel PVs of the ROI over each calibration patch. A 3.62 cm long profile was also placed across the approximate center of each calibration patch along the films' landscape axis. The maximum and minimum PV along the profile were identified, then the percent difference relative to the profile's mean PV was calculated for each. The larger percent difference is displayed in Table 3.10, all of which were within 3% uniformity per TG-235 guidelines.[28] The largest variation occurred in 400 and 620 cGy calibration films.

Table 3.10. Nominal calibration dose values, actual dose values adjusted with the linac output measurement, and largest percent difference from mean PV in each calibration patch.

Nominal Calibration Dose (cGy)	Actual Calibration Dose (cGy)	Largest Percent Difference (%)
0	0.0	0.66
24	24.3	0.38
36	36.4	-0.81
60	60.7	-0.75
80	81.0	-0.44
120	121.5	-1.04
180	182.2	-0.80
280	283.5	0.86
400	404.9	-1.38
620	627.7	-1.33
920	931.4	0.80
1380	1397.1	0.71
1600	1619.8	0.93
2000	2024.7	-0.87
2500	2530.9	-0.82

3.4. Spine Plan Film Results

Both the dose falloff difference and profile shift were obtained from the TPS-film profile pair for each trial delivered, then the metrics from the three trials were averaged for each treatment site. Table 3.11 and Table 3.12 display the average dose falloff difference ± standard deviation (σ) and average profile shifts ± σ for each treatment site, respectively. They also display the mean value of each metric ± σ across the five treatment sites for each TPS. The p-values for each statistical test are displayed as well.

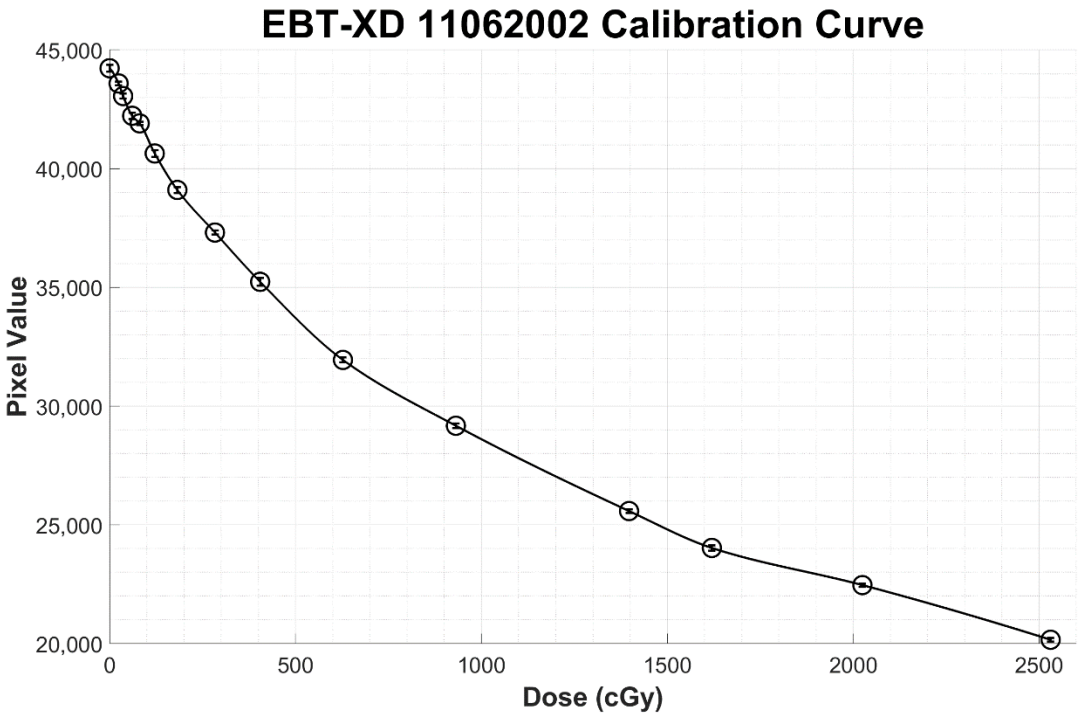

Figure 3.8. Mean RGB calibration curve for the Gafchromic EBT-XD film batch fit to a piecewise polynomial. The error bars at each point extends plus and minus one sample standard deviation (σ) of the mean PV in each calibration patch's ROI.

The largest dose falloff differences took place in the L4 TPS_{CS} plan at -1.1 ± 1.0 mm (-7.8 ± 7.1%) and the L4 TPS_{MC} plan at -1.5 ± 1.0 mm (-16.6 ± 10.7%). The smallest difference took place in both the C4 and T12 TPS_{CS} plans, at -0.3 ± 0.5 mm (-2.9 ± 5.7%) and -0.3 ± 0.8 mm (-3.5 ± 11.2%), respectively. In TPS_{MC}, the T1 plan had the smallest difference at -0.1 ± 0.3 mm (-1.3 ± 3.2%). The average dose falloff differences for all treatment sites for TPS_{CS} and TPS_{MC} were -0.0 ± 0.8 mm (+0.7 ± 7.8%) and -0.7 ± 0.5 mm (-7.8 ± 6.0%), respectively. On average, any dose falloff differences between the TPS-calculated and the film-measured AP profiles in the critical region between the PTV and cord/cauda were smaller than the resolution of the dose planes.

The largest profile shifts took place in the T1 plan for both TPS_{CS} and TPS_{MC}, -0.6 ± 0.2 mm and -0.9 ± 0.0 mm, respectively. The smallest shift in TPS_{CS} took place in both C4, +0.2 ± 0.1 mm, and L2, -0.2 ± 0.2 mm. In TPS_{MC}, the smallest shift was at L2, +0.2 ± 0.1 mm. The average profile shift across all treatment sites for TPS_{CS} and TPS_{MC} were -0.1 ± 0.3 mm and +0.0 ± 0.6 mm, respectively. Again, any profile shifts between the calculated and measured profiles in the were smaller than the dose distribution's resolution.

Each TPS sample was confirmed to come from normally distributed populations of with equal variance to its opposing TPS. No statistically significant differences were detected in the dose differences, dose falloff differences, or profile shifts between TPS_{CS} and TPS_{MC}. The dose profiles for all trials are compiled in Appendix B.

Table 3.11. AP dose falloff differences and percent dose falloff differences between the TPS-calculated and film-measured profiles of TPS_{CS}, likewise for TPS_{MC}, and the p-values of the statistical tests.

Treatment Planning System	C4	T1	T12	L2	L4	Mean ± σ across sites	Shapiro-Wilk p-value	Levene p-value	T-Test p-value
TPS_{CS} Dose Falloff Difference (mm)	-0.3 ± 0.5	+0.6 ± 0.4	-0.3 ± 0.8	+0.8 ± 0.4	-1.1 ± 1.0	-0.0 ± 0.8	0.606	0.325	0.167
TPS_{MC} Dose Falloff Difference (mm)	-0.4 ± 0.2	-0.1 ± 0.3	-0.5 ± 0.3	-0.8 ± 0.1	-1.5 ± 1.0	-0.7 ± 0.5	0.460		
TPS_{CS} Dose Falloff Difference (%)	-2.9 ± 5.7	+7.1 ± 4.7	-3.5 ± 11.2	+10.7 ± 4.7	-7.8 ± 7.1	+0.7 ± 7.8	0.436	0.341	0.088
TPS_{MC} Dose Falloff Difference (%)	-5.1 ± 2.8	-1.3 ± 3.2	-5.2 ± 3.6	-11.0 ± 1.9	-16.6 ± 10.7	-7.8 ± 6.0	0.615		

Table 3.12. AP profile shifts between the TPS-calculated and film-measured profiles of TPS_{CS}, likewise for TPS_{MC}, and the p-values of the statistical tests.

Treatment Planning System	C4	T1	T12	L2	L4	Mean ± σ across sites	Shapiro-Wilk p-value	Levene p-value	T-Test p-value
TPS_{CS} Profile shift (mm)	+0.2 ± 0.1	-0.6 ± 0.2	-0.3 ± 0.1	-0.2 ± 0.2	+0.3 ± 0.5	-0.1 ± 0.3	0.680	0.212	0.655
TPS_{MC} Profile shift (mm)	-0.3 ± 0.1	-0.9 ± 0.0	+0.4 ± 0.2	+0.2 ± 0.1	+0.7 ± 0.3	+0.0 ± 0.6	0.855		

The average GPR across the three trials for each site and TPS as well as the average GPR across all sites are displayed in Figure 3.9 and tabulated in Table 3.14 and Table 3.15. For all criteria, except 5%/1mm and 1%/1mm, Levene's test yielded unequal variances between the sample of TPS_{CS} GPRs and sample of TPS_{MC} GPRs (Table 3.16). An unpaired unequal variance t-test was performed on all samples of criteria, except for 5%/1mm and 1%/1mm, which received the equal variance t-test. Averaging across the three trials, TPS_{CS} always obtained a higher mean GPR than TPS_{MC} at all sites, except for the 1%/1mm gamma analysis of T12. The differences in GPR between each TPS were statistically significant for all criteria all except 2%/1mm and 1%/1mm.

Appendix C displays figures of the digitized film measurements for all trials, where the red pixels represent the dose points calculate that a gamma value larger than 1, i.e., failed the test, for the 2%/2mm criteria. The most common area for points to fail was inside the PTV, specifically the posterior portion, which usually had a higher measured dose than planned. TPS_{MC} consistently had more failing points inside the PTV compared to TPS_{CS}. TPS_{MC} also had overestimated dose points immediately posterior to the spinal cord and cauda equina for all sites except C4. Such failures occurred minorly in TPS_{CS} at the T1 site. Points near the edge of their ROI tended to fail for both TPSs. The area between the posterior PTV edge and anterior cord/cauda edge usually failed at either 3%/1mm, 2%/1mm, or 1%/1mm criteria (Table 3.13).

Table 3.13. Gamma criteria where dose points between the posterior PTV edge and anterior cord/cauda edge tend to fail. Each listed criterion was determined based on a qualitative observation of each site's three trials for per TPS.

Vertebral Site	TPS	ΔD/ DTA of Failure
C4	TPS_{CS}	-
	TPS_{MC}	-
T1	TPS_{CS}	3%/1mm
	TPS_{MC}	-
T12	TPS_{CS}	3%/1mm
	TPS_{MC}	3%/1mm
L2	TPS_{CS}	1%/1mm
	TPS_{MC}	3%/1mm
L4	TPS_{CS}	2%/1mm
	TPS_{MC}	1%/1mm

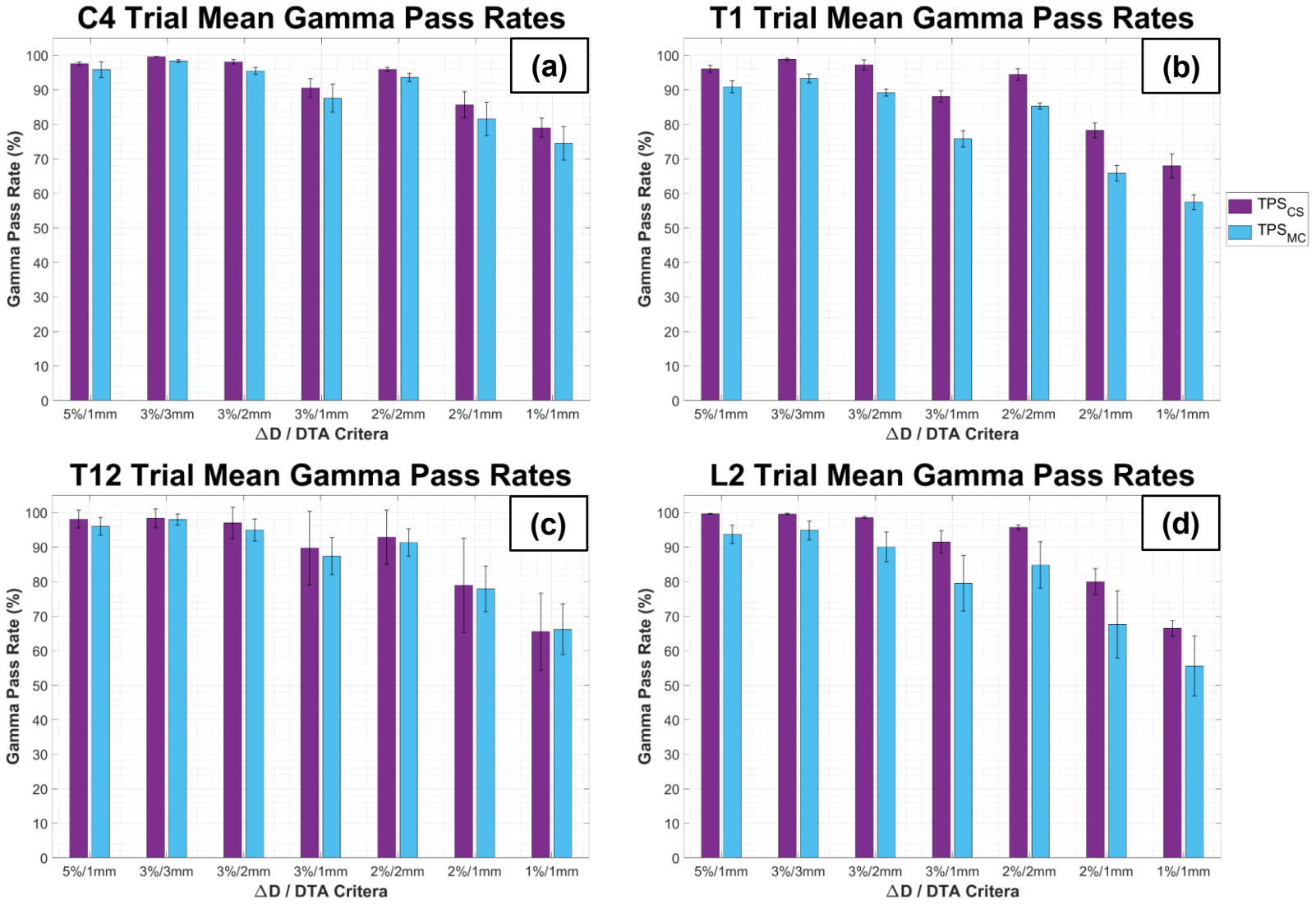

Figure 3.9. Trial average GPR at each treatment site for each TPS at multiple ΔD/DTA criteria: (a) C4, (b) T1, (c) T12, (d) L2, (e) L4, and (f) mean across all sites. The error bars extend plus and minus one sample σ of the mean.

(figure cont'd.)

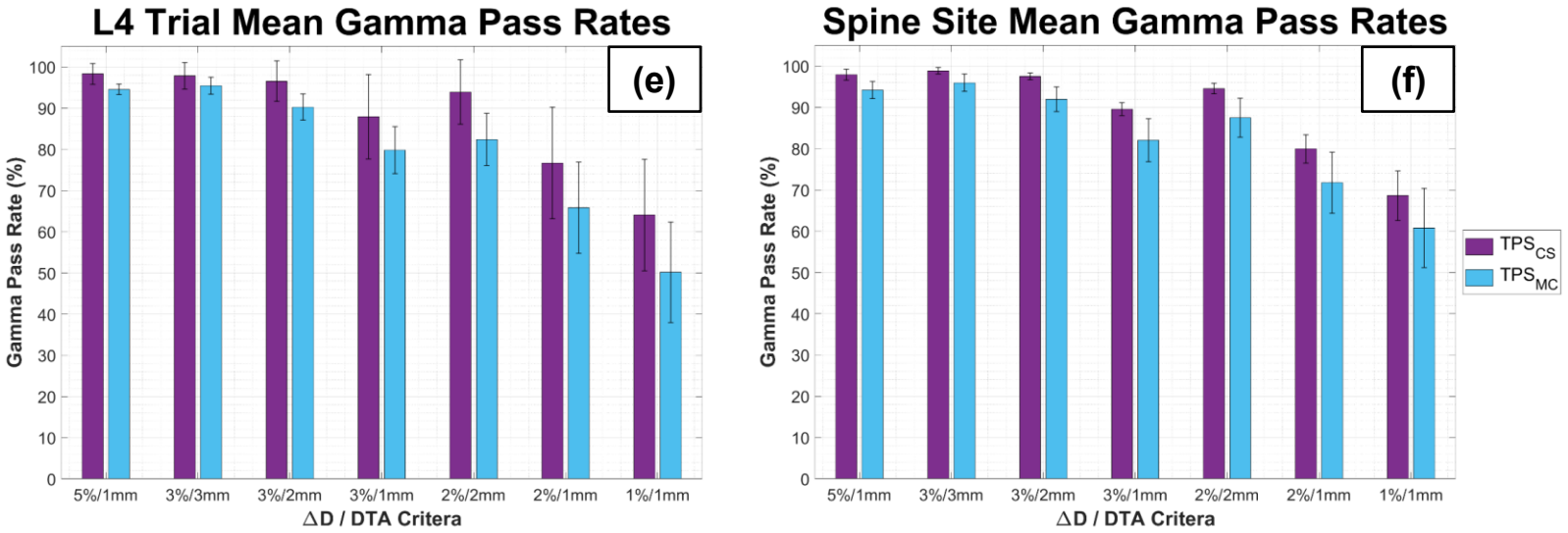
L4 Trial Mean Gamma Pass Rates
(e)
Gamma Pass Rate (%)
100
90
80
70
60
50
40
30
20
10
0
5%/1mm
3%/3mm
3%/2mm
3%/1mm
2%/2mm
2%/1mm
1%/1mm
ΔD / DTA Critera
Spine Site Mean Gamma Pass Rates
(f)
Gamma Pass Rate (%)
5%/1mm
3%/3mm
3%/2mm
3%/1mm
2%/2mm
2%/1mm
1%/1mm
ΔD / DTA Critera
TPS$_{CS}$
TPS$_{MC}$

Table 3.14. GPR ± σ at multiple ΔD/DTA criteria for the TPS_{CS} plans and Shapiro-Wilk test p-values.

ΔD/DTA Criteria	C4 (%)	T1 (%)	T12 (%)	L2 (%)	L4 (%)	Mean GPR ± σ across sites (%)	Shapiro-Wilk p-value
5%/1mm	97.57 ± 0.52	96.03 ± 1.03	98.13 ± 2.64	99.65 ± 0.13	98.33 ± 2.52	97.94 ± 1.31	0.889
3%/3mm	99.62 ± 0.05	98.80 ± 0.39	98.33 ± 2.76	99.61 ± 0.19	97.82 ± 3.22	98.84 ± 0.79	0.439
3%/2mm	98.13 ± 0.62	97.23 ± 1.45	97.03 ± 4.56	98.61 ± 0.30	96.56 ± 4.93	97.51 ± 0.84	0.699
3%/1mm	90.53 ± 2.68	88.10 ± 1.67	89.74 ± 10.70	91.49 ± 3.28	87.89 ± 10.27	89.55 ± 1.55	0.548
2%/2mm	95.95 ± 0.56	94.41 ± 1.70	92.87 ± 7.89	95.72 ± 0.71	93.90 ± 7.81	94.57 ± 1.29	0.651
2%/1mm	85.68 ± 3.78	78.24 ± 2.12	78.99 ± 13.63	80.01 ± 3.73	76.70 ± 13.53	79.93 ± 3.44	0.250
1%/1mm	79.00 ± 2.76	67.96 ± 3.52	65.52 ± 11.14	66.50 ± 2.22	64.08 ± 13.53	68.61 ± 5.98	0.047

Table 3.15. GPR ± σ at multiple ΔD/DTA criteria for the TPS_{MC} plans and Shapiro-Wilk test p-values.

ΔD/DTA Criteria	C4 (%)	T1 (%)	T12 (%)	L2 (%)	L4 (%)	Mean GPR ± σ across sites (%)	Shapiro-Wilk p-value
5%/1mm	95.87 ± 2.29	90.90 ± 1.74	96.03 ± 2.56	93.71 ± 2.62	94.57 ± 1.28	94.22 ± 2.09	0.347
3%/3mm	98.32 ± 0.43	93.30 ± 1.27	98.00 ± 1.57	94.83 ± 2.76	95.44 ± 2.05	95.98 ± 2.14	0.509
3%/2mm	95.48 ± 1.00	89.16 ± 1.03	94.98 ± 3.17	90.09 ± 4.31	90.25 ± 3.19	91.99 ± 2.99	0.097
3%/1mm	87.60 ± 4.04	75.82 ± 2.35	87.43 ± 5.39	79.55 ± 8.00	79.83 ± 5.72	82.04 ± 5.24	0.239
2%/2mm	93.60 ± 1.20	85.26 ± 0.91	91.35 ± 3.94	84.86 ± 6.69	82.39 ± 6.34	87.49 ± 4.74	0.422
2%/1mm	81.56 ± 4.84	65.84 ± 2.29	77.89 ± 6.63	67.61 ± 9.72	65.80 ± 11.07	71.74 ± 7.44	0.096
1%/1mm	74.51 ± 4.88	57.45 ± 2.18	66.17 ± 7.34	55.55 ± 8.70	50.15 ± 12.22	60.77 ± 9.61	0.760

Table 3.16. Mean GPR ± σ across the treatment sites at multiple ΔD/DTA criteria for TPS_{CS} and TPS_{MC}.

ΔD/DTA Criteria	TPS_{CS} Mean GPR ± σ across sites (%)	TPS_{MC} Mean GPR ± σ across sites (%)	Levene p-value	T-test p-value
5%/1mm	97.94 ± 1.31	94.22 ± 2.09	0.371	0.010
3%/3mm	98.84 ± 0.79	95.98 ± 2.14	0.031	0.038
3%/2mm	97.51 ± 0.84	91.99 ± 2.99	0.001	0.012
3%/1mm	89.55 ± 1.55	82.04 ± 5.24	0.008	0.030
2%/2mm	94.57 ± 1.29	87.49 ± 4.74	0.005	0.027
2%/1mm	79.93 ± 3.44	71.74 ± 7.44	0.018	0.070
1%/1mm	68.61 ± 5.98	60.77 ± 9.61	0.210	0.160

3.5. Uncertainty

Three main sources of measurement uncertainty were independently documented: The inherent profile shift, the registration standard deviation, and the imaging-radiation isocenter coincidence.

The inherent profile shift for the film was determined by planning a simple 6 MV 4-field box plan in TPS_{CS} with the flattening filter included (4 beams: Anterior-Posterior, Posterior-Anterior, Right-Left, and Left-Right). This plan was dubbed 'RegTestFF.' Following the same film dosimetry procedure as the spine plans, AP and LAT profiles were obtained through the center of dose distribution (Figure B.42 through Figure B.44). The TPS_{CS} profile compared with three trials of film profiles for this plan yielded an average -0.1 ± 0.3 mm AP profile shift at the 1250 cGy dose point (negative signifying an anterior shift). If this shift is accounted for in each site's average profile shift, that is, add +0.1 mm to each, the TPS_{CS} and TPS_{MC} mean profile shifts across all sites become +0.0 mm and +0.1 mm, respectively. These values remain smaller than the dose plane resolution, suggesting high accuracy between the planned and measured film profiles.

The RegTestFF film AP and LAT dose profiles also exhibited an average of 61.74 cGy underestimation (-3.9% relative to Rx) compared to the TPS_{CS} profiles. This dose difference was not specifically seen in the spine plans' film measurements, however. Most film dose profiles were higher inside the PTV compared to their TPS profile.

The registration standard deviation between the TPS dose plane and each film scan was outputted by the film analysis software, shown in Table 3.17 below. The software's technical manual recommends the standard deviation be less than the inverse of the 'Reference' image's resolution (1 mm in this case).[32] For each treatment site, all standard deviations met this requirement. The T1 site's standard deviation was the highest, which may explain its high mean profile shift (Table 3.12). Regardless, the registration for all trials appeared very accurate.

Table 3.17. Registration standard deviation for each film measurement trial (A, B, and C) and the trial average for each site.

Treatment Site	Trial	TPS_{CS} Registration Standard Deviation (mm)	TPS_{MC} Registration Standard Deviation (mm)
C4	A	0.143	0.166
	B	0.141	0.136
	C	0.154	0.117
	AVG	0.146	0.140
T1	A	0.873	0.894
	B	0.843	0.874
	C	0.877	0.841
	AVG	0.864	0.870
T12	A	0.278	0.292
	B	0.346	0.313
	C	0.292	0.308
	AVG	0.305	0.304

(table cont'd.)

Treatment Site	Trial	TPS_{CS} Registration Standard Deviation (mm)	TPS_{MC} Registration Standard Deviation (mm)
L2	A	0.158	0.173
	B	0.194	0.148
	C	0.163	0.163
	AVG	0.172	0.161
L4	A	0.189	0.199
	B	0.198	0.242
	C	0.169	0.194
	AVG	0.185	0.212
RegTestFF (4-field Box Plan)	A	0.147	-
	B	0.209	-
	C	0.216	-
	AVG	0.191	-

The imaging-radiation isocenter coincidence was determined by examining the linac's daily Winston-Lutz planar images of a cubic phantom (MIMI, REF 91240, Standard Imaging, Inc., Middleton, Wisconsin) taken as part of the linac's daily QA procedure. The selected images were acquired on the same day of each spinal treatment delivery (or previous day for Saturday measurements). The center of a BB in the imaged QA phantom (imaging isocenter) and the center of the MLC window (radiation isocenter) were estimated, then the distance between them was measured. The distances measured between the isocenters were averaged across the spine treatment days, yielding the values in Table 3.18 below. The SI and AP distances were measured on the Left-Right planar images to avoid the extra offset caused by the gantry's forward sag. The lateral (LAT) distances were measured with the AP planar image. If the AP isocenter coincidence is accounted for in each treatment site's average profile shift, that is, add +0.2 mm to each, the TPS_{CS} and TPS_{MC} mean profile shifts across all sites become +0.1 mm and +0.2 mm, respectively. Again, these values remain below the dose plane's resolution, implying highly accurate measurements within the linac's tolerance. Note that these shifts in Table 3.18 are limited to a 0.25 mm image resolution.

Table 3.18. Imaging isocenter shifts relative to the radiation isocenter for each day of film measurement. Positive values indicate a shift in the superior, anterior, or left direction. Negative values indicate a shift in the inferior, posterior, or right direction.

Treatment (Site-TPS_{Trial})	Date	SI Shift (mm)	AP Shift (mm)	LAT Shift (mm)
C4-$CS_{A,B}$	09/02/2021	0.00	0.00	0.00
T1-$CS_{A,B,C}$	09/13/2021	0.00	+0.25	-0.25
C4-CS_{C}, T1-$MC_{A,B,C}$	09/21/2021	-1.25	+0.25	-0.75
C4-$MC_{A,B,C}$, T12-$CS_{A,B,C}$	10/16/2021	+0.25	+0.25	0.00
T12-$MC_{A,B,C}$	10/19/2021	0.00	+0.50	-0.25
L2-$CS_{A,B,C}$	10/26/2021	0.00	+0.50	0.00
L2-$MC_{A,B,C}$	10/27/2021	+0.25	+0.25	-0.25
L4-$CS_{A,B,C}$, L4-$MC_{A,B,C}$	10/30/2021	0.00	-0.25	0.00
RegTestFF (4-Field Box Plan)	12/11/2021	-0.50	0.00	+1.00
	Mean Shift	-0.1 ± 0.5	+0.2 ± 0.2	-0.1 ± 0.5

Chapter 4. Discussion and Conclusion

4.1. Validation Plan Summary

In the TG-119 validation plans, TPS_{MC} was, on average, slightly more accurate than TPS_{CS}, in terms of point dose measurements and average GPR. It is possible that a thinner slice thickness would have produced more accurate low dose measurements in the Multitarget plan since they involved SI shifts of the water slabs. The Cshape plan experienced many 'Terminated Fault' linac errors during treatment delivery (for both TPSs), which stopped the treatment and usually required readjustment of the gantry angle before continuing. These interruptions occasionally occurred during the C4 and T12 spine plan deliveries as well. The high degree of plan modulation may be the cause of this and could explain why the Cshape plan had the highest dose differences compared to the other validation plans.

With these thoughts in mind and considering the very high GPR for the validation plans, the newly commissioned 6 MV FFF beam model in TPS_{MC} appeared to be accurate enough for research purposes. It should also be noted that the task group report's institutional results were based on plans that used seven or nine IMRT fields with the flattening filter in place, rather than FFF VMAT fields.

4.2. Spine Film Profiles and GPR Summary

In the critical region between the PTV and cord/cauda, both planning systems, on average, calculated the dose gradient with no significant difference in accuracy in terms of dose falloff and profile shift. The dose points in this region tended to pass the gamma analyses very well, but usually failed when the DTA reached 1 mm, (excluding 5%/1mm criteria). These specific results do not support the hypothesis of this work. The higher GPRs from the TPS_{CS} spine plans compared to those from TPS_{MC}, were surprising, given the fact that MC-based dose calculation algorithms are generally considered more accurate than CS-based.[3, 11, 38]

The TPS_{MC} spine plans used many more MU, and thus were more modulated than the TPS_{CS} spine plans (Table 3.1). The lower GPRs seen on the film measurements of the TPS_{MC} spine plans suggest that the resulting high modulation pushed the linac to its mechanical limits.[39] At some instances during the TPS_{MC} plan deliveries, all except for one row of MLCs were blocked by the linac jaws. The following settings specific to TPS_{MC} may have contributed to the lower GPR: the minimum segment width, maximum leaf travel per gantry rotation, and maximum number of control points.

The minimum segment width in TPS_{MC} was set to 0.5 cm, as recommended by one of the vendor training manuals.[24] The corresponding setting in TPS_{CS}, minimum dynamic leaf gap, was 1 cm. Wang et al. found that re-planning in TPS_{MC} with a minimum segment width of either 1.0 or 1.5 cm resulted in an increased GPR and a decreased total number of MU generated per plan compared with a 0.5 cm minimum segment width.[40] A study by Saenz et al. comparing plans calculated and optimized in the TPSs used in this work also found that TPS_{MC} generated more MU than TPS_{CS}.[15] Saenz et al. also used a 0.5 cm minimum segment width in TPS_{MC}. Conversely, a study by Lee et al. found that TPS_{CS} generated more MU than TPS_{MC},[14] but minimum segment width used was not disclosed. Both these studies used higher prescriptions doses, though (20 Gy in one fraction and 24 Gy in 2 fractions, respectively), and neither one confirmed their plans with ion chamber or film measurements.

Limiting the MLC movement speed (in mm per degree of gantry rotation) has been shown by Yang et al. to increase GPR while reducing the number of MU in TPS_{CS}.[41] The leaves were limited to 4.6 mm per degree in our TPS_{CS} spine plans, but in TPS_{MC}, this setting was left blank by default.

The VMAT control point spacing (degrees) is determined in TPS_{MC} automatically during segmentation, increasing the number of control points at gantry angles where high modulation is required and decreasing the number at angles where less modulation is needed.[24] The result is varied control point spacing at each segment in TPS_{MC}. This cannot be manually changed, as opposed to TPS_{CS}, where the control point spacing is a single user-entered value. Reducing the maximum number of control points allowed in TPS_{MC}, however, may slightly reduce the total MU delivered as it does for TPS_{CS}, decreasing plan modulation.[41] Determining the effect of plan modulation on plan deliverability by examining relationships between these three TPS_{MC} settings and the resulting measurements may be pursued in a future study.

One possible explanation for the lower GPR inside the PTVs of TPS_{MC} specifically is the auto-filling of the hollow ring contours when importing the structures from TPS_{CS}. While the shrink margin feature in TPS_{MC} was used to create optimization goals for each plan, the imported ring structures were used to measure the volume outside the CTV that the 105% dose hotspots occupied. If this volume exceeded 2 cc, the plan was optimized further to reduce the hotspot volume, following RTOG 0631.[21] Mistakenly, the filled portions of the ring structures were not noticed and corrected until after all film measurements and analyses were completed. This meant that the hotspot volume measurements included portions of the PTV volumes. RTOG 0631 does not prohibit dose inhomogeneity or hotspots inside the target,[21] so relying on the incorrect ring structure volumes possibly caused TPS_{MC} to limit the hotspots more than necessary. This could be why the internal PTV of the vertebral sites in TPS_{MC} had colder dose distributions than TPS_{CS}. The push for colder doses combined with the TPS settings described previously may have contributed to the higher plan modulation and lower GPR inside the PTVs. However, this would only explain the decreased GPR in the T12, L2, and L4 sites, as the C4 and T1 sites' ring contours were only filled near the superior and inferior edges of the targets.

A study by Haga et al. involved planning treatments at a variety of anatomical sites in TPS_{CS}, then transferring the optimized VMAT segments to TPS_{MC}. TPS-calculated point doses were then compared with ion chamber measurements in a water phantom and cork phantom.[13] Directly importing the control points enables detection of dose differences between each TPS independent of the differences between optimization methods and TPS-specific settings. Performing anthropomorphic phantom film measurements of plans in each TPS with identical beam data as Haga did is another potential avenue of future study.

4.3. Limitations

Although both TPS_{CS} and TPS_{MC} used identical CT images and structure sets, the TPS-calculated volumes of the structures slightly differed between the two. The contours for the spine plans were created in TPS_{CS} in 'Poly' mode, which displays the contours at the edge of the CT voxels. When the structures were imported to TPS_{MC}, the structures were shifted to the center of the CT voxels, which created 1 mm gaps between some contours in TPS_{MC} where they previously were adjacent in TPS_{CS}. This caused the structures in TPS_{MC} to have slightly smaller defined volumes compared to those in TPS_{CS}, though it is difficult to determine whether this would produce a significant dosimetric effect in the planning results.

Another difference between TPS_{CS} and TPS_{MC} is how the CT number to density tables are defined. In TPS_{CS}, it is defined in terms of physical density vs. Hounsfield units + 1000, but in TPS_{MC}, it is defined in terms of electron density relative to water (RED) vs. Hounsfield units. TPS_{MC} converts the RED values to physical density using analytical equations.[25] However, the vendor recommends that, for non-human media such as tissue equivalent material, the RED values be adjusted in order to produce a physical density that matches its actual value instead of solely relying on the conversion equations. This was not performed when commissioning TPS_{MC}. A test spine SBRT plan was calculated on a previously treated patient in TPS_{MC} using both a CT number to density table with nominal RED values and one with adjusted RED values. The highest observed mean dose difference between the two tables relative to 1600 cGy was 1.1% at the vertebra's posterior edge (data not shown). This is smaller than the systematic dose underestimation of the film observed in the RegTestFF plan (see the Uncertainty subsection in Results), so compared to the settings discussed previously, it is not likely a crucial source of dose differences between each TPS.

When analyzing the film measurements, some sources of uncertainty were not considered. The calibration films were arranged in three rows while scanned (Figure 2.6), with the central row approximately aligned with the scanner's central axis (parallel to the scan direction). It is possible that the calibration films in the outer rows experienced some lateral response artifact, in which the measured PV decreases laterally (perpendicular from the scan direction) from the scanner central axis.[29, 42–45] The film analysis software used in this project does not currently offer a method to correct for this artifact. If it were corrected on the scanned image of the calibration films, the measured PV of the lateral calibration film patches would increase slightly, ultimately increasing the dose of the whole calibration curve. In the film measurements of the spine plans, however, this artifact was not visibly seen. This is likely because of the relatively small lateral size of the vertebral treatment targets. The largest vertebral site was L4, about 5.2 cm across. The lateral response artifact also would have no effect on the AP dose profiles since each film's AP axis was aligned perpendicular to the scan direction and approximately centered near the scanner axis. This artifact is currently being characterized for our institution's scanner for Gafchromic EBT3 film as part of another graduate student's project.

The film analysis software was also limited to reading either the PV of one color channel or simply measuring the mean of all three channels. Some studies suggest a number of triple-channel dosimetry methods that can improve film measurement accuracy.[46, 47] Such methods are currently not available in the software used, and time-constraints prevented the hand-coding of it.

4.4. Conclusion

The end-to-end accuracy of single-fraction spine SBRT plans at several vertebral sites in a CS-based TPS and MC-based TPS were evaluated with radiochromic film measurements. On average, each TPS calculated the dose profiles between the vertebral bodies and spinal cord within 1 mm accuracy. Gamma analyses in this specific region showed good agreement with the calculated doses for all ΔD/DTA criteria tested, except for 3%/1mm, 2%/1mm, and 1%/1mm sometimes. The lower GPR throughout other areas in the TPS_{MC} sites, specifically at 2%/2mm criteria, may be improved by placing appropriate optimization limits that reflect the capabilities of the linac used in the treatments. Specific settings identified in this work were minimum segment width, maximum leaf travel per gantry rotation, and maximum number of control points.

Appendix A. Spine Treatment Planning Methodology

The overall inverse planning philosophy in each TPS was to attempt to meet the PTV dose coverage while limiting OAR dose and reducing dose hotspots outside of the CTV to the limits specified in ROTG 0631.[21]

All DICOM structures (CTVs, PTV, OARs, etc.) in the phantom were contoured in TPS_{CS}. After contouring the CTV and PTV structures of each site (named [Site]_CTV and [Site]_2mm_PTV in the TPS, respectively), two ring structures were created. Each ring was a 1 cm expansion the CTV and PTV, named [Site]_Ring1_1cm_PTV and [Site]_Ring1_1cm_CTV, respectively. The rings were expanded in all directions, but settings were specified to avoid the spinal cord structure (named [Site]_PartCord0.25mm_contract) and cauda equina structure (Figure A.1). Either one ring or both rings were used as an objective during inverse optimization for each site to control the maximum dose around each vertebral body. TPS_{CS} has a Scorecard feature that quickly calculates doses to individual structures and compares them with user-entered dosimetric criteria. Both rings were included in the Scorecard in order to evaluate the dose hotspot volume up to 1 cm outside the CTV as well as the maximum dose outside the CTV and PTV.

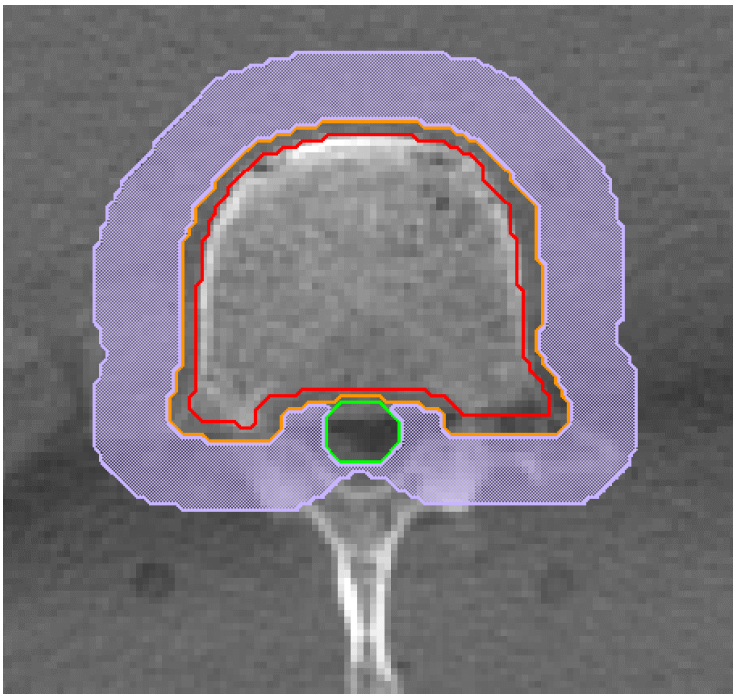

Figure A.1. The L4 site in TPS_{CS} with L4_CTV contoured in red, L4_2mm_PTV in orange, Cauda Equina in green, and L4_Ring1_1cm_PTV shaded in purple.

In addition, structures named [Site]_Cold_Post were made to cover some site's pedicles and portions of the internal posterior CTV to improve target coverage. Irregularly-shaped structures named [Site]_Limit Back were placed a few centimeters posterior to the cord / cauda to decrease circumferential dose around them. Both the Cold_Post and Limit Back contours were occasionally edited throughout the optimization in attempts to shift some isodose lines.

The inverse planning objectives were revised and adjusted as needed throughout the planning process. The last used criteria for the plans in TPS_{CS} are shown in Table A.1 through

Table A.5. The objective value for each row gives a measure of how close the dose goal was to being met. A lower value implies that the dose goal was met and signals the optimization algorithm to focus on meeting other goals. The weight parameter may be manually adjusted on some objectives to increase the objective value, which in turn increases the optimization algorithm's focus on that goal. The composite objective value is the sum of all objective values.

Table A.1. Final IMRT optimization objectives for the C4 plan in TPS_{CS}.

Structure	Type	Target Dose (cGy)	Volume (%)	Weight	Objective Value
C4_2mm_PTV	Max Dose	1720	97	5	7.44088e-05
	Min DVH	1680	-	5	0.00122388
	Min Dose	1520	-	5	0.000204882
C4_Cold_Post	Min Dose	1480	-	1	0
C4_Limit Back	Max DVH	500	20	1	0
C4_PartCord0.25mm_contract	Max DVH	940	9	4	0.000109722
	Max Dose	1340	-	2	4.44104e-06
C4_Ring1_1cm_PTV	Max Dose	1480	-	3	0.00165311
Skin	Max Dose	2300	-	1	0
Trachea & Larynx	Max DVH	1050	24	1	0
	Max Dose	2020	-	1	0
				Composite Objective Value	0.00327045

Table A.2. Final IMRT optimization objectives for the T1 plan in TPS_{CS}.

Structure	Type	Target Dose (cGy)	Volume (%)	Weight	Objective Value
BrachPlex close	Max DVH	1400	50	1	0
	Max Dose	1750	-	1	0
Esophagus	Max DVH	1190	20	1	0
	Max Dose	1460	-	1	6.85621e-06
Lung_Tot	Max DVH	740	20	1	0
Skin	Max Dose	2300	-	1	0
T1_2mm_PTV	Max Dose	1720	-	6	0.000128042
	Min DVH	1680	97	8	0.00345028
	Min Dose	1520	-	8	0.000936043
T1_Cold_Post	Min Dose	1480	-	5	0.000960953
T1_Limit Back	Max DVH	950	10	1	0.000195212
T1_PartCord0.25mm_contract	Max DVH	920	9	8	0.00018757
	Max Dose	1250	-	8	3.88076e-05
T1_Ring1_1cm_CTV	Max Dose	1650	-	5	0.000103189
T1_Ring1_1cm_PTV	Max Dose	1480	-	5	0.0010349
				Composite Objective Value	0.00704185

Table A.3. Final IMRT optimization objectives for the T12 plan in TPS_{CS}.

Structure	Type	Target Dose (cGy)	Volume (%)	Weight	Objective Value
Duodenum	Max DVH	1120	7	1	0
	Max Dose	1600	-	1	0
Lung_Tot	Max DVH	740	21	1	0
Renal Cortex L & R	Max Dose	840	-	1	3.34729e-11
Renal Hilum L & R	Max DVH	1060	66	1	0
Skin	Max Dose	2300	-	1	0
Stomach	Max DVH	1120	15	1	0
	Max Dose	1600	-	1	0
T12_2mm_PTV	Max Dose	1740	-	5	3.20092e-06
	Min DVH	1680	97	5	0.00171851
	Min Dose	1540	-	5	0.000985871
T12_Cold Post	Min Dose	1520	-	1	0.000418885
T12_Limit Back	Max DVH	900	10	1	0
T12_PartCord0.25mm_contract	Max DVH	960	9	8	0.00018884
	Max Dose	1300	-	8	2.48648e-07
T12_Ring1_1cm_CTV	Max Dose	1650	-	1	1.96845e-05
T12_Ring1_1cm_PTV	Max Dose	1480	-	1	0.00043729
				Composite Objective Value	0.00377253

Table A.4. Final IMRT optimization objectives for the L2 plan in TPS_{CS}.

Structure	Type	Target Dose (cGy)	Volume (%)	Weight	Objective Value
Cauda Equina	Max DVH	1000	7	1	4.54262e-05
	Max Dose	1300	-	1	0.000137597
Duodenum	Max DVH	1120	7	1	0
	Max Dose	1600	-	1	0
L2_Cold Post	Min Dose	1520	-	4	3.38985e-05
L2_Limit Back	Max DVH	900	10	1	0
L2_PartCord0.25mm_contract	Max DVH	960	9	1	2.38277e-05
	Max Dose	1400	-	1	0
L2_Ring1_1cm_CTV	Max Dose	1440	-	1	0.00343336
L2_2mm_PTV	Max Dose	1760	-	5	1.20001e-06
	Min DVH	1680	97	5	0.00173833
	Min Dose	1540	-	5	0.00020188
	Min DVH	1600	90	4	0
Renal Cortex L & R	Max Dose	840	-	1	0
Renal Hilum L & R	Max DVH	1060	66	1	0
Stomach	Max DVH	1120	10	1	0
	Max Dose	1600	-	1	0
				Composite Objective Value	0.00561551

Table A.5. Final IMRT optimization objectives for the L4 plan in TPS_{CS}.

Structure	Type	Target Dose (cGy)	Volume (%)	Weight	Objective Value
Cauda Equina	Max DVH	1350	20	1	0
	Max Dose	1500	-	1	1.06784e-05
Duodenum	Max DVH	1120	7	1	0
	Max Dose	1600	-	1	0
L4_Cold Post	Min Dose	1560	-	2	7.96038e-07
L4_Limit Back	Max DVH	900	10	1	0
L4_Ring1_1cm_PTV	Max Dose	1440	-	1	0.000391367
L4_2mm_PTV	Max Dose	1760	-	5	0
	Min DVH	1680	98	5	0.00168039
	Min Dose	1560	-	5	8.1144e-05
Renal Cortex L & R	Max Dose	840	-	1	0
Renal Hilum L & R	Max DVH	1060	66	1	0
				Composite Objective Value	0.00216437

When all the contoured structures were imported from TPS_{CS} to TPS_{MC}, the system automatically filled the hollow areas of ring-shaped contours, i.e., donut shaped contours became filled circles. This increased the volume of the Ring contours. Similar to the Scorecard feature in TPS_{CS}, TPS_{MC} displays user-customizable dosimetric criteria. This dosimetric criteria was checked during the plan optimization to confirm adequate target coverage, OAR sparing, and dose hotspot limits 1 cm outside of the CTV. However, because the Ring structures included the interior of the vertebral body in some slices, the hotspot volumes were overestimated. The plans in TPS_{MC} were mistakenly chosen to be optimized further, unnecessarily decreasing overall dose inside the target. The filled Ring structures were noticed months after the plan delivery and data analysis. They were corrected by manually trimming the Rings from the PTV and CTV and allowing a thin hollow channel to extend from the inner to outer border of each Ring, as shown in Figure A.2. These corrections allowed the true values for the hotspot volumes outside of the CTV and the maximum point doses outside of the CTV and PTV to be recorded in Table 3.1.

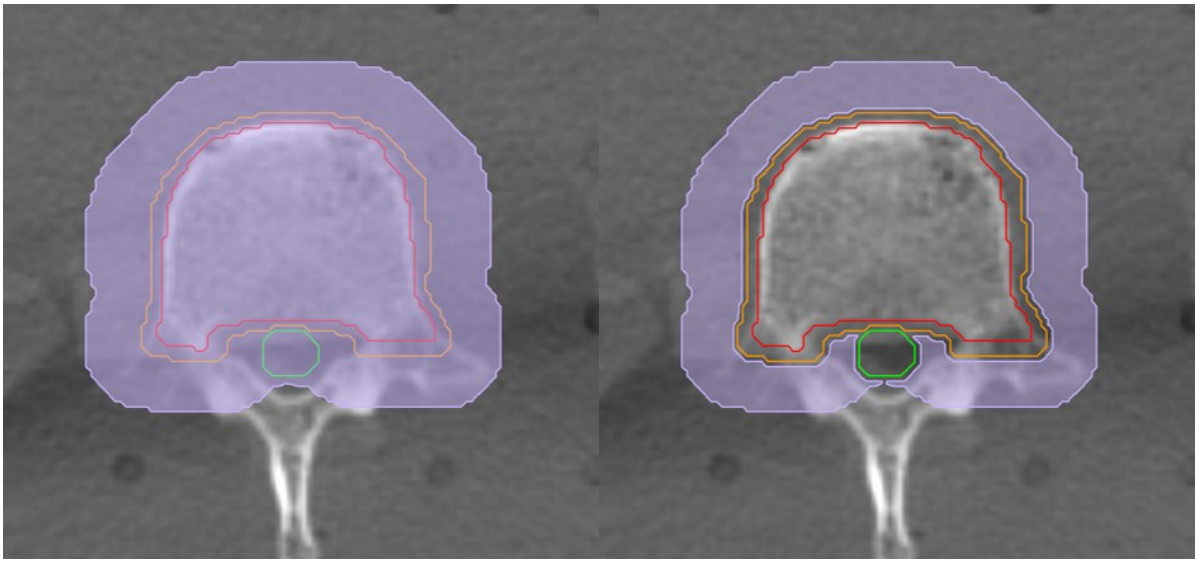

Figure A.2. L4_Ring1_1cm_PTV shaded in purple in TPS_{MC} upon direct import from TPS_{CS} (Left). L4_Ring1_1cm_PTV in TPS_{MC} after manually correcting the contour (Right). Note the small opening directly posterior to the green cauda equina structure which prevents the ring from being filled.

As in $TPS_{CS,}$ the optimization criteria in the TPS_{MC} plans were adjusted throughout the inverse planning process. 'Constrained' optimization was used as opposed to 'Pareto' to prioritize OAR dose constraints over target coverage. The last used criteria for each TPS_{MC} plan are displayed in Table A.6 through Table A.10. The 'cost functions' are analogous to the dose goals in Table A.1 through Table A.5, but the significance of the reference dose and 'isoconstraint' values depends on the cost function used.

'Target Penalty' is analogous to 'Minimum DVH,' with the isoconstraint representing the minimum dose desired for a user-specified minimum volume (%) of coverage (shown in the table caption). 'Quadratic Overdose' is similar to a 'Max Dose' constraint, with its reference dose representing the maximum dose, and the isoconstraint representing the root mean square dose excess, a user-entered dose value that allows the structure to exceed the reference dose by a small amount. 'Overdose DVH' acts similarly to 'Max DVH,' with its reference dose representing the objective dose and the isoconstraint representing the maximum volume (%) of the structure the dose will occupy. 'Maximum Dose' is a hard physical dose limit, and its isoconstraint is simply the maximum allowed dose in the structure. 'Conformality' pushes high dose areas to the target area, increasing conformity as its isoconstraint is lowered.[24]

The weights in TPS_{MC} were automatically adjusted by the system, as opposed to the weights in TPS_{CS}, which were manually adjusted. The shrink margin feature in TPS_{MC} essentially mimics the Ring structures from TPS_{CS}. For example, in Table A.6, there are three shrink margins for the structure 'External ROI with Rods.' This structure contains the entire phantom contour and the frame rods. Without the shrink margins, the optimizer would attempt to meet the dose goal (1680.0 cGy) in every location inside the phantom except for the interior of the PTV. With the shrink margins enabled as shown, the optimizer attempted to limit the dose to 1680.0 cGy immediately outside of the PTV, 1520.0 cGy 2 mm away from the PTV, and 1440.0 cGy 4 mm away from the PTV and beyond.

Table A.6. Final IMRT optimization objectives for the C4 plan in TPS_{MC}. The target penalty minimum volume for C4_2mm_PTV is 96%.

Structure	Cost Function	Weight	Reference Dose (cGy)	Shrink Margin (cm)	Isoconstraint
BrachPlex close	Overdose DVH	0.01	1400.0	-	30.00
C4_2mm_PTV	Target Penalty	1.00	-	-	1640.0
	Quadratic Overdose	0.01	1740.0	-	40.0
	Maximum Dose	2.23	-	-	1800.0
C4_PartCord0.25cm_contract	Maximum Dose	0.03	-	0.00	1380.0
	Overdose DVH	7.65	1000.0	0.00	9.50
External ROI with Rods	Conformality	0.02	-	-	0.63
	Quadratic Overdose	0.01	1680.0	0.00	40.0
	Quadratic Overdose	0.01	1520.0	0.20	40.0
	Quadratic Overdose	0.01	1440.0	0.40	40.0

Table A.7. Final IMRT optimization objectives for the T1 plan in TPS_{MC}. The target penalty minimum volume for T1_2mm_PTV is 96%.

Structure	Cost Function	Weight	Reference Dose (cGy)	Shrink Margin (cm)	Isoconstraint
Esophagus	Maximum Dose	0.16	-	-	1580.0
	Overdose DVH	0.01	1190.0	-	15.00
BrachPlex close	Overdose DVH	1.33	1400.0	-	40.00
T1_2mm_PTV	Target Penalty	1.00	-	-	1640.0
	Quadratic Overdose	0.01	1740.0	-	40.0
	Maximum Dose	2.42	-	-	1780.0
T1_PartCord0.25cm_contract	Maximum Dose	0.01	-	0.00	1380.0
	Overdose DVH	12.37	1000.0	0.00	9.50
External ROI with Rods	Conformality	0.01	-	-	0.63
	Quadratic Overdose	0.01	1680.0	0.00	40.0
	Quadratic Overdose	0.01	1520.0	0.20	40.0
	Quadratic Overdose	0.01	1440.0	0.40	40.0

Table A.8. Final IMRT optimization objectives for the T12 plan in TPS_{MC}. The target penalty minimum volume for T12_2mm_PTV is 96%.

Structure	Cost Function	Weight	Reference Dose (cGy)	Shrink Margin (cm)	Isoconstraint
T12_2mm_PTV	Target Penalty	1.00	-	-	1680.0
	Quadratic Overdose	0.01	1720.0	-	40.0
	Maximum Dose	1.28	-	-	1800.0
T12_PartCord0.25cm_contract	Maximum Dose	0.01	-	0.00	1380.0
	Overdose DVH	24.21	1000.0	0.00	9.00
External ROI with Rods	Conformality	0.01	-	-	0.60
	Quadratic Overdose	0.01	1660.0	0.00	40.0
	Quadratic Overdose	0.01	1500.0	0.20	40.0
	Quadratic Overdose	0.01	1420.0	0.40	40.0

Table A.9. Final IMRT optimization objectives for the L2 plan in TPS_{MC}. The target penalty minimum volume for L2_2mm_PTV is 95%.

Structure	Cost Function	Weight	Reference Dose (cGy)	Shrink Margin (cm)	Isoconstraint
L2_2mm_PTV	Target Penalty	1.00	-	-	1640.0
	Quadratic Overdose	0.01	1740.0	-	40.0
	Maximum Dose	0.62	-	-	1780.0
L2_PartCord0.25cm_contract	Maximum Dose	0.01	-	0.00	1380.0
	Overdose DVH	0.99	1000.0	0.00	9.50
Cauda Equina	Maximum Dose	0.28	-	0.00	1580.0
	Overdose DVH	0.01	1400.0	0.00	25.00
External ROI with Rods	Conformality	0.01	-	-	0.60
	Quadratic Overdose	0.01	1660.0	0.00	40.0
	Quadratic Overdose	0.01	1500.0	0.20	40.0
	Quadratic Overdose	0.01	1420.0	0.40	40.0

Table A.10. Final IMRT optimization objectives for the L4 plan in TPS_{MC}. The target penalty minimum volume for L4_2mm_PTV is 96%.

Structure	Cost Function	Weight	Reference Dose (cGy)	Shrink Margin (cm)	Isoconstraint
L4_2mm_PTV	Target Penalty	1.00	-	-	1660.0
	Quadratic Overdose	0.01	1720.0	-	40.0
	Maximum Dose	1.22	-	-	1780.0
SacrPlex close	Overdose DVH	0.06	1420.0	0.00	30.00
Cauda Equina	Maximum Dose	1.64	-	0.00	1570.0
	Overdose DVH	0.01	1440.0	0.00	20.00
External ROI with Rods	Conformality	0.01	-	-	0.60
	Quadratic Overdose	0.01	1660.0	0.00	40.0
	Quadratic Overdose	0.01	1500.0	0.20	40.0
	Quadratic Overdose	0.01	1420.0	0.40	40.0

Appendix B. Full Dose Profile Results

Table B.1 and Table B.2 display the AP dose falloffs of the TPS_{CS}-calculated profiles, each individual trial (A, B, and C) of film-measured AP profiles, and the differences and percent differences between the TPS and film. Table B.3 and Table B.4 display the same for the TPS_{MC}-calculated profiles. Table B.5 and Table B.6 display the AP profile shift between each TPS and film for each trial.

Figure B.1 through Figure B.40 display all planned dose distributions with the red AP profile marked followed by plots of the planned AP profile and the measured AP profile of each trial. For the cervical and thoracic profile, the shaded region represents the area between the posterior contour edge of the PTV and anterior contour edge of the spinal cord. For the lumbar profiles, the PTV contour edge and cauda equina contour edge were directly adjacent. Figure B.41 through Figure B.47 show the same for the three RegTestFF trials in TPS_{CS}, including planned and measured AP and LAT profiles.

Table B.1. AP dose falloff, dose falloff difference and percent dose falloff difference for each trial (A, B, and C), and average (AVG) value ± σ for the TPS_{CS} cervical and thoracic sites.

Treatment Site	C4				T1				T12			
Trial	A	B	C	AVG	A	B	C	AVG	A	B	C	AVG
TPS_{CS} Dose Falloff (mm)	8.9	8.9	8.9	8.9	8.6	8.6	8.6	8.6	7.2	7.2	7.2	7.2
Film Dose Falloff (mm)	9.2	8.3	8.4	8.6 ± 0.5	9.6	8.8	9.2	9.2 ± 0.4	6.4	7.9	6.6	7.0 ± 0.8
Difference (mm)	+0.3	-0.6	-0.5	-0.3 ± 0.5	+1.0	+0.2	+0.6	+0.6 ± 0.4	-0.8	+0.7	-0.6	-0.3 ± 0.8
Difference (%)	+3.6	-6.8	-5.6	-2.9 ± 5.7	+11.8	+2.4	+7.1	+7.1 ± 4.7	-10.9	+9.4	-9.0	-3.5 ± 11.2

Table B.2. AP dose falloff, dose falloff difference and percent dose falloff difference for each trial (A, B, and C), and average (AVG) value ± σ for the TPS_{CS} lumbar sites.

Treatment Site	L2				L4			
Trial	A	B	C	AVG	A	B	C	AVG
TPS_{CS} Dose Falloff (mm)	7.9	7.9	7.9	7.9	13.7	13.7	13.7	13.7
Film Dose Falloff (mm)	8.3	9.0	8.8	8.7 ± 0.4	13.3	13.1	11.6	12.7 ± 1.0
Difference (mm)	+0.4	+1.1	+1.0	+0.8 ± 0.4	-0.4	-0.6	-2.2	-1.1 ± 1.0
Difference (%)	+5.5	+14.3	+12.3	+10.7 ± 4.7	-3.1	-4.4	-15.9	-7.8 ± 7.1

Table B.3. AP dose falloff, dose falloff difference and percent dose falloff difference for each trial (A, B, and C), and average (AVG) value ± σ for the TPS_{MC} cervical and thoracic sites.

Treatment Site	C4				T1				T12			
Trial	A	B	C	AVG	A	B	C	AVG	A	B	C	AVG
TPS_{MC} Dose Falloff (mm)	8.2	8.2	8.2	8.2	9.8	9.8	9.8	9.8	9.2	9.2	9.2	9.2
Film Dose Falloff (mm)	7.9	7.6	8.0	7.8 ± 0.2	10.1	9.5	9.5	9.7 ± 0.3	9.0	8.3	8.8	8.7 ± 0.3
Difference (mm)	-0.3	-0.7	-0.3	-0.4 ± 0.2	+0.2	-0.3	-0.3	-0.1 ± 0.3	-0.2	-0.9	-0.4	-0.5 ± 0.3
Difference (%)	-3.6	-8.3	-3.3	-5.1 ± 2.8	+2.4	-2.8	-3.5	-1.3 ± 3.2	-2.4	-9.3	-3.9	-5.2 ± 3.6

Table B.4. AP dose falloff, dose falloff difference and percent dose falloff difference for each trial (A, B, and C), and average (AVG) value ± σ for the TPS_{MC} lumbar sites.

Treatment Site	L2				L4			
Trial	A	B	C	AVG	A	B	C	AVG
TPS_{MC} Dose Falloff (mm)	6.9	6.9	6.9	6.9	9.0	9.0	9.0	9.0
Film Dose Falloff (mm)	6.2	6.3	6.0	6.2 ± 0.1	6.4	8.2	7.8	7.5 ± 1.0
Difference (mm)	-0.8	-0.6	-0.9	-0.8 ± 0.1	-2.6	-0.7	-1.2	-1.5 ± 1.0
Difference (%)	-11.3	-9.0	-12.8	-11.0 ± 1.9	-28.7	-8.3	-13.0	-16.6 ± 10.7

Table B.5. AP profile shift for each trial (A, B, and C) and average (AVG) value ± σ for the cervical and thoracic sites.

Treatment Site	C4				T1				T12			
Trial	A	B	C	AVG	A	B	C	AVG	A	B	C	AVG
TPS_{CS} Profile shift (mm)	+0.2	+0.2	+0.1	+0.2 ± 0.1	-0.7	-0.6	-0.4	-0.6 ± 0.2	-0.3	-0.2	-0.2	-0.3 ± 0.1
TPS_{MC} Profile shift (mm)	-0.1	-0.4	-0.3	-0.3 ± 0.1	-0.9	-0.9	-0.9	-0.9 ± 0.0	+0.2	+0.4	+0.7	+0.4 ± 0.2

Table B.6. AP profile shift for each trial (A, B, and C) and average (AVG) value ± σ for the lumbar sites.

Treatment Site	L2				L4			
Trial	A	B	C	AVG	A	B	C	AVG
TPS_{CS} Profile shift (mm)	+0.0	-0.3	-0.4	-0.2 ± 0.2	+0.1	-0.1	+0.8	+0.3 ± 0.5
TPS_{MC} Profile shift (mm)	+0.1	+0.2	+0.2	+0.2 ± 0.1	+0.8	+1.1	+0.4	+0.7 ± 0.3

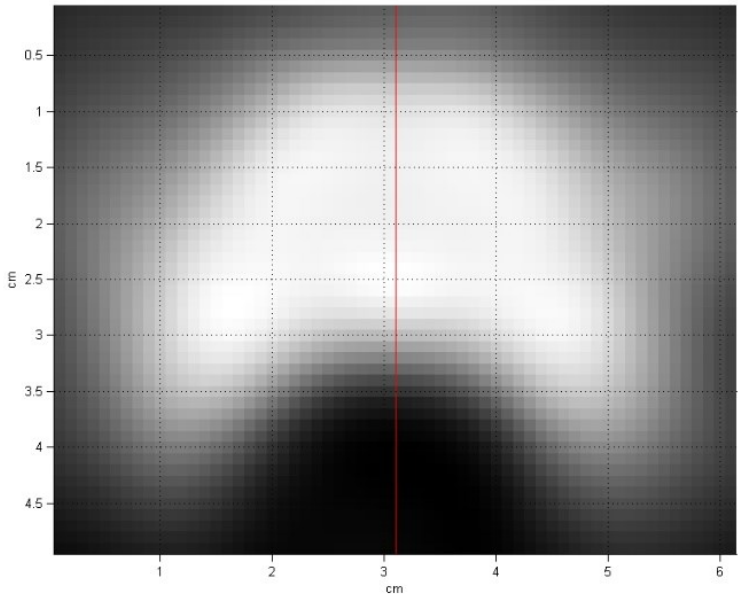

Figure B.1. AP dose profile over the TPS_{CS} C4 planned dose distribution.

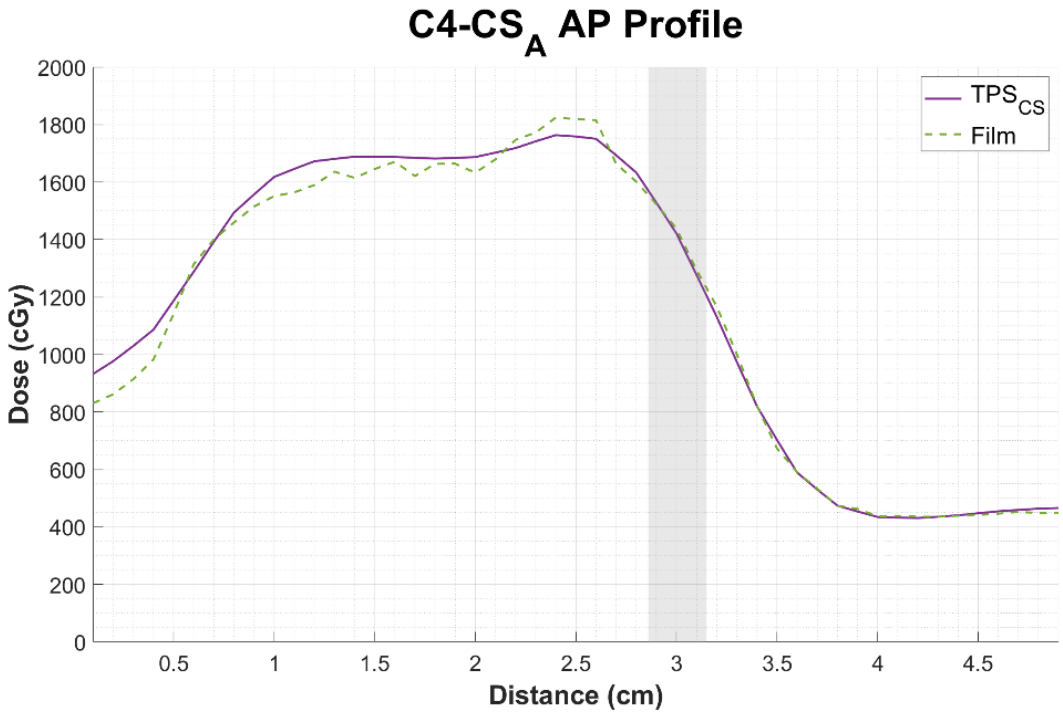

Figure B.2. Planned AP TPS_{CS} dose profile with its respective film-measured dose profile for the C4 site, trial A.

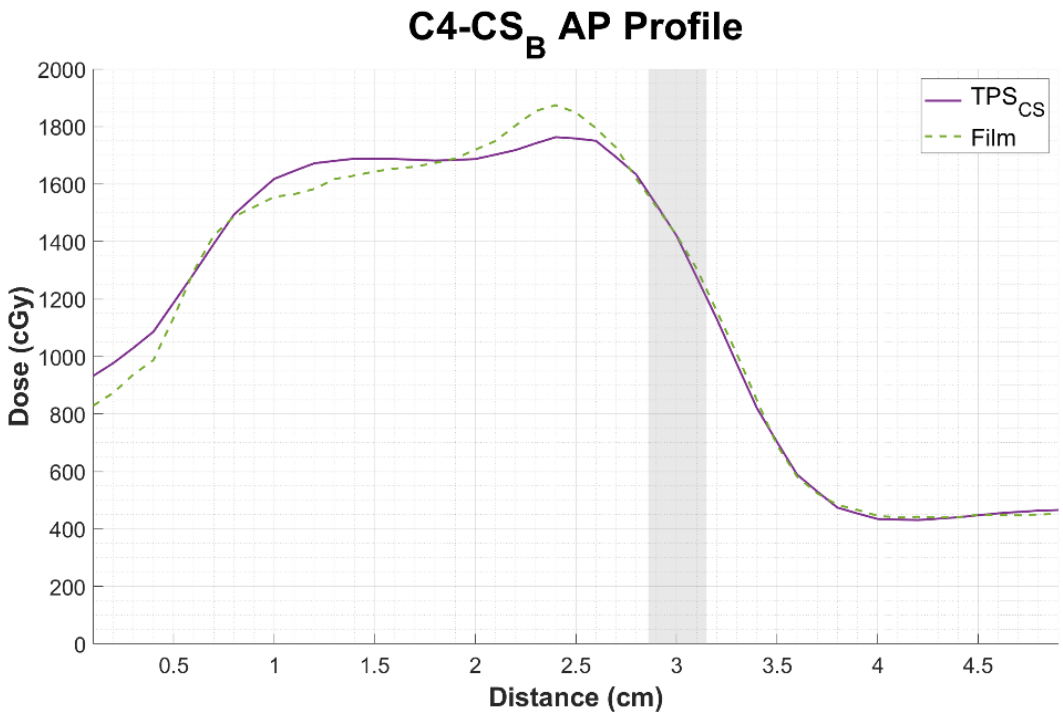

Figure B.3. Planned AP TPS_{CS} dose profile with its respective film-measured dose profile for the C4 site, trial B.

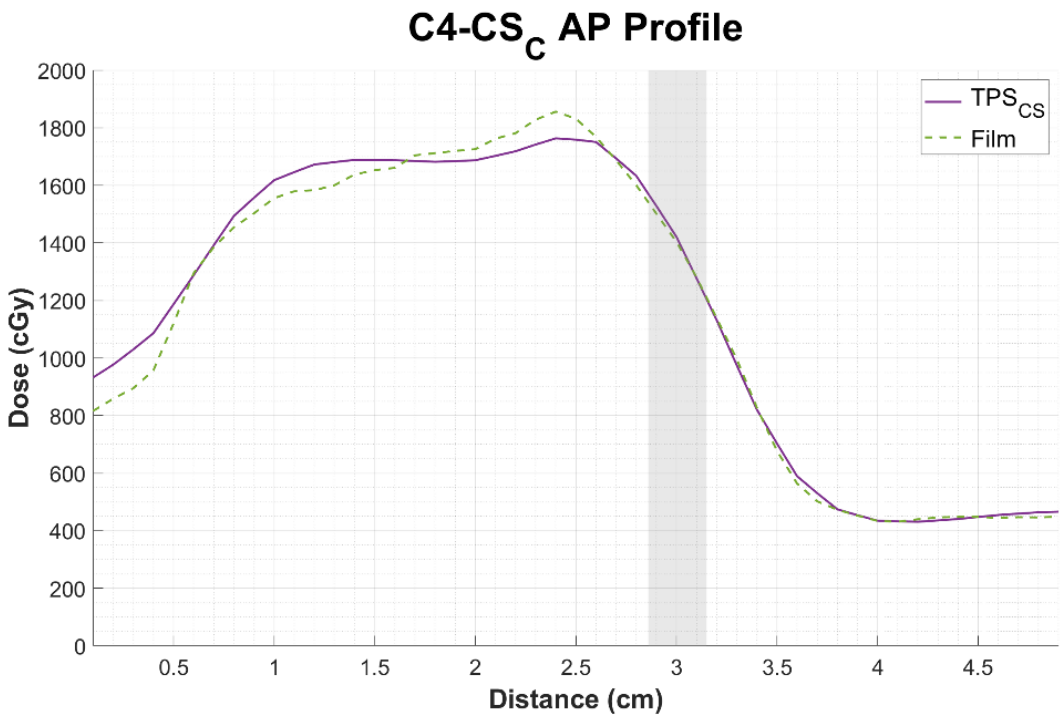

Figure B.4. Planned AP TPS_{CS} dose profile with its respective film-measured dose profile for the C4 site, trial C.

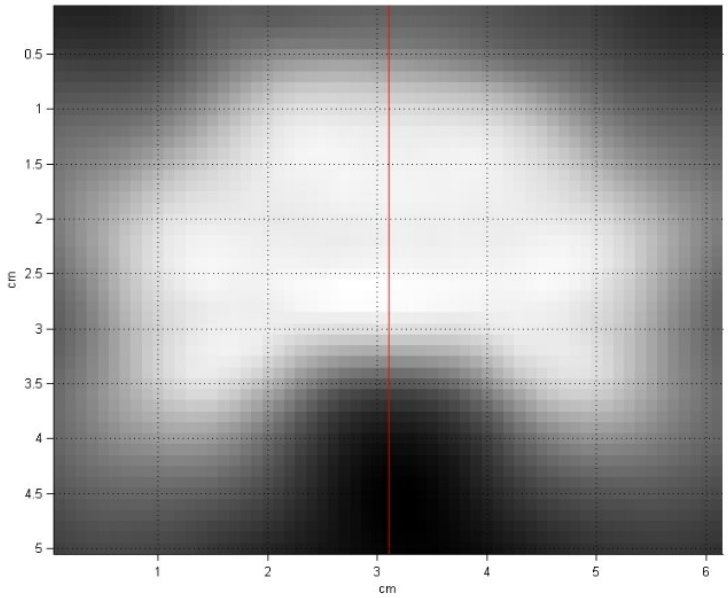

Figure B.5. AP dose profile over the TPS_{MC} C4 planned dose distribution.

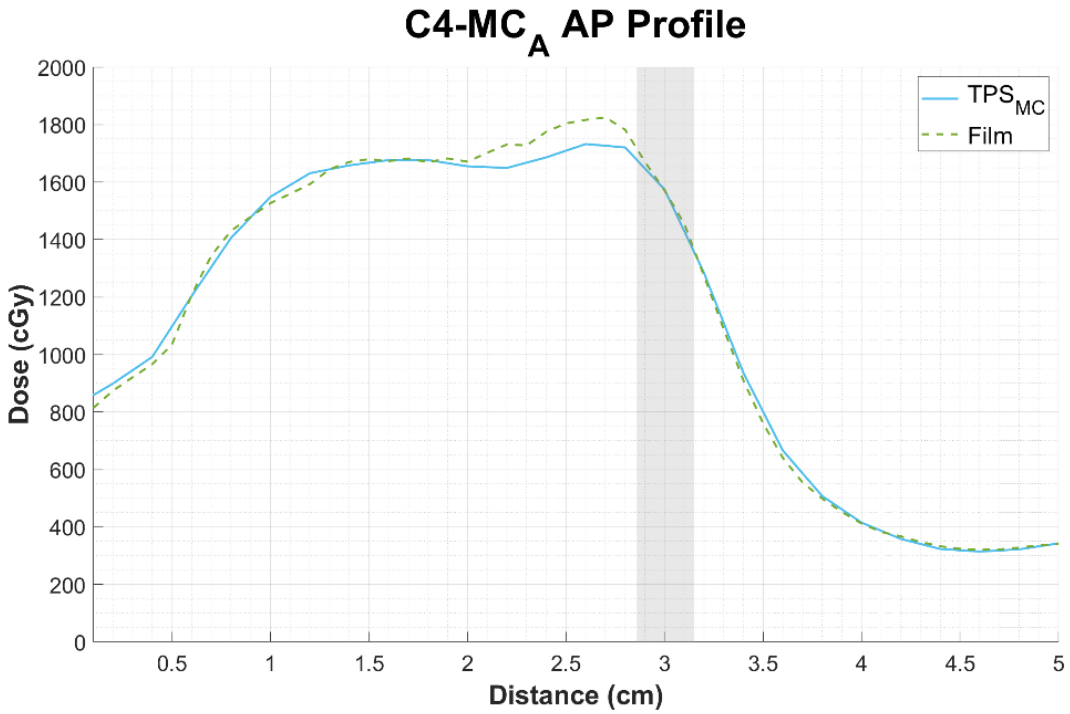

Figure B.6. Planned AP TPS_{MC} dose profile with its respective film-measured dose profile for the C4 site, trial A.

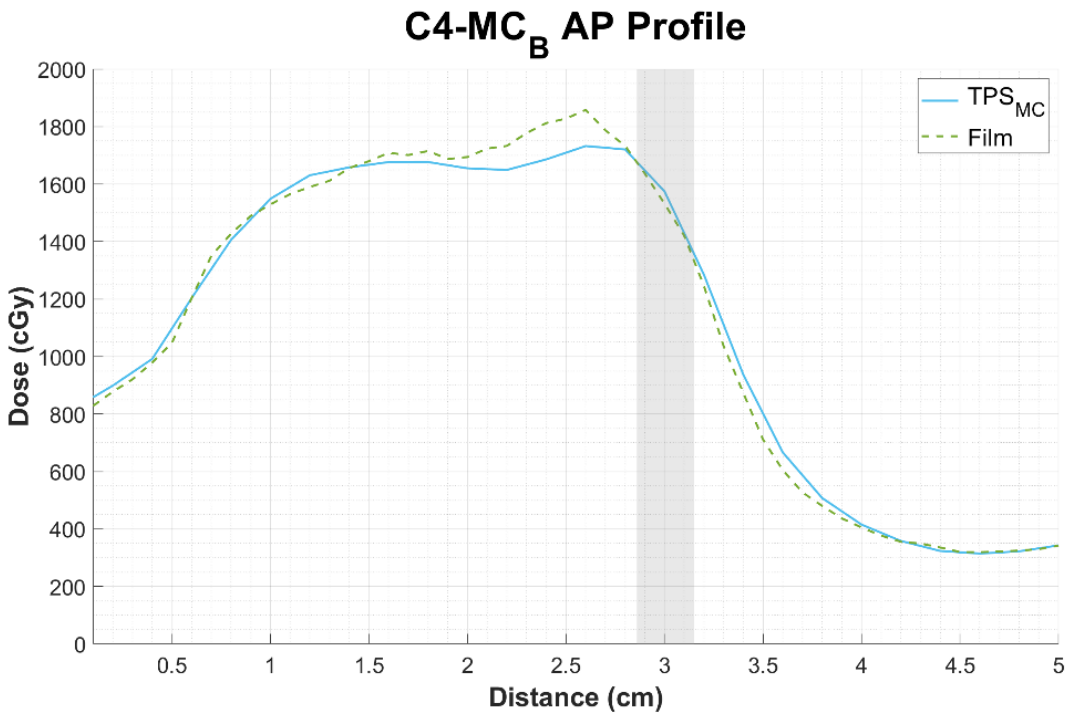

Figure B.7. Planned AP TPS_{MC} dose profile with its respective film-measured dose profile for the C4 site, trial B.

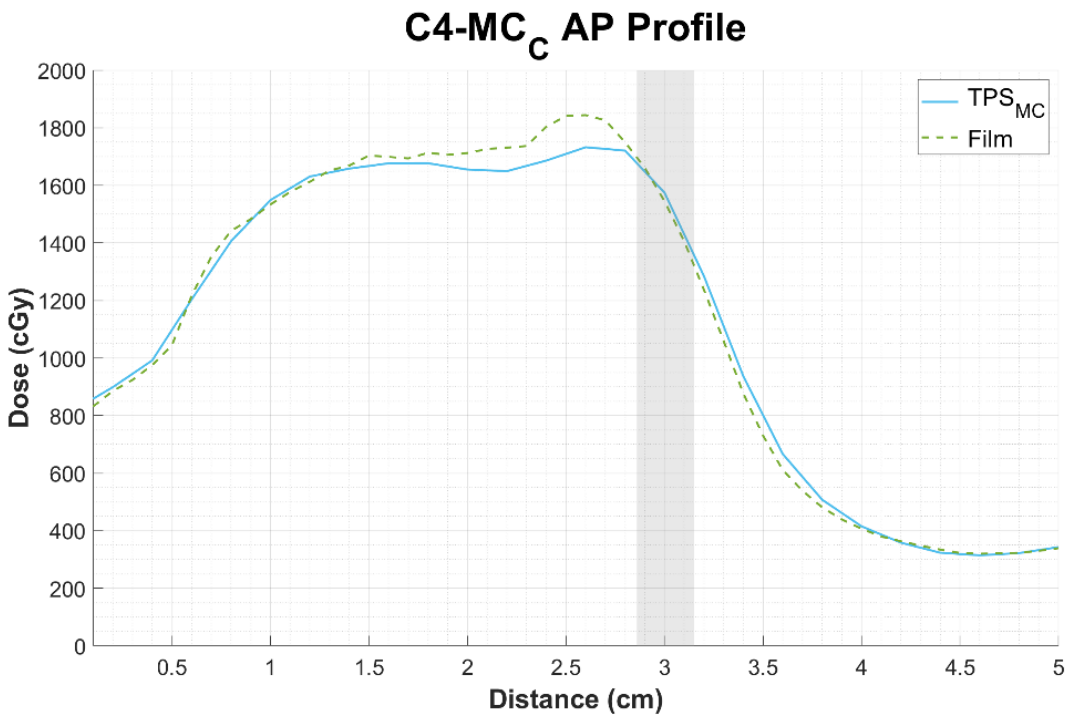

Figure B.8. Planned AP TPS_{MC} dose profile with its respective film-measured dose profile for the C4 site, trial C.

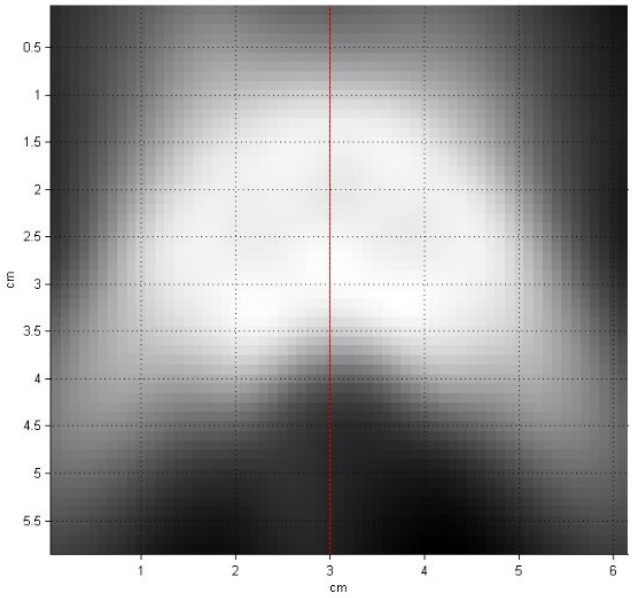

Figure B.9. AP dose profile over the TPS_{CS} T1 planned dose distribution.

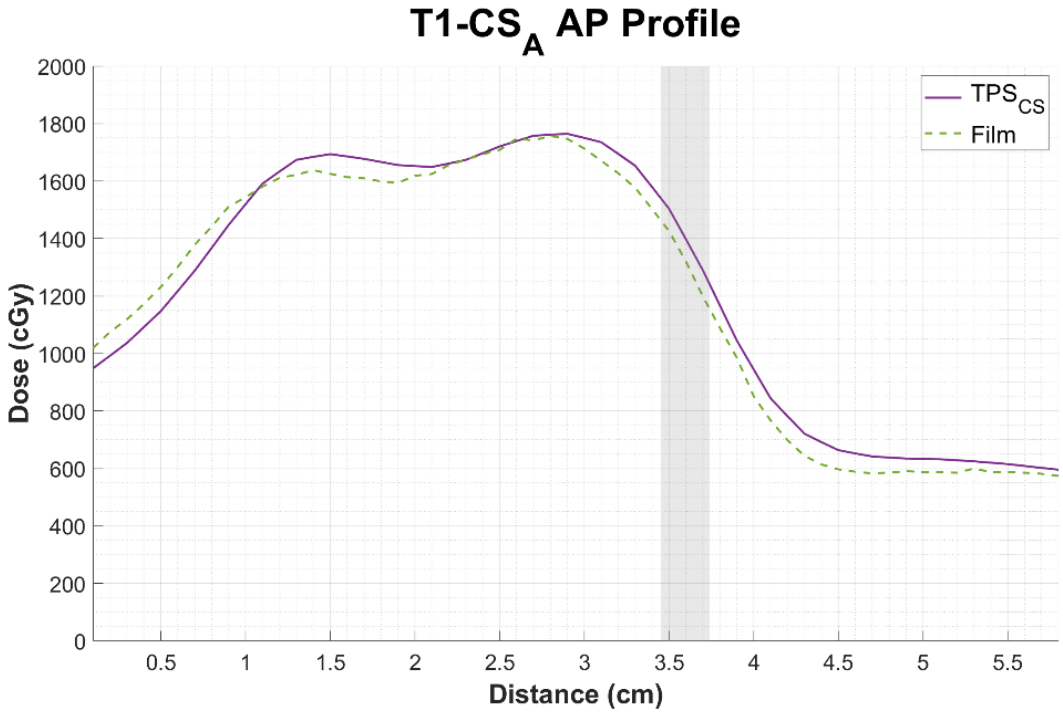

Figure B.10. Planned AP TPS_{CS} dose profile with its respective film-measured dose profile for the T1 site, trial A.

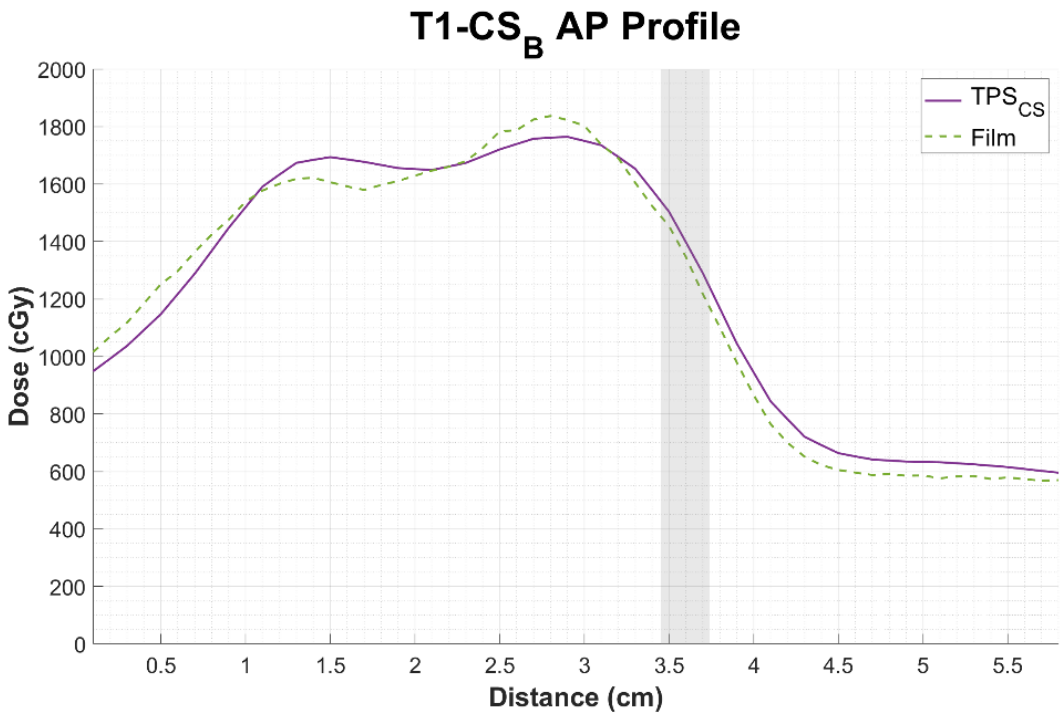

Figure B.11. Planned AP TPS_{CS} dose profile with its respective film-measured dose profile for the T1 site, trial B.

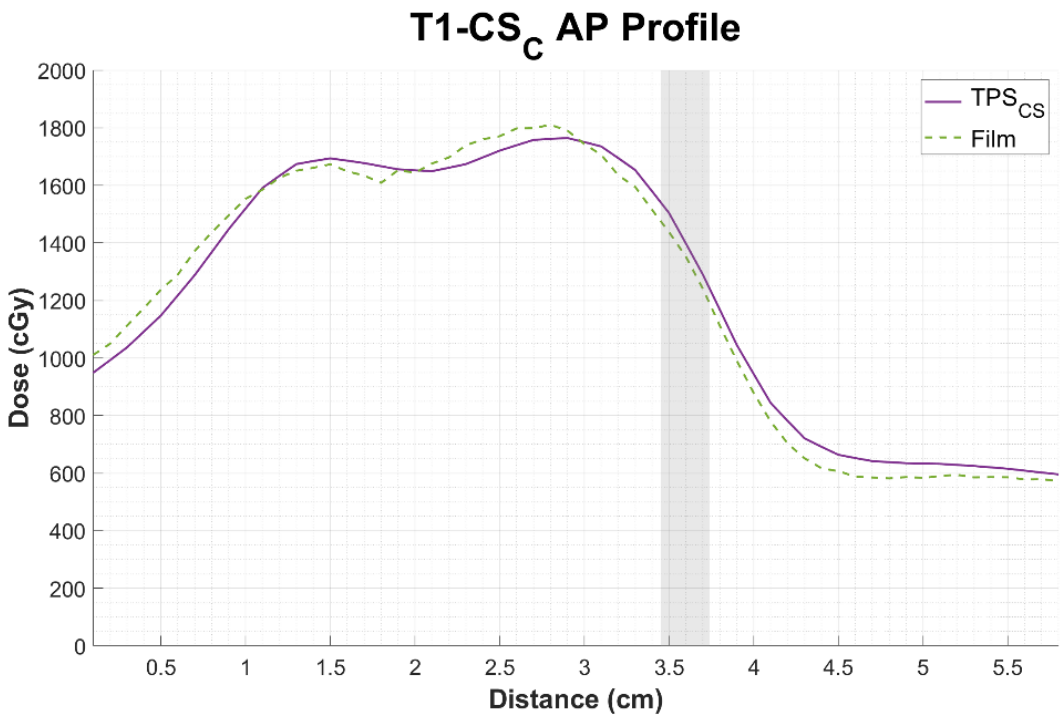

Figure B.12. Planned AP TPS_{CS} dose profile with its respective film-measured dose profile for the T1 site, trial C.

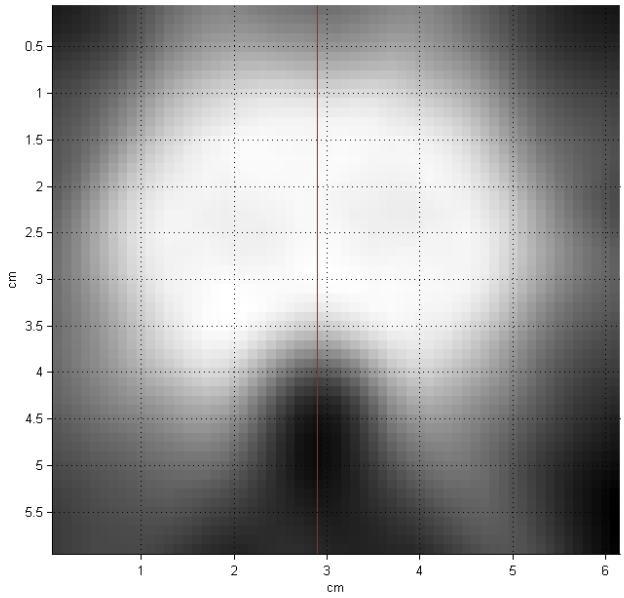

Figure B.13. AP dose profile over the TPS_{MC} T1 planned dose distribution.

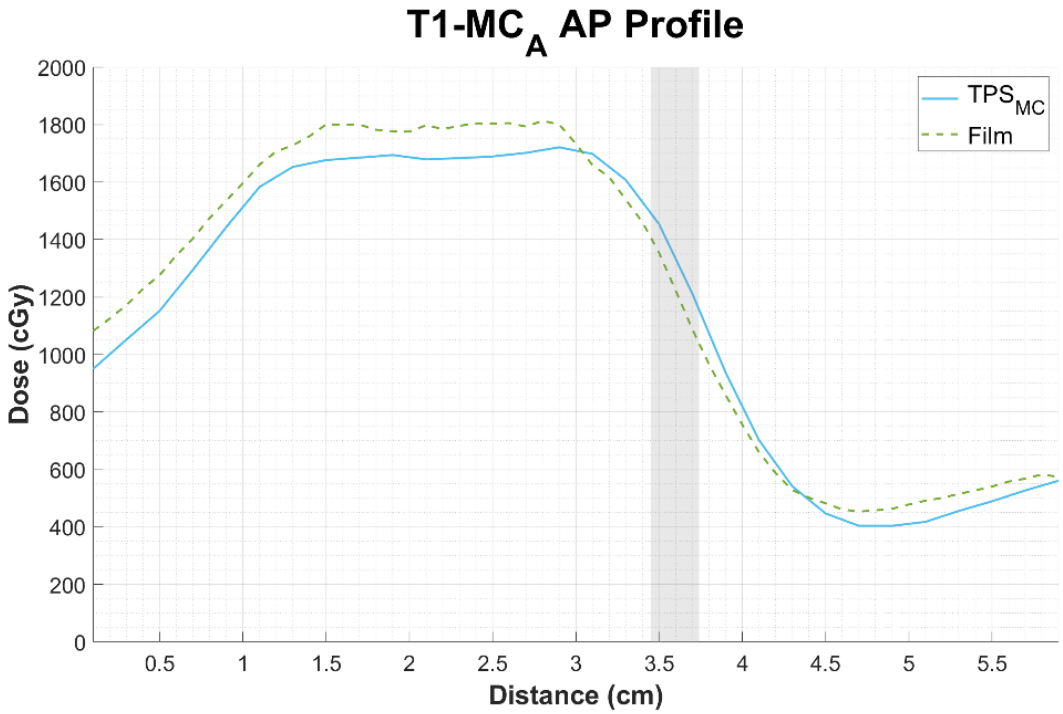

Figure B.14. Planned AP TPS_{MC} dose profile with its respective film-measured dose profile for the T1 site, trial A.

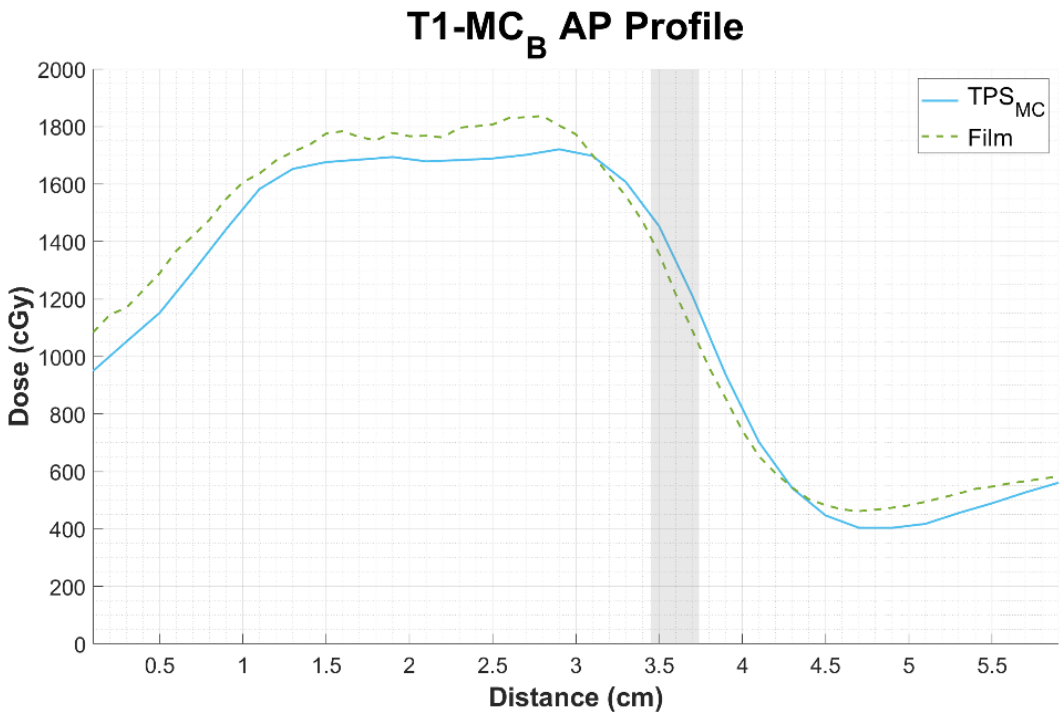

Figure B.15. Planned AP TPS_{MC} dose profile with its respective film-measured dose profile for the T1 site, trial B.

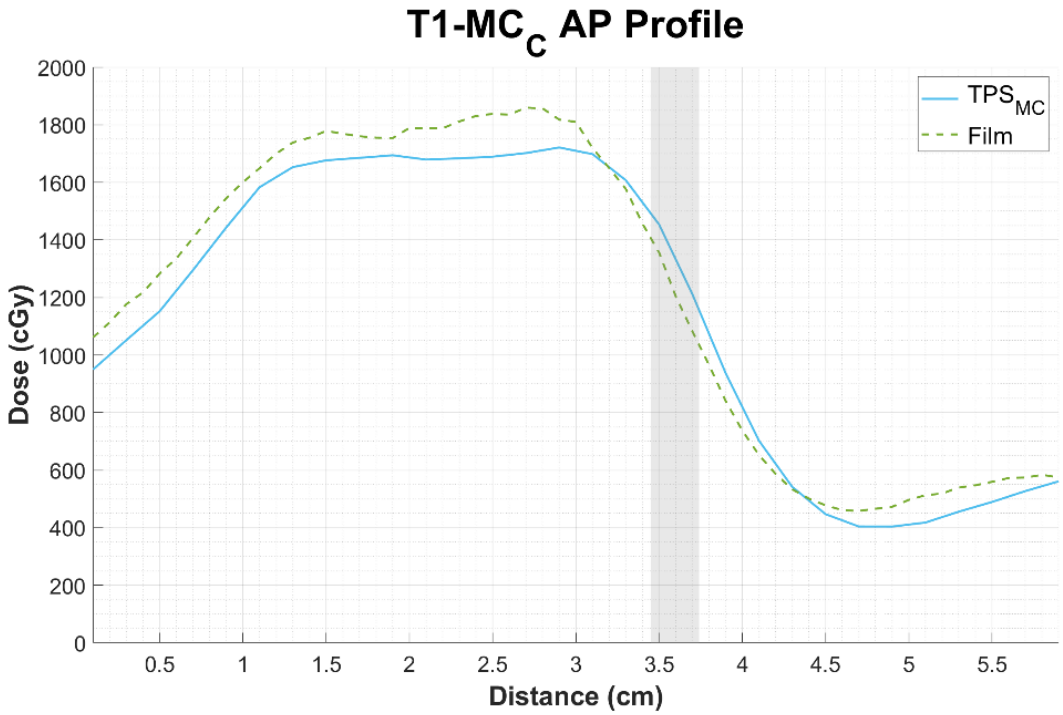

Figure B.16. Planned AP TPS_{MC} dose profile with its respective film-measured dose profile for the T1 site, trial C.

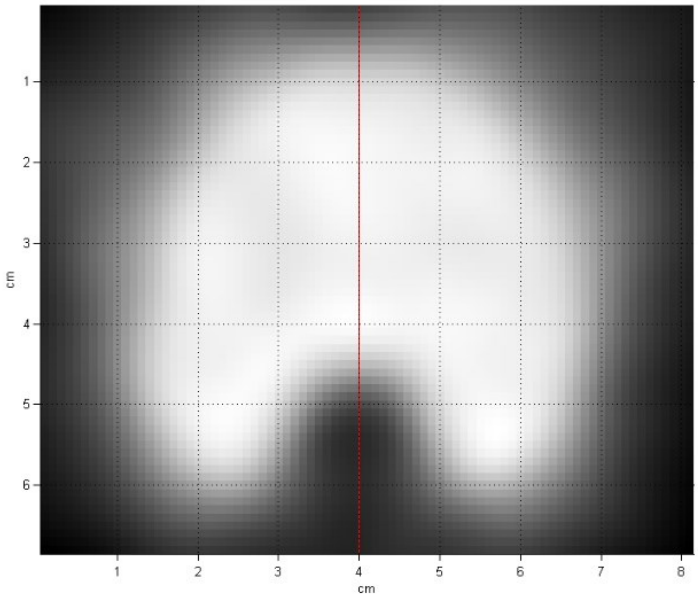

Figure B.17. AP dose profile over the TPS_{CS} T12 planned dose distribution.

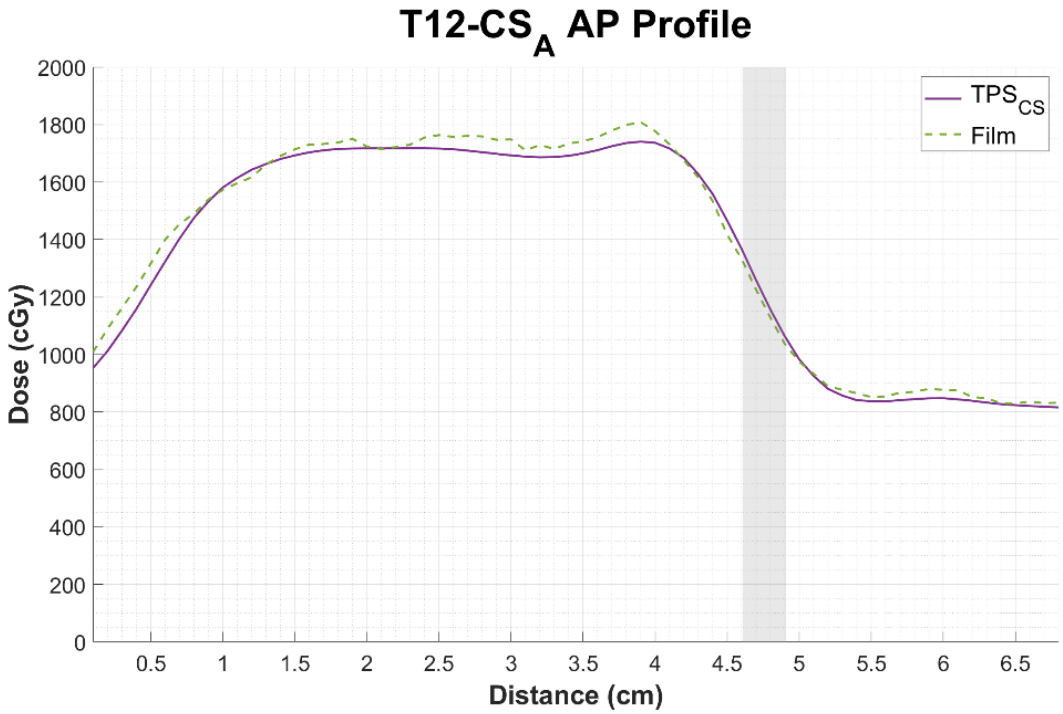

Figure B.18. Planned AP TPS_{CS} dose profile with its respective film-measured dose profile for the T12 site, trial A.

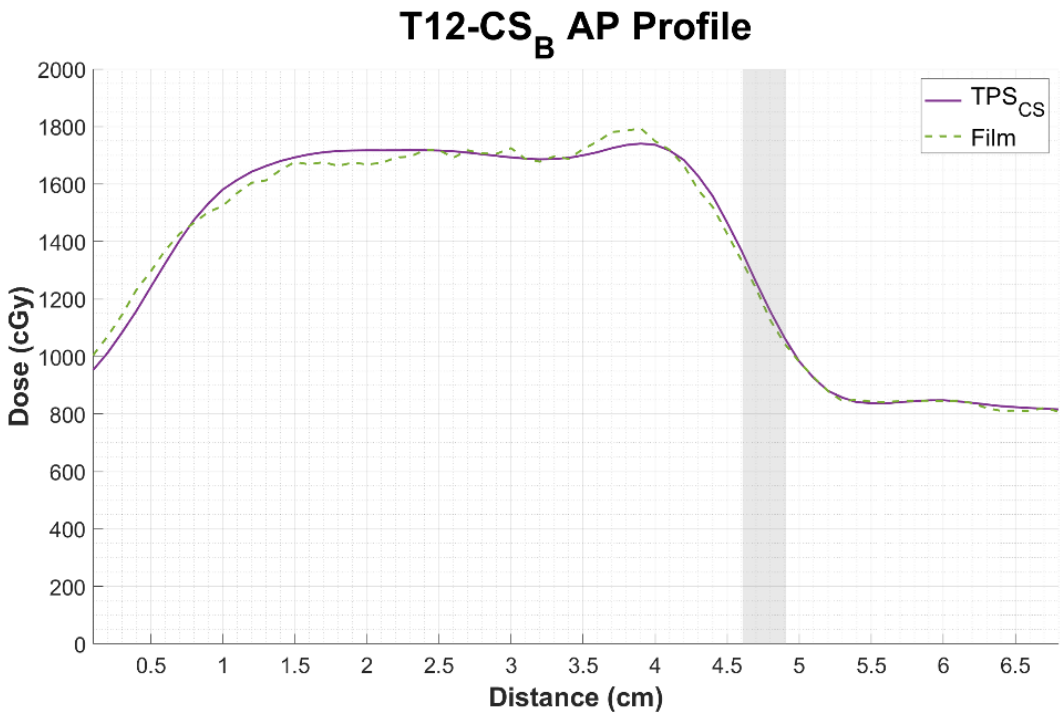

Figure B.19. Planned AP TPS_{CS} dose profile with its respective film-measured dose profile for the T12 site, trial B.

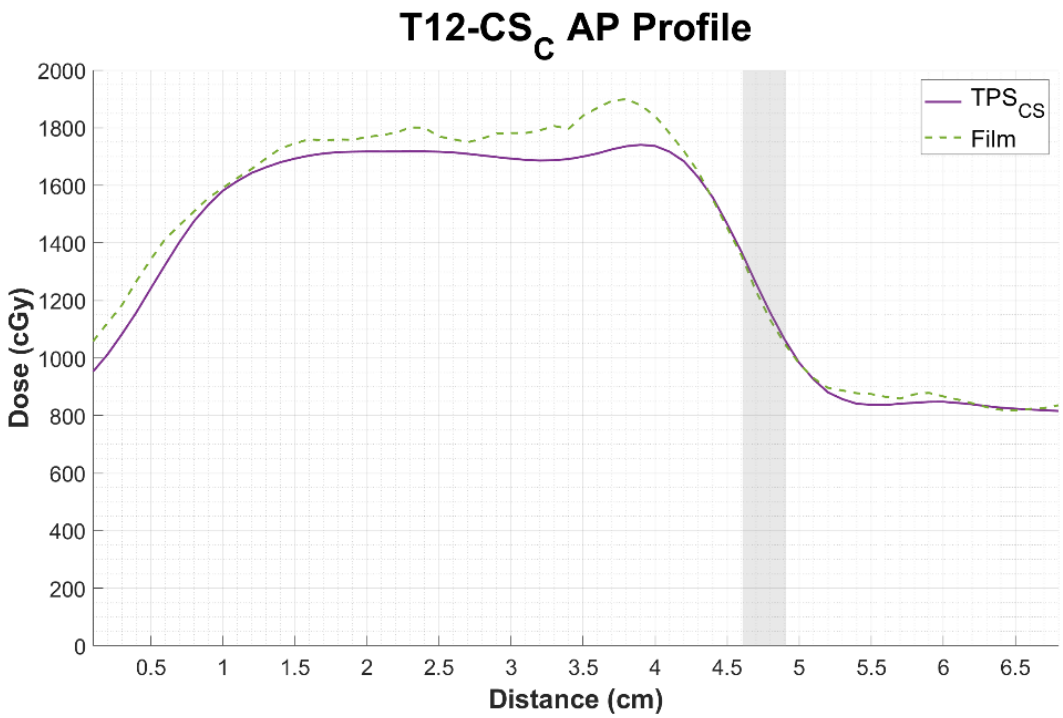

Figure B.20. Planned AP TPS_{CS} dose profile with its respective film-measured dose profile for the T12 site, trial C.

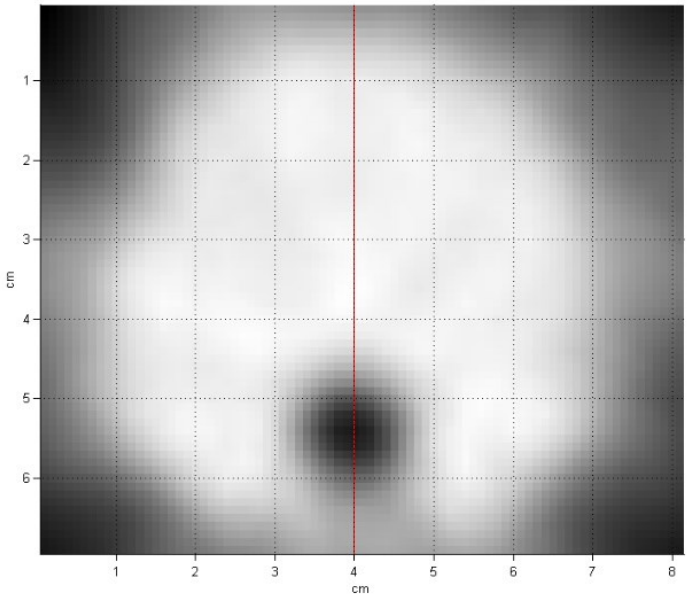

Figure B.21. AP dose profile over the TPS_{MC} T12 planned dose distribution.

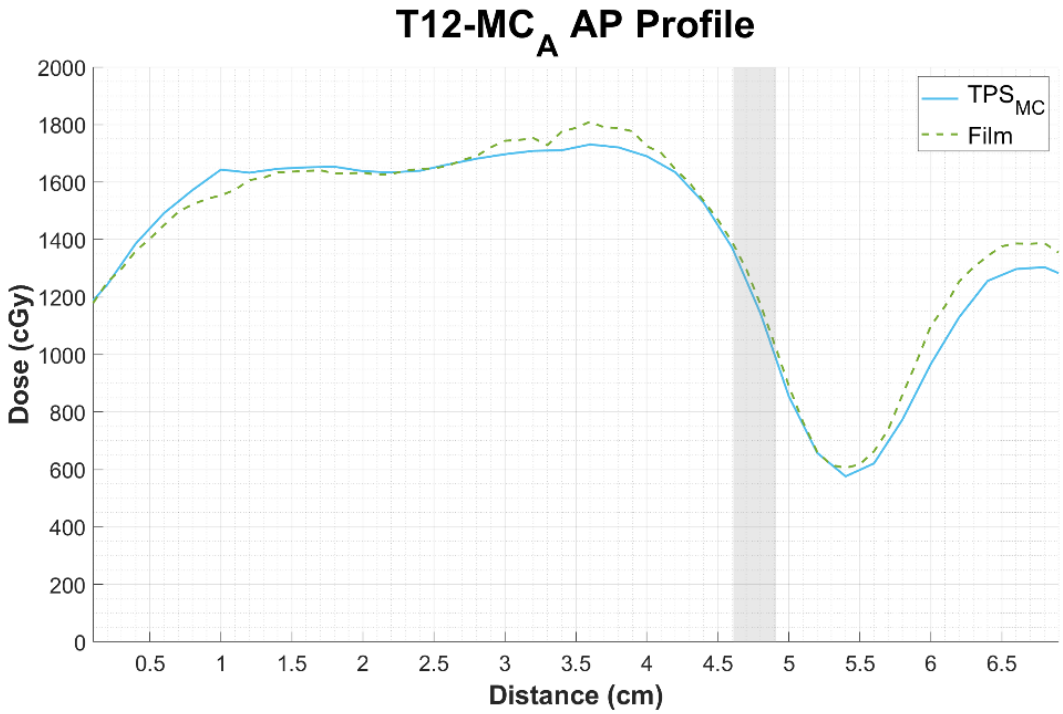

Figure B.22. Planned AP TPS_{MC} dose profile with its respective film-measured dose profile for the T12 site, trial A.

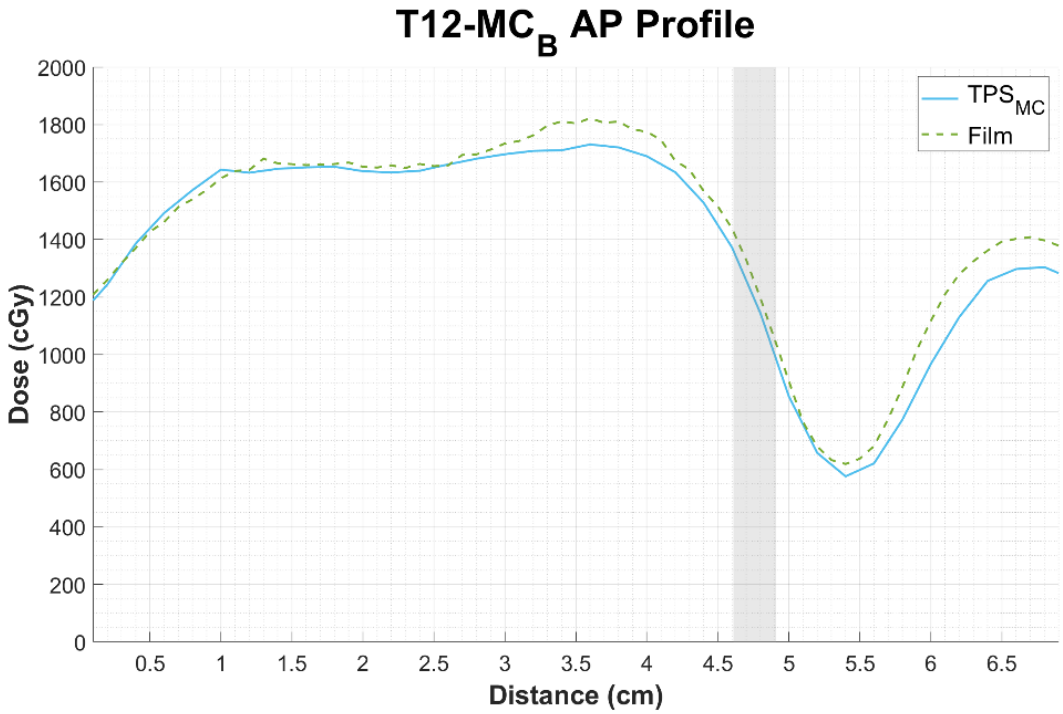

Figure B.23. Planned AP TPS_{MC} dose profile with its respective film-measured dose profile for the T12 site, trial B.

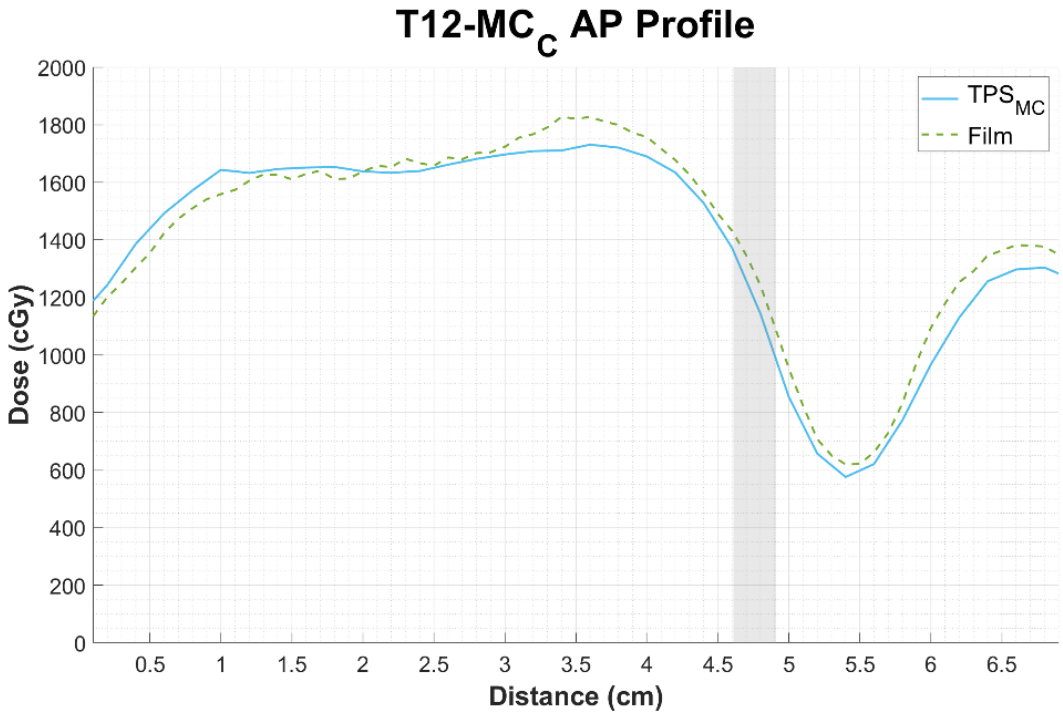

Figure B.24. Planned AP TPS_{MC} dose profile with its respective film-measured dose profile for the T12 site, trial C.

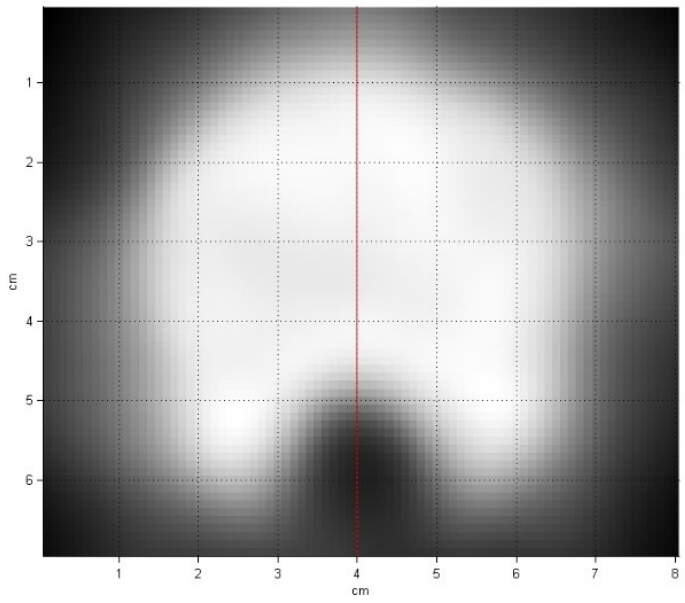

Figure B.25. AP dose profile over the TPS_{CS} L2 planned dose distribution.

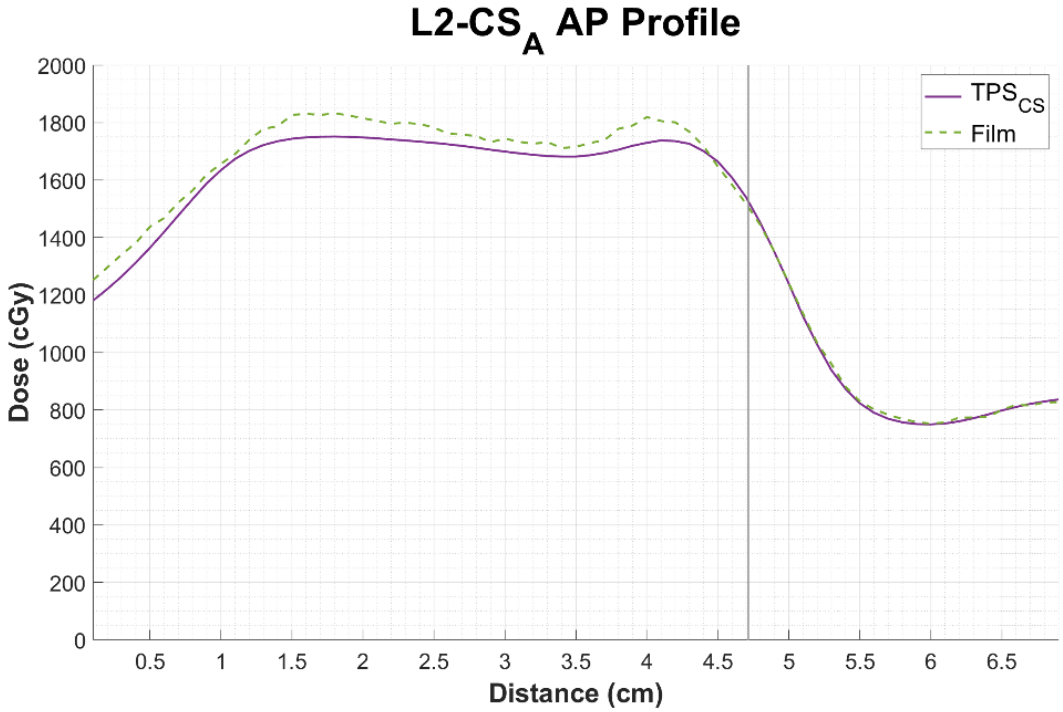

Figure B.26. Planned AP TPS_{CS} dose profile with its respective film-measured dose profile for the L2 site, trial A.

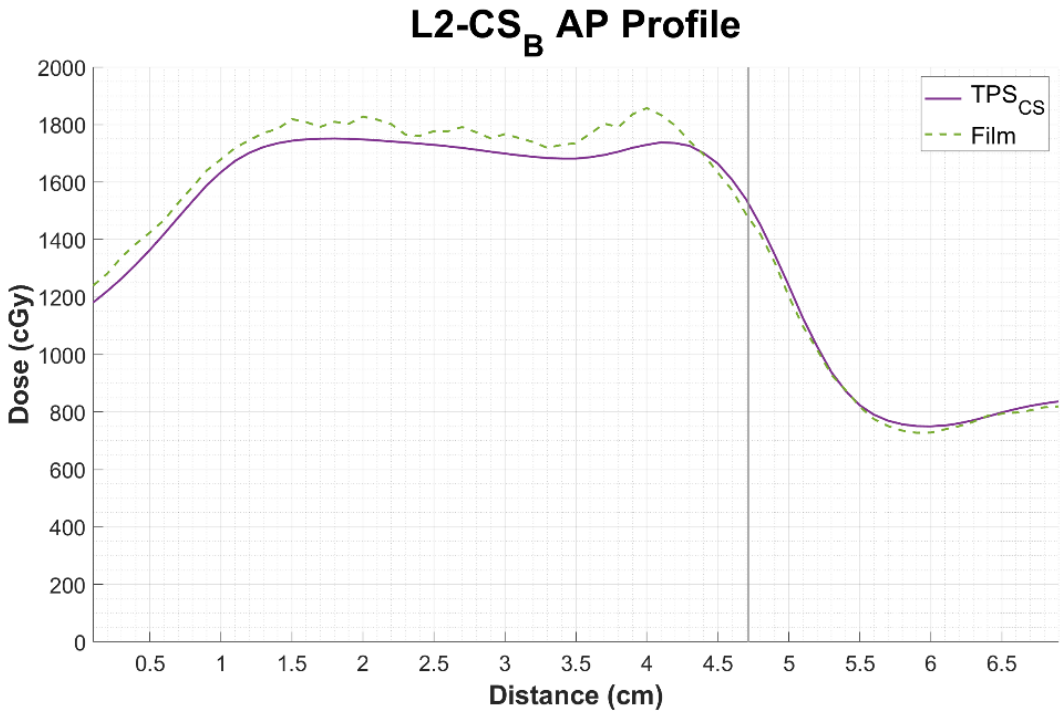

Figure B.27. Planned AP TPS_{CS} dose profile with its respective film-measured dose profile for the L2 site, trial B.

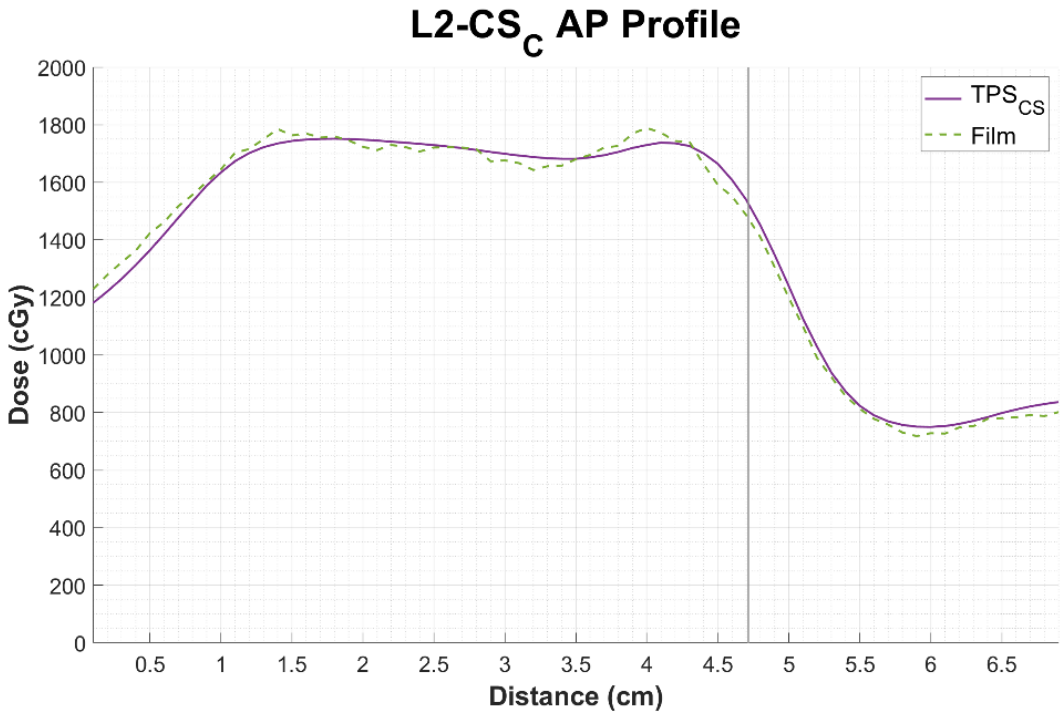

Figure B.28. Planned AP TPS_{CS} dose profile with its respective film-measured dose profile for the L2 site, trial C.

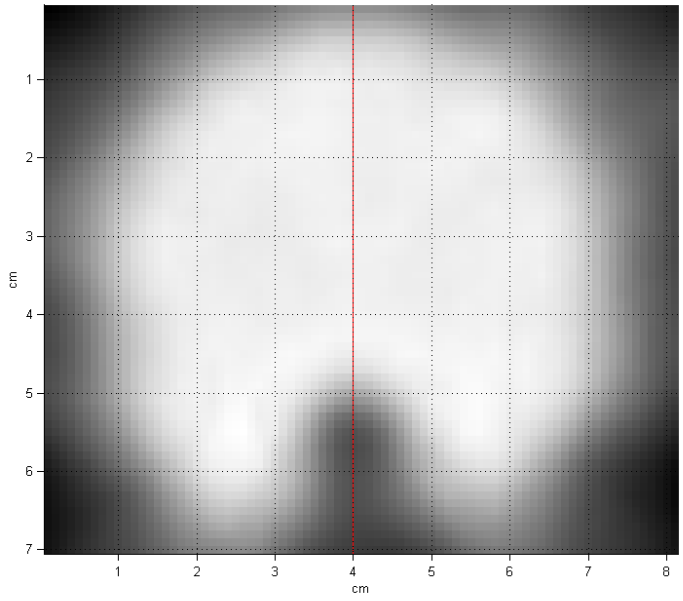

Figure B.29. AP dose profile over the TPS_{MC} L2 planned dose distribution.

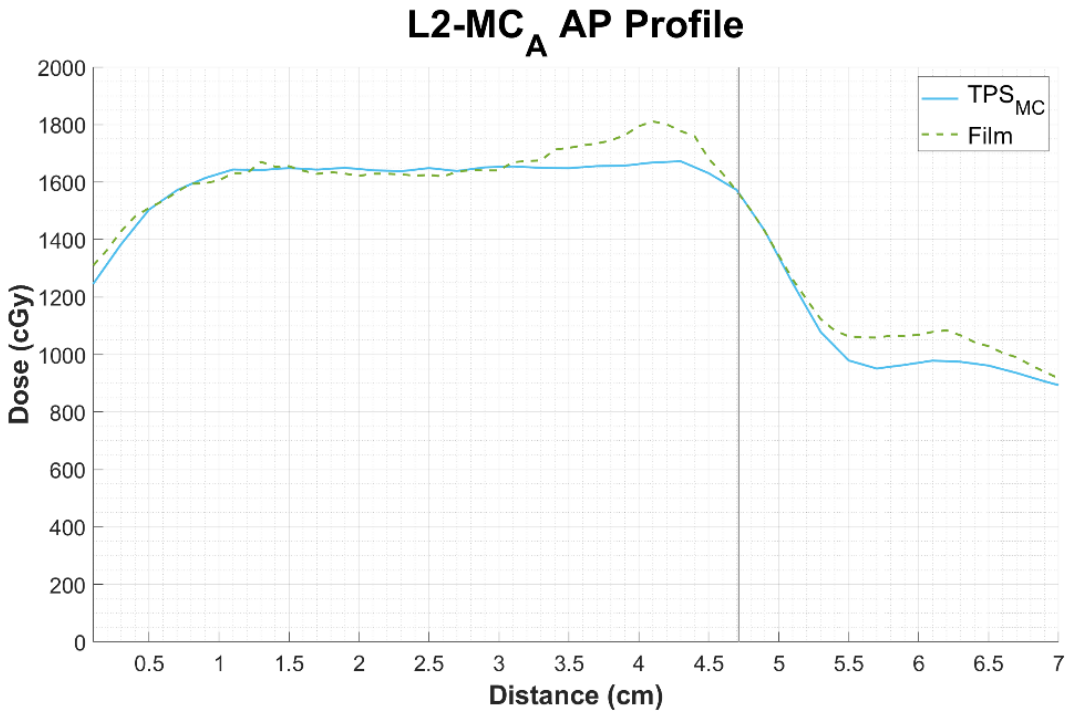

Figure B.30. Planned AP TPS_{MC} dose profile with its respective film-measured dose profile for the L2 site, trial A.

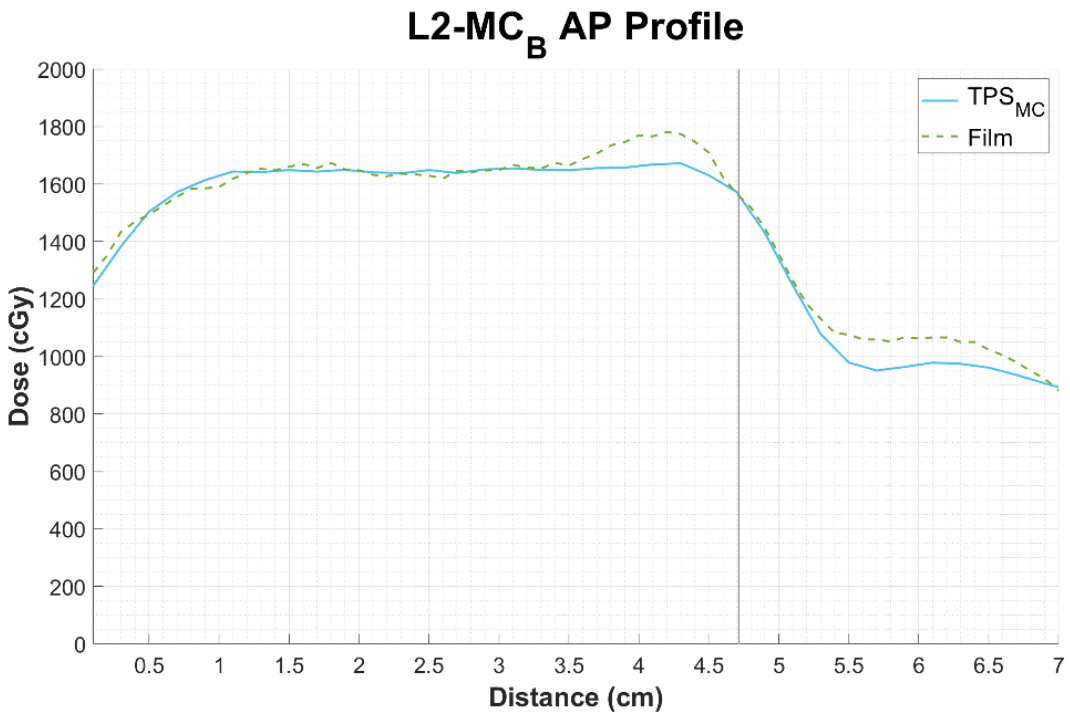

Figure B.31. Planned AP TPS_{MC} dose profile with its respective film-measured dose profile for the L2 site, trial B.

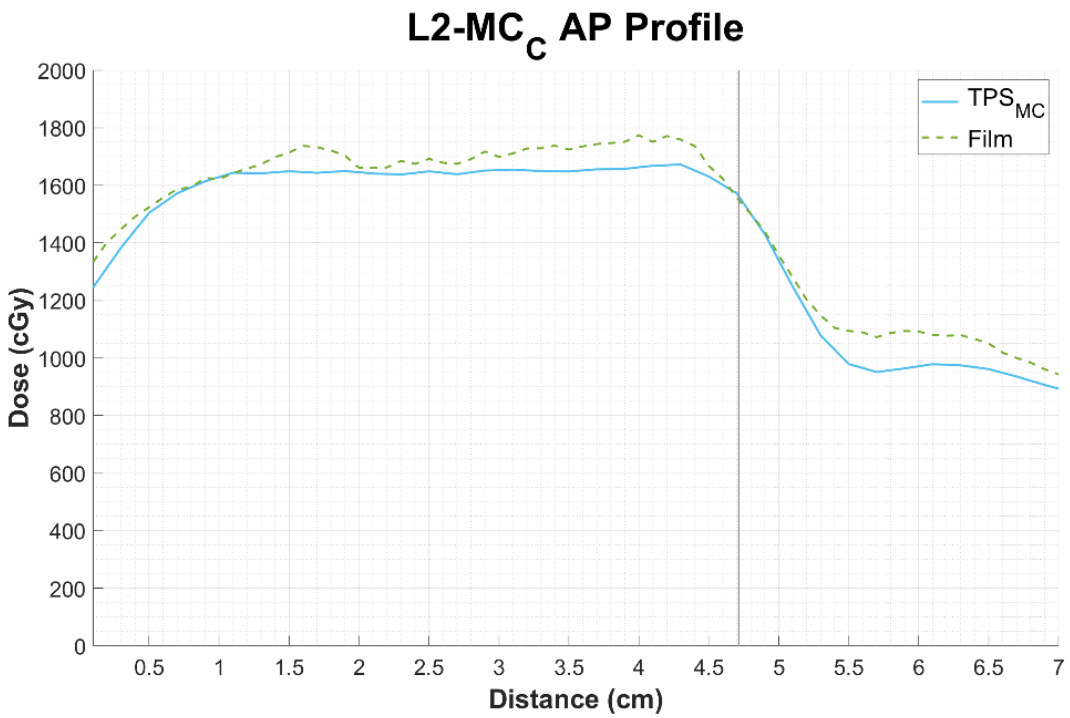

Figure B.32. Planned AP TPS_{MC} dose profile with its respective film-measured dose profile for the L2 site, trial C.

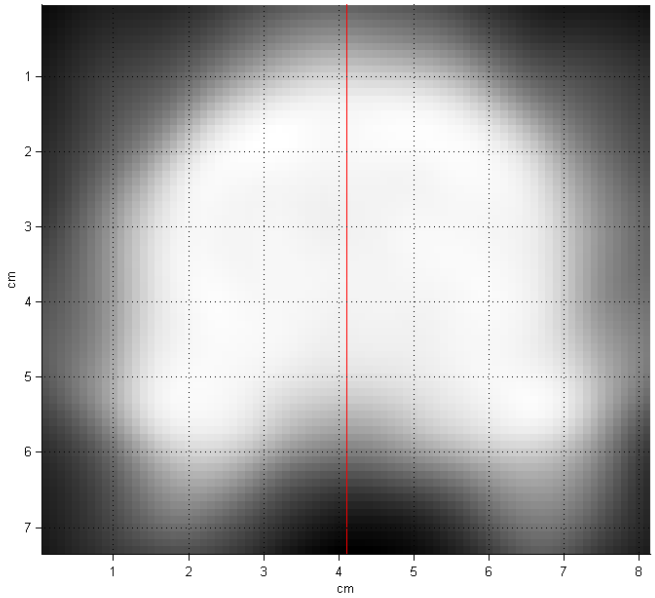

Figure B.33. AP dose profile over the TPS_{CS} L4 planned dose distribution.

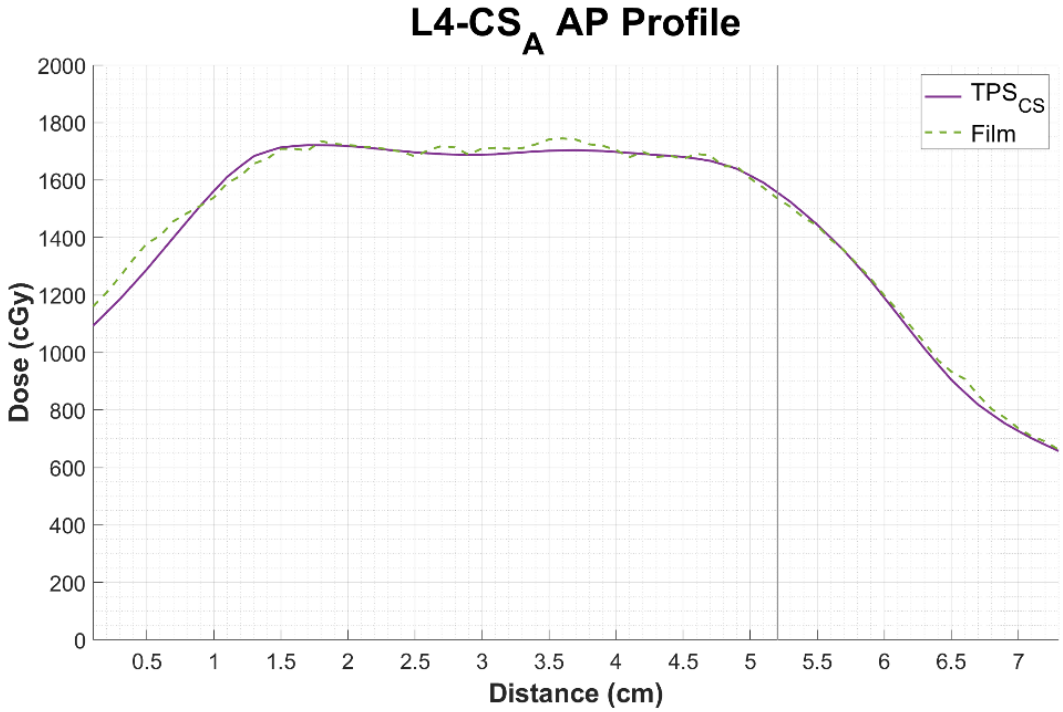

Figure B.34. Planned AP TPS_{CS} dose profile with its respective film-measured dose profile for the L4 site, trial A.

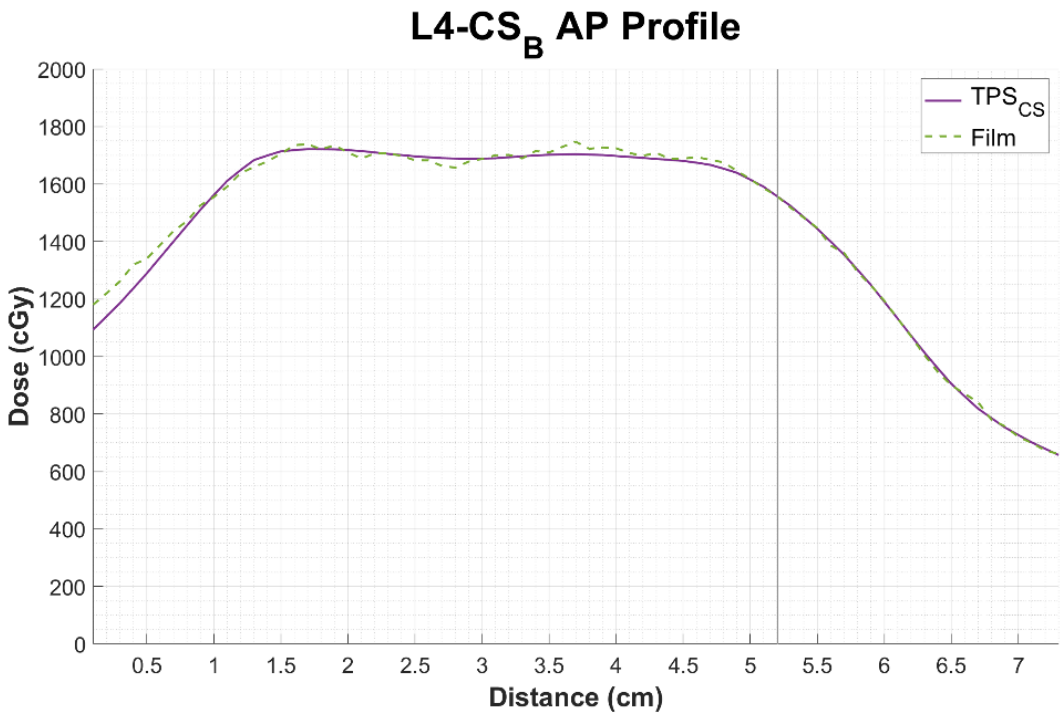

Figure B.35. Planned AP TPS_{CS} dose profile with its respective film-measured dose profile for the L4 site, trial B.

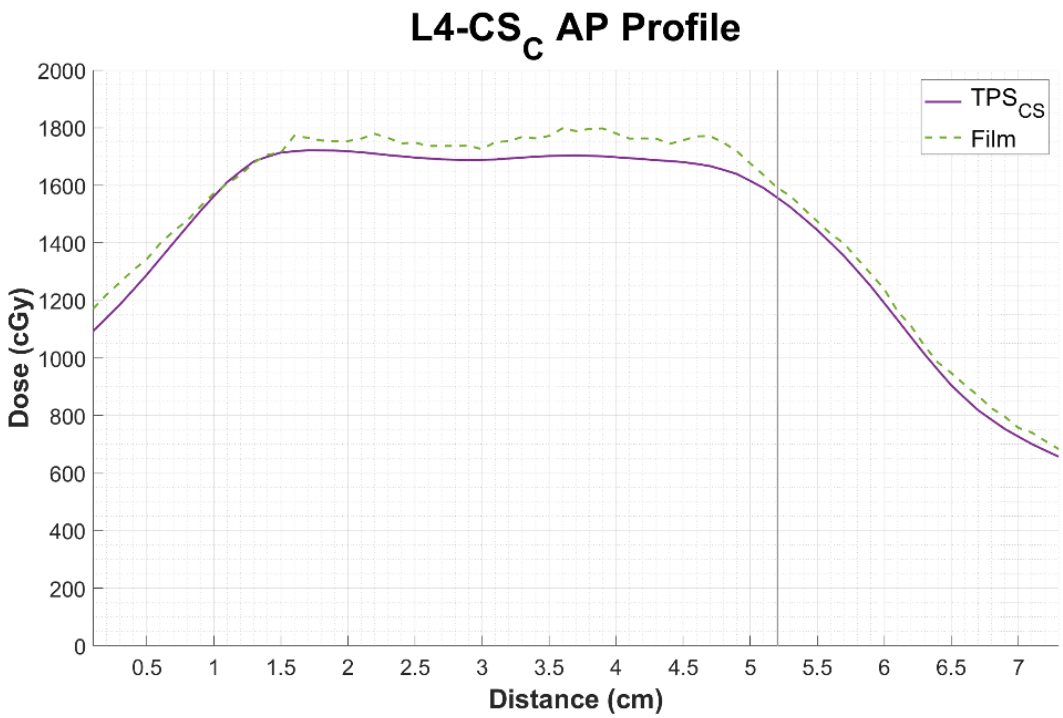

Figure B.36. Planned AP TPS_{CS} dose profile with its respective film-measured dose profile for the L4 site, trial C.

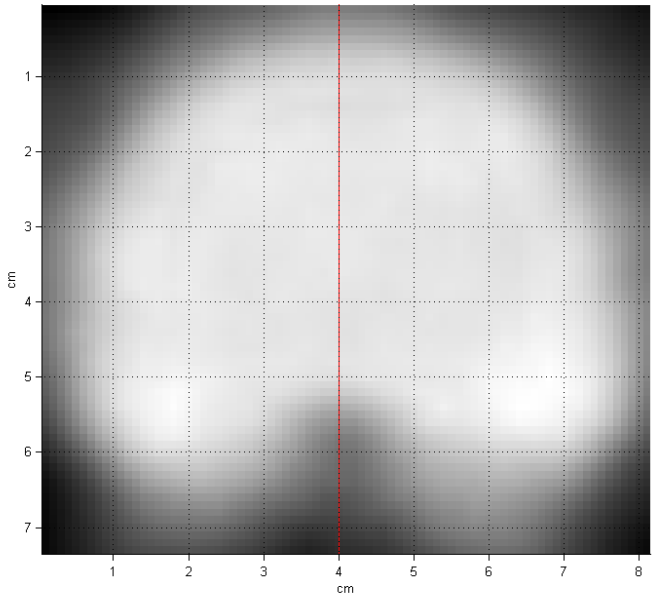

Figure B.37. AP dose profile over the TPS_{MC} L4 planned dose distribution.

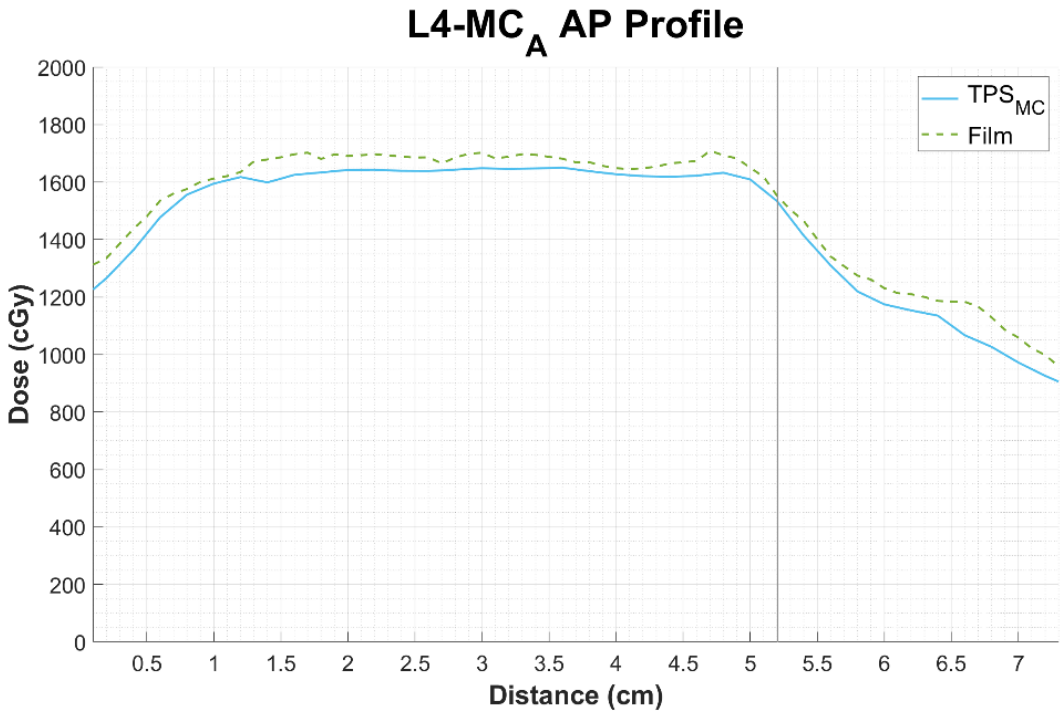

Figure B.38. Planned AP TPS_{MC} dose profile with its respective film-measured dose profile for the L4 site, trial A.

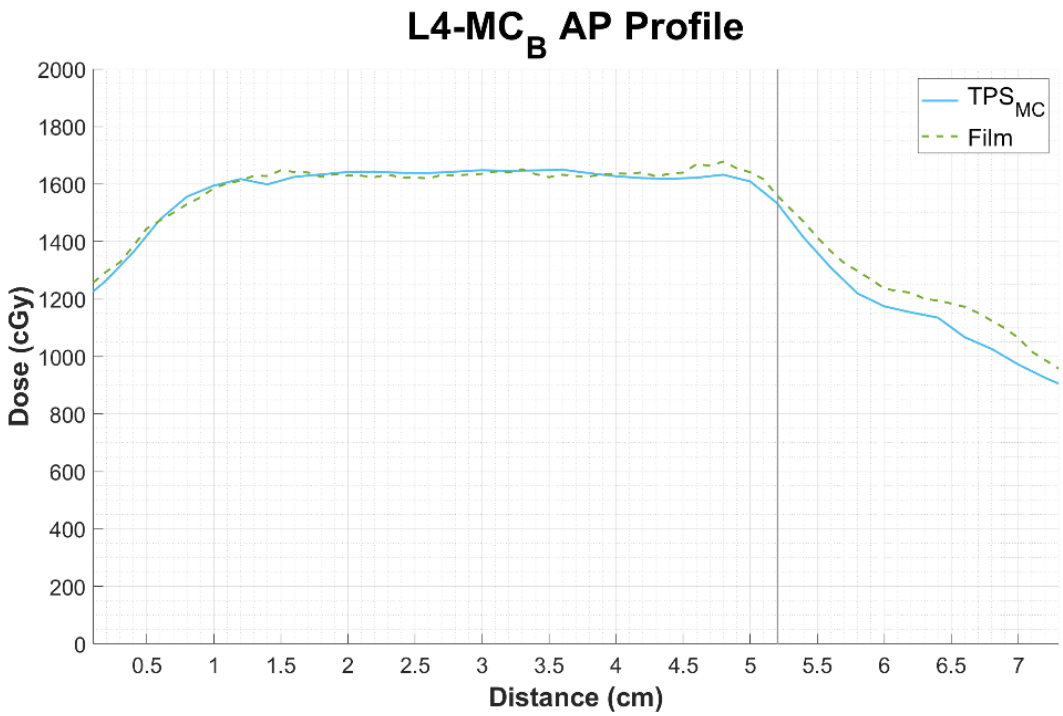

Figure B.39. Planned AP TPS_{MC} dose profile with its respective film-measured dose profile for the L4 site, trial B.

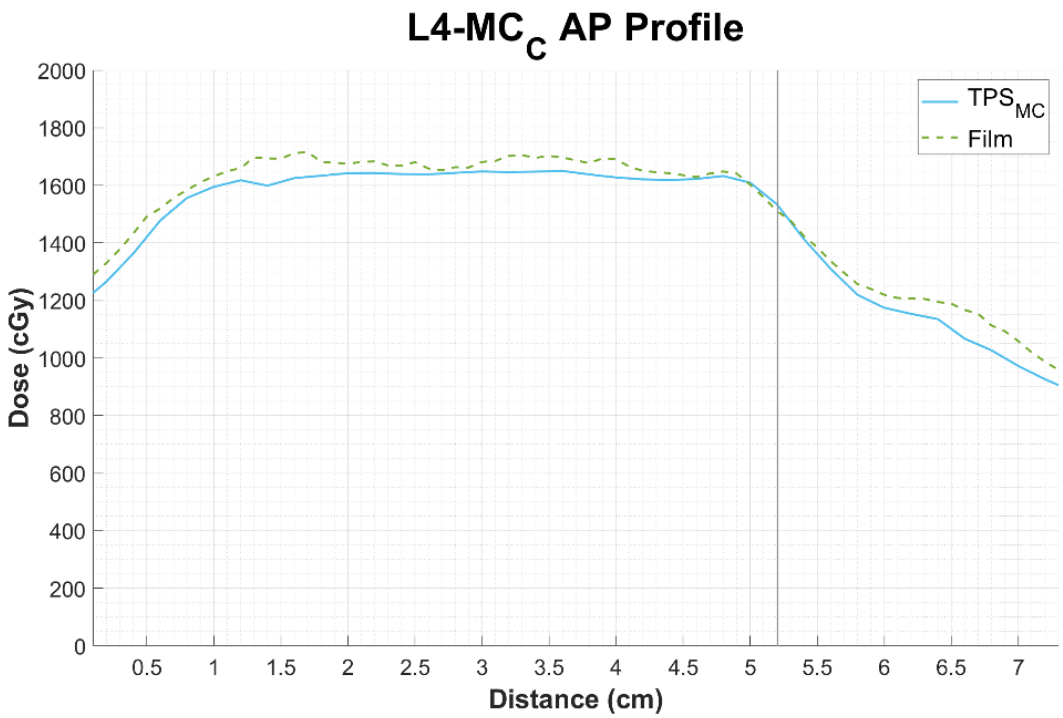

Figure B.40. Planned AP TPS_{MC} dose profile with its respective film-measured dose profile for the L4 site, trial C.

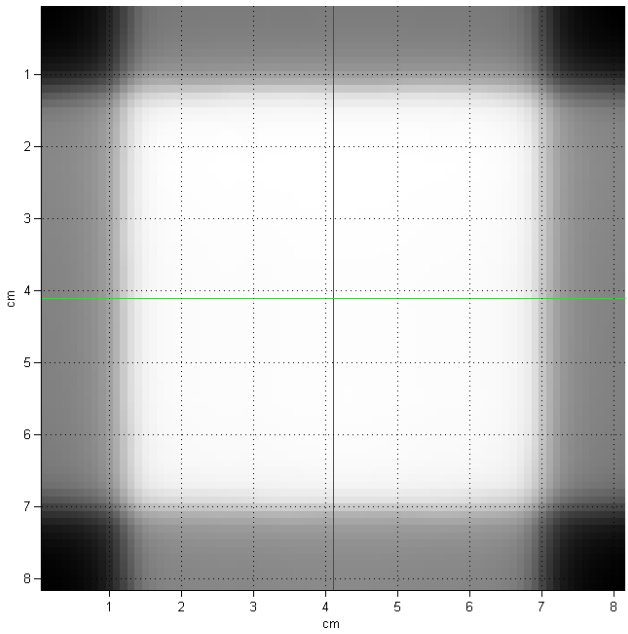

Figure B.41. AP and LAT dose profiles over the TPS_{CS} 4-field box (RegTestFF) planned dose distribution.

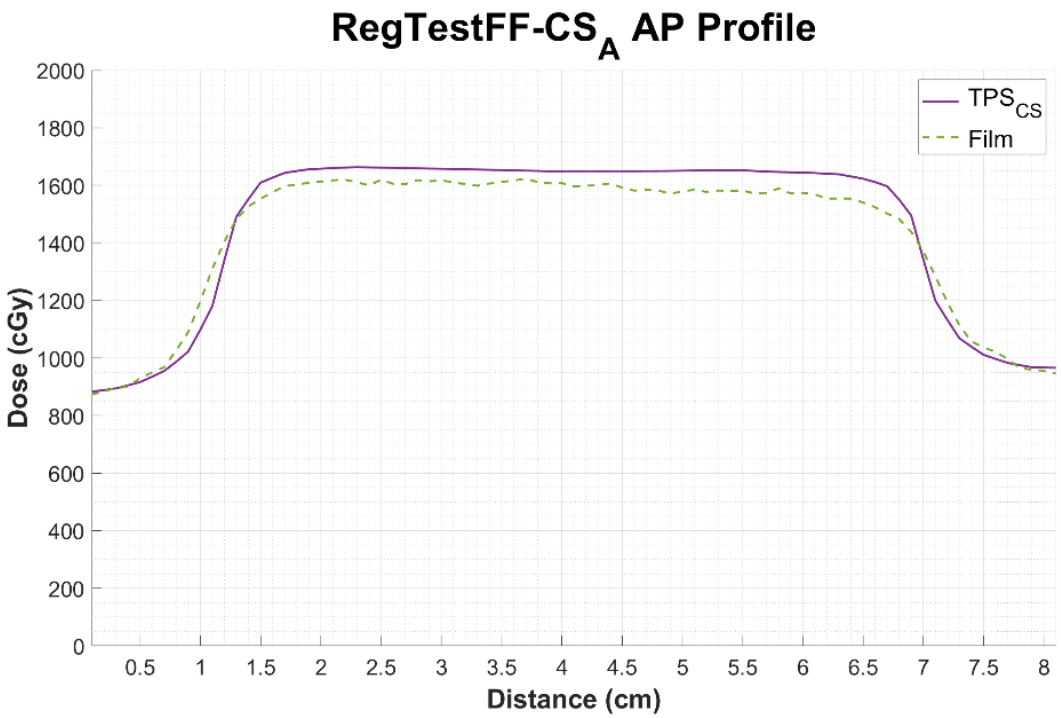

Figure B.42. Planned AP TPS_{CS} dose profile with its respective film-measured dose profile for RegTestFF, trial A.

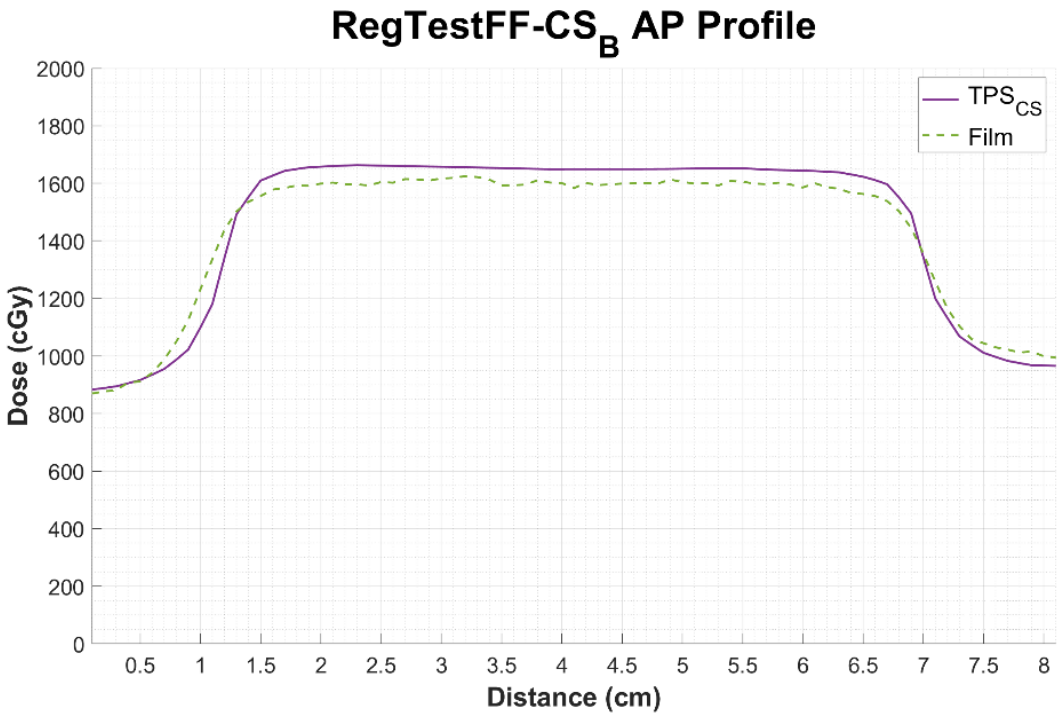

Figure B.43. Planned AP TPS_{CS} dose profile with its respective film-measured dose profile for RegTestFF, trial B.

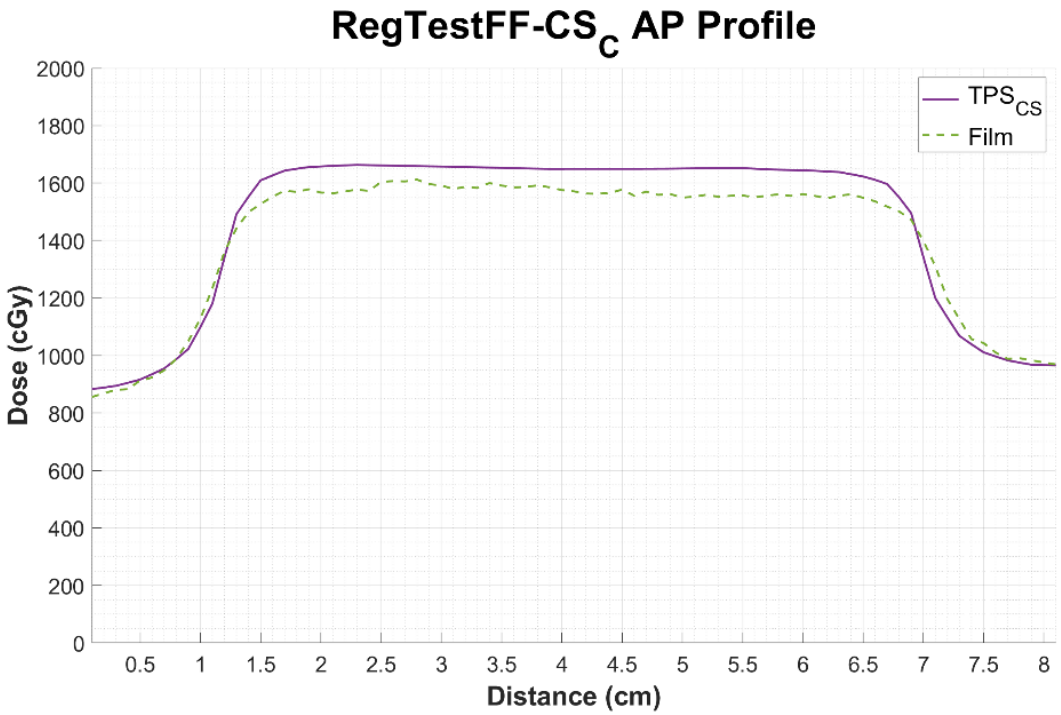

Figure B.44. Planned AP TPS_{CS} dose profile with its respective film-measured dose profile for RegTestFF, trial C.

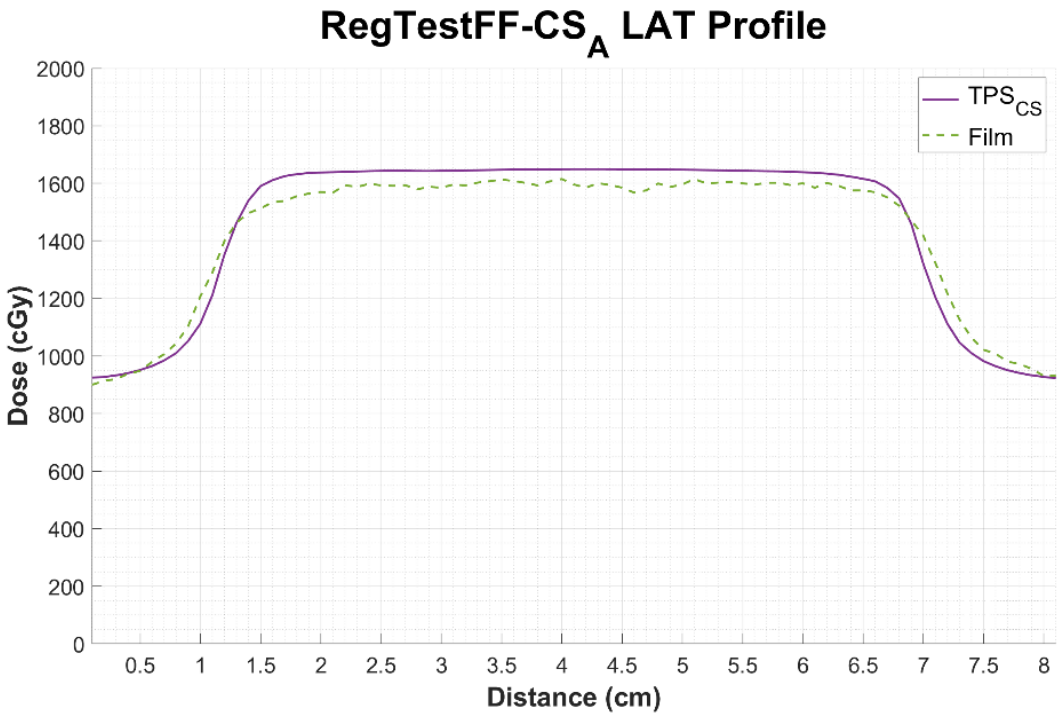

Figure B.45. Planned LAT TPS_{CS} dose profile with its respective film-measured dose profile for RegTestFF, trial A.

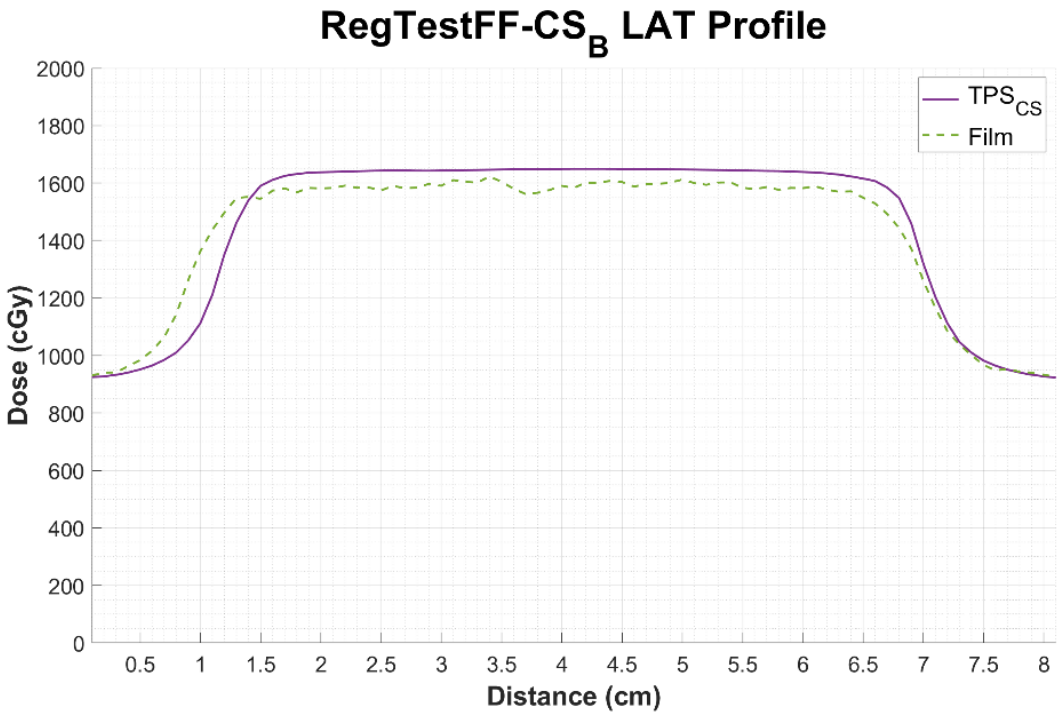

Figure B.46. Planned LAT TPS_{CS} dose profile with its respective film-measured dose profile for RegTestFF, trial B.

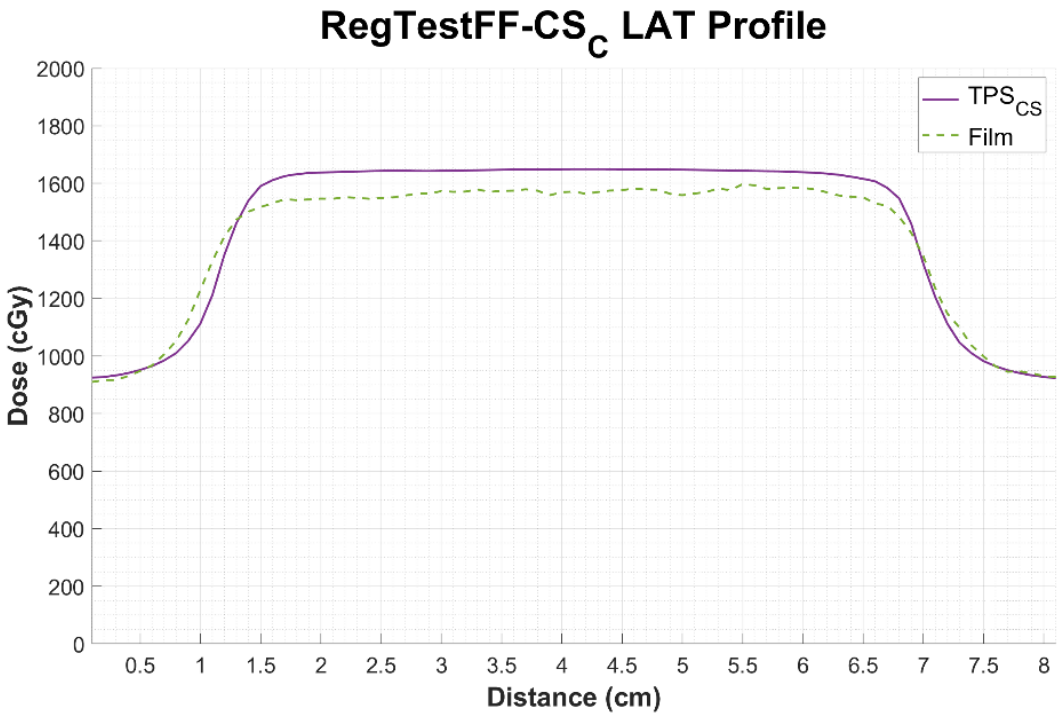

Figure B.47. Planned LAT TPS_{CS} dose profile with its respective film-measured dose profile for RegTestFF, trial C.

Appendix C. Full Gamma Analysis Results

Table C.1 through Table C.4 display the GPR of each individual trial (A, B, and C) for all treatments sites from each TPS. Figure C.1 through Figure C.15 show the film-measured dose distribution of each trial in both TPS_{CS} and TPS_{MC}. The red pixels have a gamma calculated greater than 1, failing the 2%/2mm ΔD/DTA criteria. Figure C.16 through Figure C.19 show the same for the TG-119 validation plans.

Table C.1. GPR of each trial (A, B, and C) and average (AVG) GPR ± σ for the TPS_{CS} cervical and thoracic sites.

Site	C4				T1				T12			
Trial	A	B	C	AVG	A	B	C	AVG	A	B	C	AVG
5%/1mm	98.09	97.56	97.06	97.57 ± 0.52	97.12	95.08	95.90	96.03 ± 1.03	99.75	99.56	95.08	98.13 ± 2.64
3%/3mm	99.57	99.67	99.63	99.62 ± 0.05	98.95	98.36	99.10	98.80 ± 0.39	99.96	99.89	95.15	98.33 ± 2.76
3%/2mm	98.80	97.99	97.59	98.13 ± 0.62	97.94	95.56	98.19	97.23 ± 1.45	99.66	99.67	91.76	97.03 ± 4.56
3%/1mm	90.40	87.92	93.28	90.53 ± 2.68	88.72	86.21	89.37	88.10 ± 1.67	97.51	94.17	77.54	89.74 ± 10.70
2%/2mm	96.59	95.58	95.68	95.95 ± 0.56	95.65	92.48	95.11	94.41 ± 1.70	97.04	97.79	83.77	92.87 ± 7.89
2%/1mm	85.55	81.97	89.53	85.68 ± 3.78	76.26	77.98	80.47	78.24 ± 2.12	87.38	86.33	63.27	78.99 ± 13.63
1%/1mm	78.92	76.28	81.80	79.00 ± 2.76	64.25	68.37	71.25	67.96 ± 3.52	70.21	73.55	52.81	65.52 ± 11.14
ROI (cm^2)	6×4.84				6×5.71				8×6.78			

Table C.2. GPR of each trial (A, B, and C) and average (AVG) GPR ± σ for the TPS_{CS} lumbar sites.

Site	L2				L4			
Trial	A	B	C	AVG	A	B	C	AVG
5%/1mm	99.53	99.78	99.64	99.65 ± 0.13	99.58	99.97	95.43	98.33 ± 2.52
3%/3mm	99.40	99.66	99.78	99.61 ± 0.19	99.68	99.68	94.10	97.82 ± 3.22
3%/2mm	98.33	98.57	98.93	98.61 ± 0.30	99.54	99.27	90.87	96.56 ± 4.93
3%/1mm	88.10	91.74	94.64	91.49 ± 3.28	92.19	95.32	76.17	87.89 ± 10.27
2%/2mm	95.85	94.96	96.36	95.72 ± 0.71	98.44	98.38	84.88	93.90 ± 7.81
2%/1mm	77.50	78.24	84.29	80.01 ± 3.73	82.99	85.95	61.17	76.70 ± 13.53
1%/1mm	66.50	64.28	68.71	66.50 ± 2.22	70.02	73.63	48.60	64.08 ± 13.53
ROI (cm^2)	8×6.88				8×7.17			

Table C.3. GPR of each trial (A, B, and C) and average (AVG) GPR ± σ for the TPS_{MC} cervical and thoracic sites.

Site	C4				T1				T12			
Trial	A	B	C	AVG	A	B	C	AVG	A	B	C	AVG
5%/1mm	97.51	93.25	96.85	95.87 ± 2.29	88.94	92.25	91.50	90.90 ± 1.74	98.53	96.15	93.42	96.03 ± 2.56
3%/3mm	98.66	97.84	98.46	98.32 ± 0.43	92.28	94.72	92.91	93.30 ± 1.27	99.39	98.32	96.30	98.00 ± 1.57
3%/2mm	96.20	94.33	95.90	95.48 ± 1.00	88.05	90.08	89.36	89.16 ± 1.03	97.92	95.40	91.63	94.98 ± 3.17
3%/1mm	92.13	84.36	86.30	87.60 ± 4.04	73.58	75.60	78.27	75.82 ± 2.35	93.34	86.15	82.79	87.43 ± 5.39
2%/2mm	94.79	92.39	93.61	93.60 ± 1.20	84.58	86.30	84.91	85.26 ± 0.91	94.92	92.00	87.12	91.35 ± 3.94
2%/1mm	87.02	77.79	79.87	81.56 ± 4.84	64.10	64.99	68.44	65.84 ± 2.29	85.22	76.15	72.30	77.89 ± 6.63
1%/1mm	80.13	71.34	72.07	74.51 ± 4.88	55.74	56.71	59.91	57.45 ± 2.18	73.86	65.41	59.24	66.17 ± 7.34
ROI (cm^2)	6×4.84				6×5.71				8×6.79			

Table C.4. GPR of each trial (A, B, and C) and average (AVG) GPR ± σ for the TPS_{MC} lumbar sites.

Site	L2				L4			
Trial	A	B	C	AVG	A	B	C	AVG
5%/1mm	91.08	96.31	93.74	93.71 ± 2.62	93.24	94.67	95.79	94.57 ± 1.28
3%/3mm	95.01	97.50	91.98	94.83 ± 2.76	93.10	96.31	96.92	95.44 ± 2.05
3%/2mm	89.40	94.71	86.17	90.09 ± 4.31	86.66	92.73	91.37	90.25 ± 3.19
3%/1mm	74.76	88.78	75.10	79.55 ± 8.00	75.33	86.27	77.88	79.83 ± 5.72
2%/2mm	84.37	91.78	78.43	84.86 ± 6.69	76.34	88.99	81.85	82.39 ± 6.34
2%/1mm	63.62	78.69	60.53	67.61 ± 9.72	57.52	78.37	61.51	65.80 ± 11.07
1%/1mm	52.05	65.45	49.15	55.55 ± 8.70	41.37	64.11	44.97	50.15 ± 12.22
ROI (cm^2)	8×6.88				8×7.17			

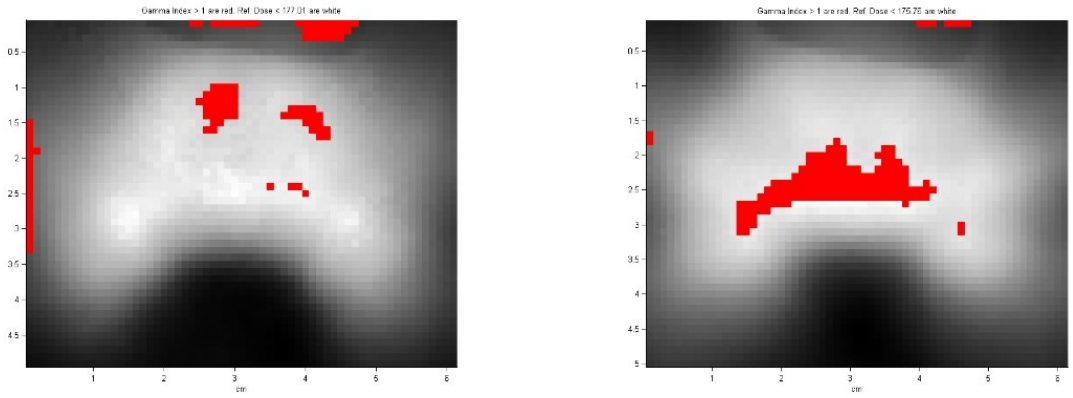

Figure C.1. C4-TPS$_{CS}$-A (Left) and C4-TPS$_{MC}$-A (Right) dose points failing gamma criteria 2%/2mm.

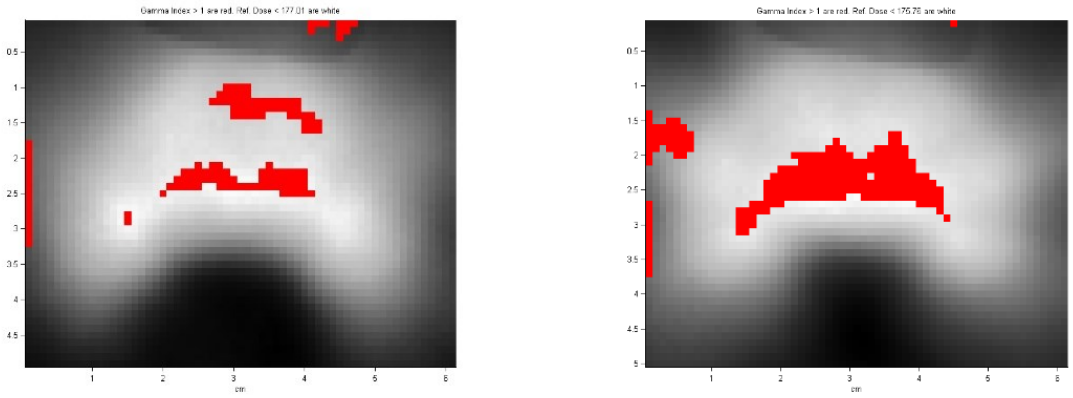

Figure C.2. C4-TPS$_{CS}$-B (Left) and C4-TPS$_{MC}$-B (Right) dose points failing gamma criteria 2%/2mm.

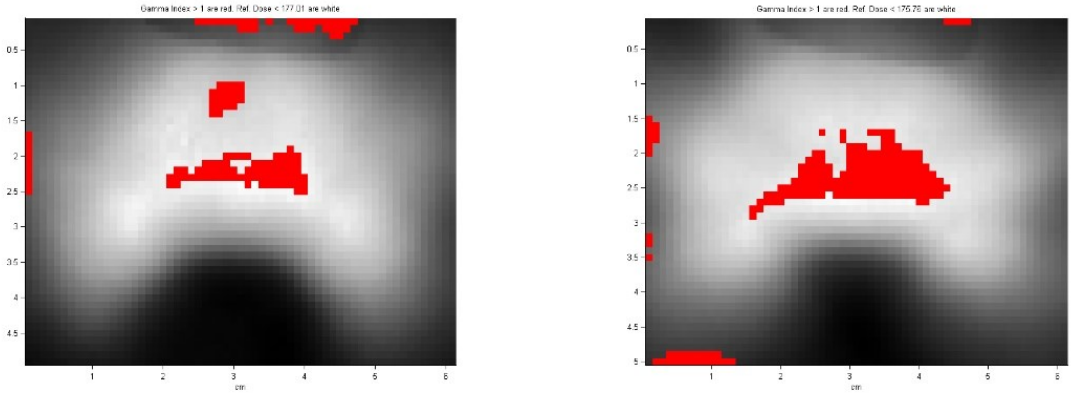

Figure C.3. C4-TPS$_{CS}$-C (Left) and C4-TPS$_{MC}$-C (Right) dose points failing gamma criteria 2%/2mm.

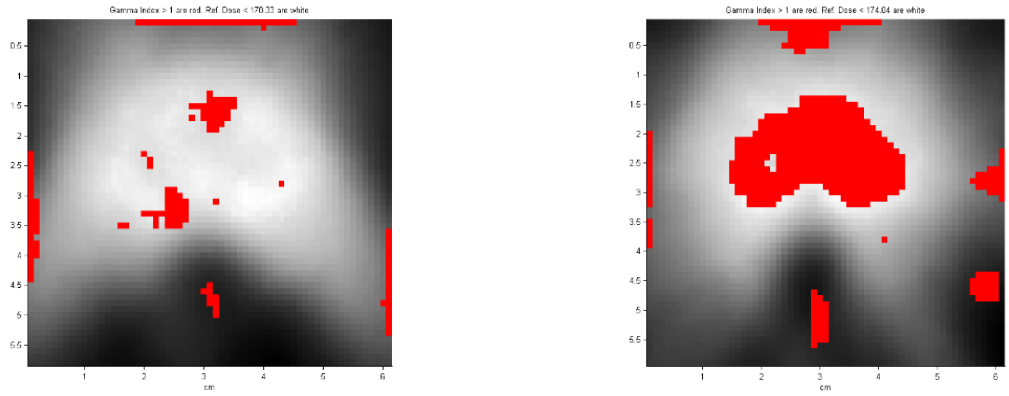

Figure C.4. T1-TPS$_{CS}$-A (Left) and T1-TPS$_{MC}$-A (Right) dose points failing gamma criteria 2%/2mm.

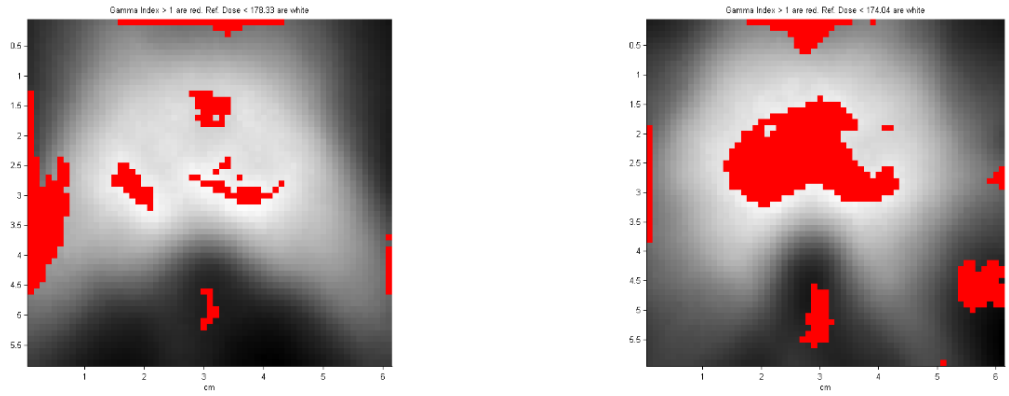

Figure C.5. T1-TPS$_{CS}$-B (Left) and T1-TPS$_{MC}$-B (Right) dose points failing gamma criteria 2%/2mm.

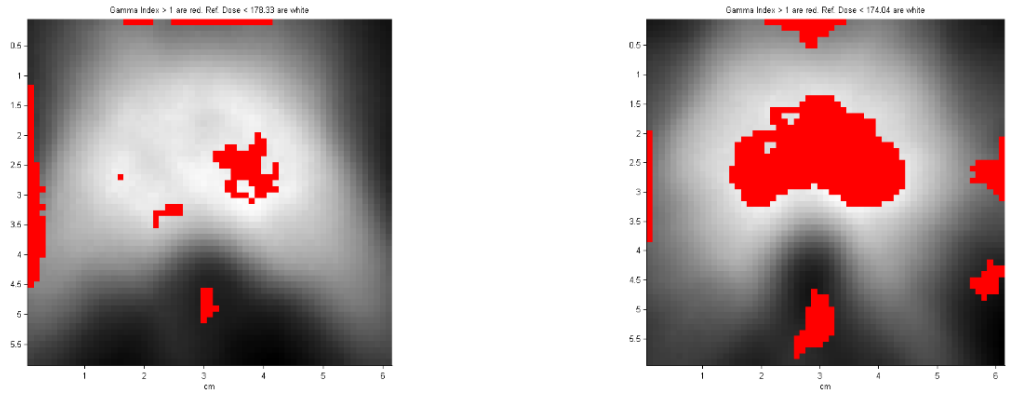

Figure C.6. T1-TPS$_{CS}$-C (Left) and T1-TPS$_{MC}$-C (Right) dose points failing gamma criteria 2%/2mm.

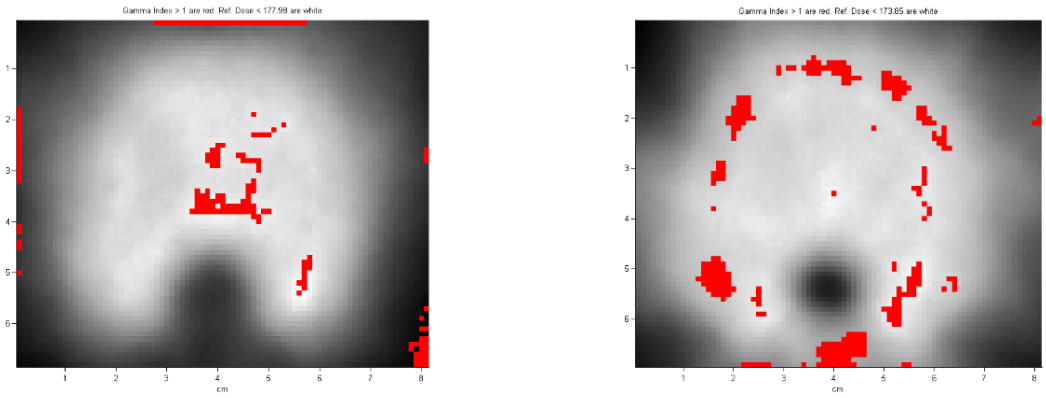

Figure C.7. T12-TPS$_{CS}$-A (Left) and T12-TPS$_{MC}$-A (Right) dose points failing gamma criteria 2%/2mm.

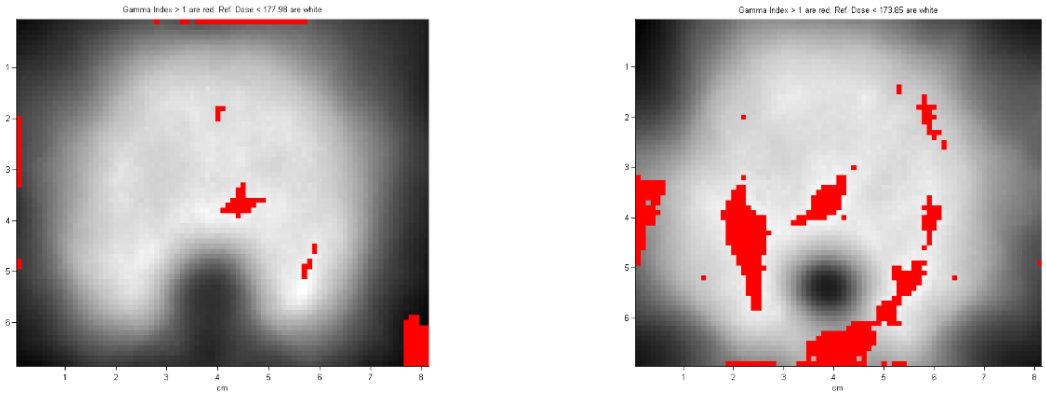

Figure C.8. T12-TPS$_{CS}$-B (Left) and T12-TPS$_{MC}$-B (Right) dose points failing gamma criteria 2%/2mm.

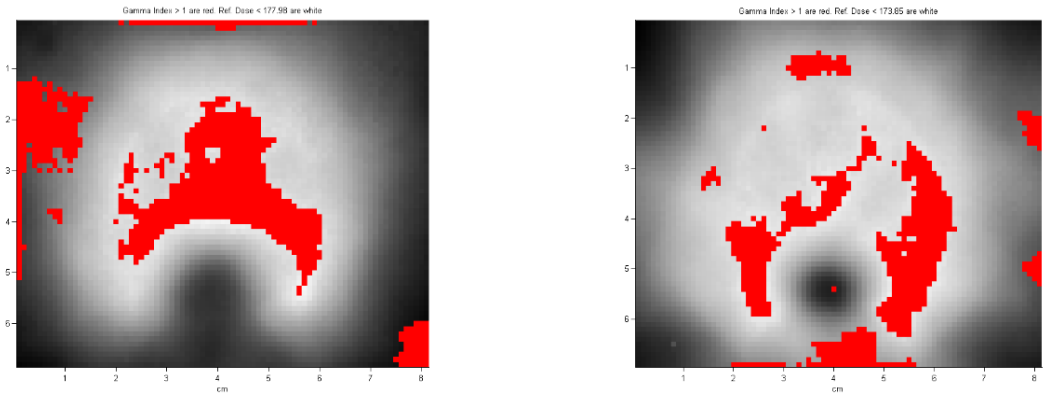

Figure C.9. T12-TPS$_{CS}$-C (Left) and T12-TPS$_{MC}$-C (Right) dose points failing gamma criteria 2%/2mm.

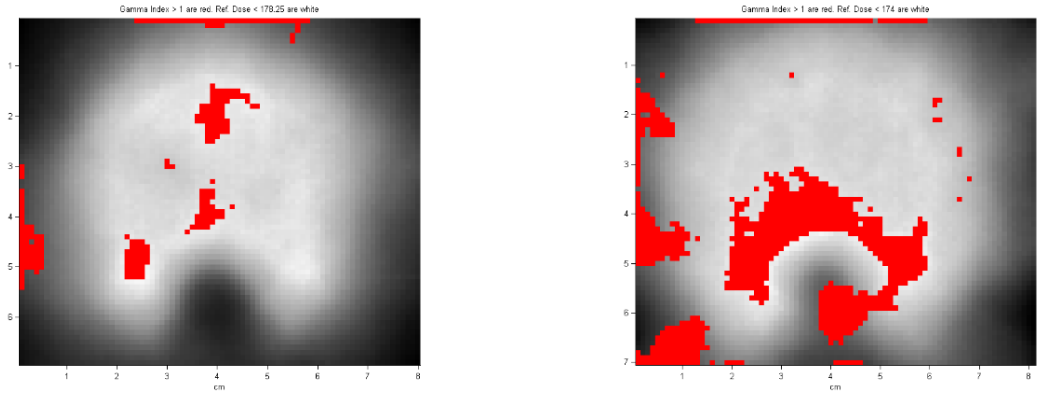

Figure C.10. L2-TPS$_{CS}$-A (Left) and L2-TPS$_{MC}$-A (Right) dose points failing gamma criteria 2%/2mm.

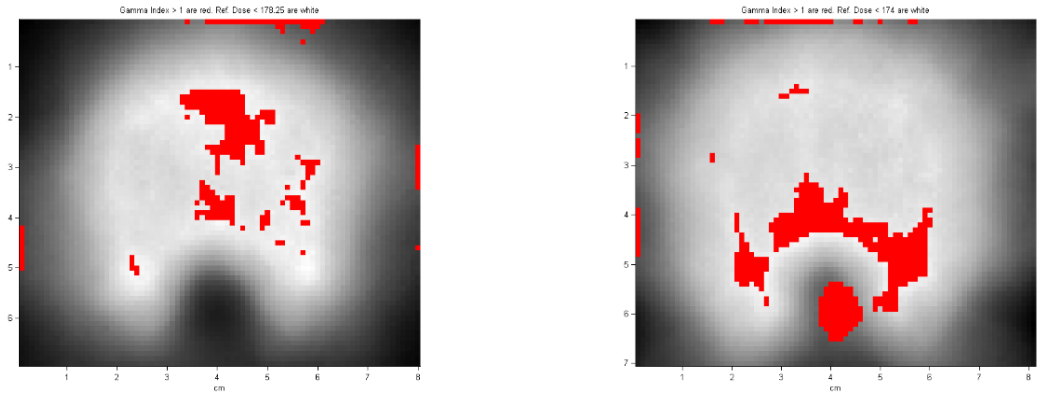

Figure C.11. L2-TPS$_{CS}$-B (Left) and L2-TPS$_{MC}$-B (Right) dose points failing gamma criteria 2%/2mm.

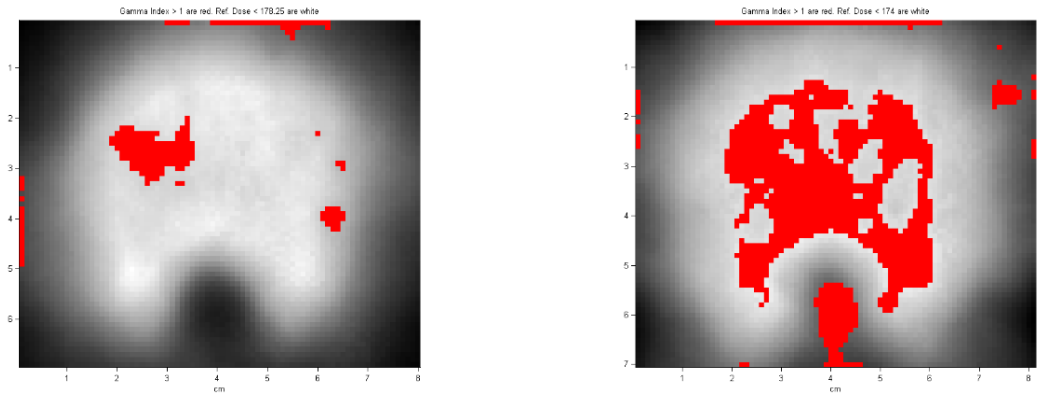

Figure C.12. L2-TPS$_{CS}$-C (Left) and L2-TPS$_{MC}$-C (Right) dose points failing gamma criteria 2%/2mm.

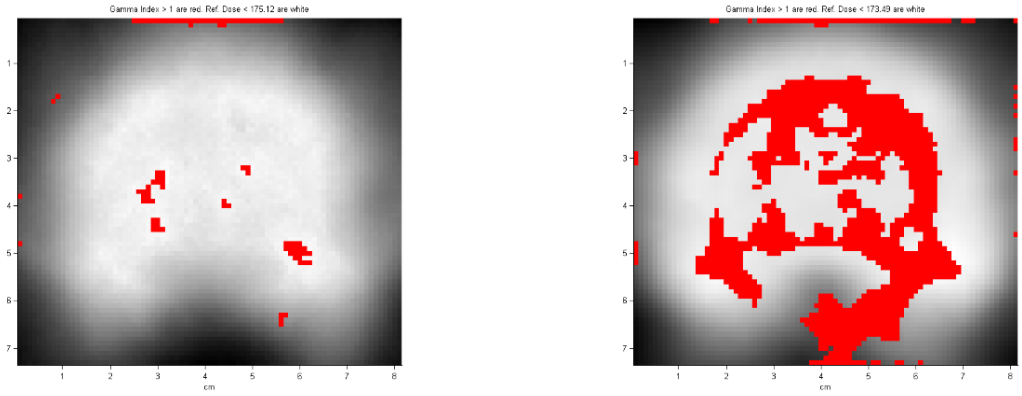

Figure C.13. L4-TPS$_{CS}$-A (Left) and L4-TPS$_{MC}$-A (Right) dose points failing gamma criteria 2%/2mm.

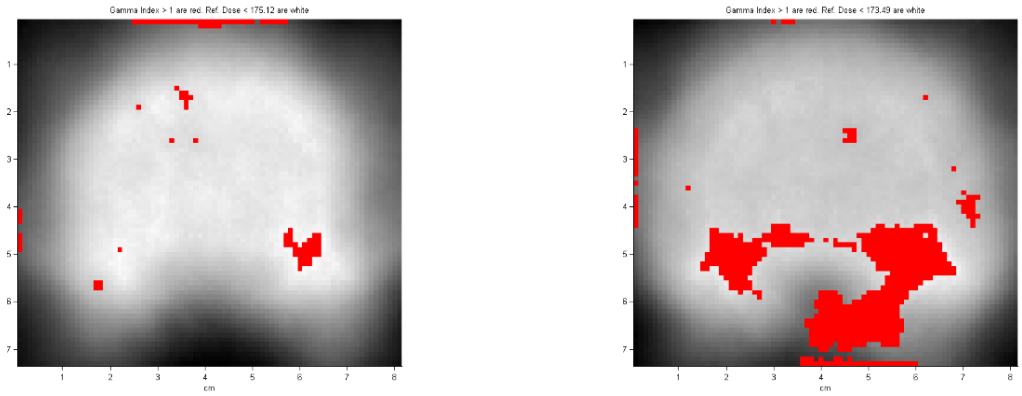

Figure C.14. L4-TPS$_{CS}$-B (Left) and L4-TPS$_{MC}$-B (Right) dose points failing gamma criteria 2%/2mm.

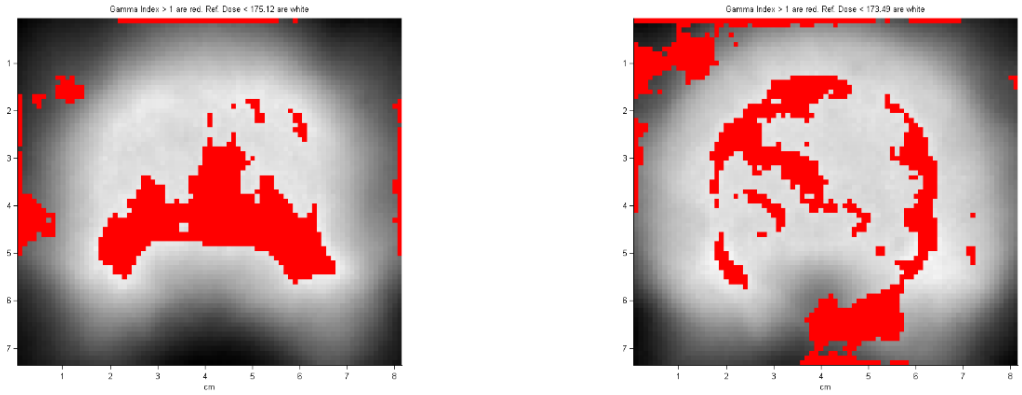

Figure C.15. L4-TPS$_{CS}$-C (Left) and L4-TPS$_{MC}$-C (Right) dose points failing gamma criteria 2%/2mm.

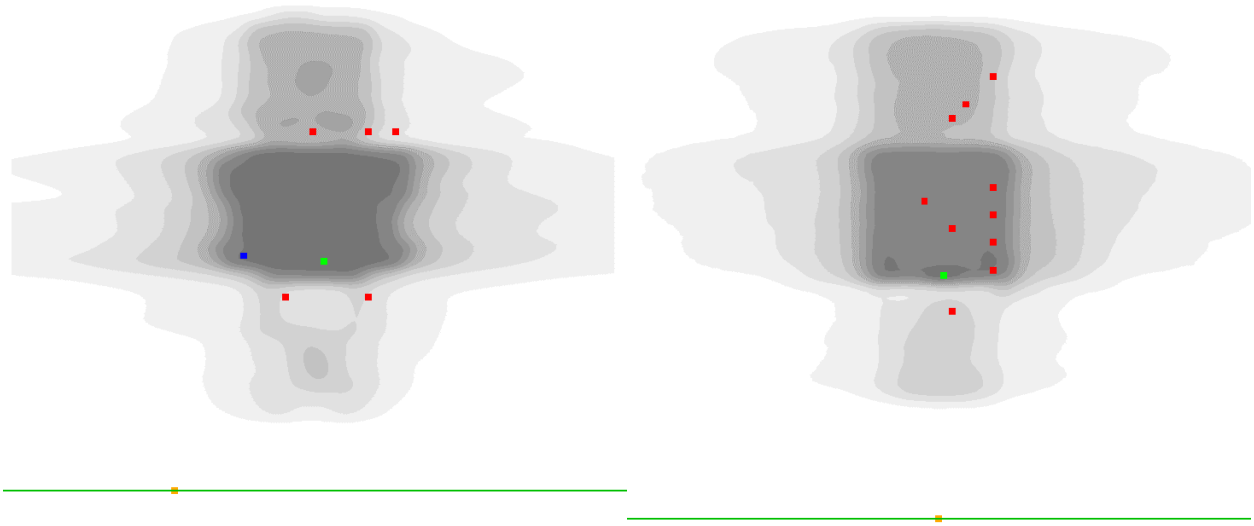

Figure C.16. TG-119 Multitarget site diode array measurements failing (red) gamma criteria 2%/2mm in TPS_{CS} (Left) and TPS_{MC} (Right).

Figure C.17. TG-119 Prostate site diode array measurements failing (red) gamma criteria 2%/2mm in TPS_{CS} (Left) and TPS_{MC} (Right).

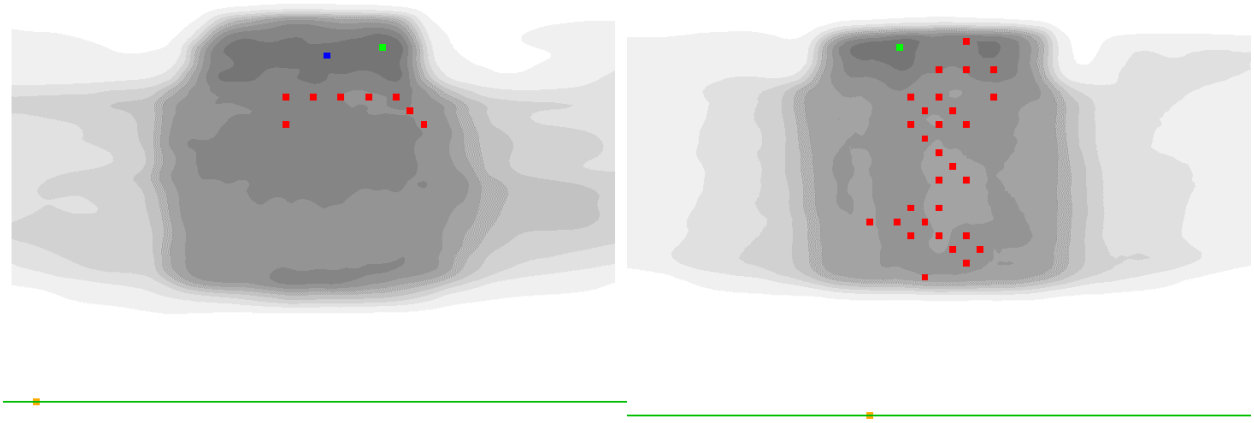

Figure C.18. TG-119 Head/Neck site diode array measurements failing (red) gamma criteria 2%/2mm in TPS_{CS} (Left) and TPS_{MC} (Right).

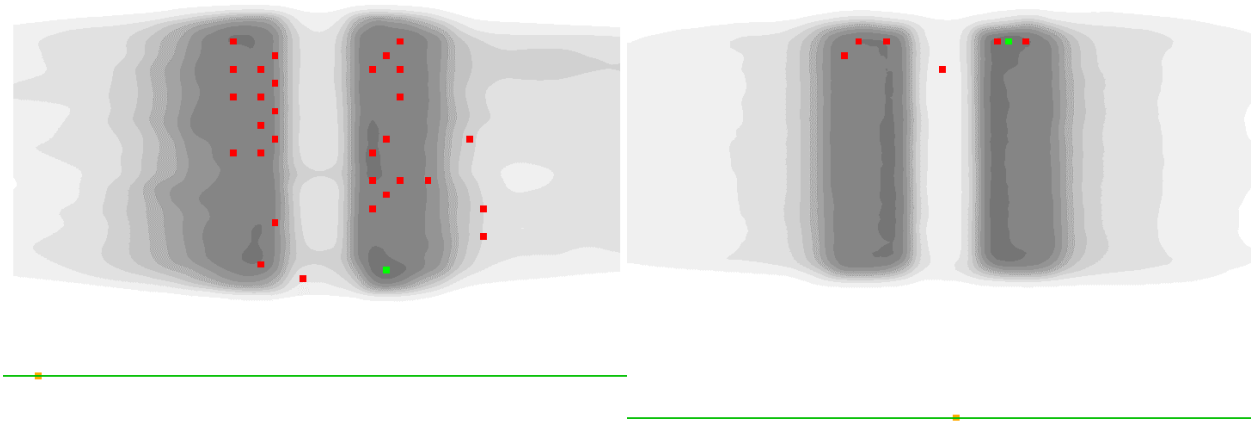

Figure C.19. TG-119 Cshape site diode array measurements failing (red) gamma criteria 2%/2mm in TPS_{CS} (Left) and TPS_{MC} (Right).

References

[1] Rijken J, Crowe S, Trapp J, Kairn T. A review of stereotactic body radiotherapy for the spine. *Phys Eng Sci Med*. 2020; 43(3):799–824. https://doi.org/10.1007/s13246-020-00889-w.

[2] Nalichowski A, Kaufman I, Gallo J, et al. Single fraction radiosurgery/stereotactic body radiation therapy (SBRT) for spine metastasis: A dosimetric comparison of multiple delivery platforms. *J Appl Clin Med Phys*. 2017; 18(1):164–169. https://doi.org/10.1002/acm2.12022.

[3] Paudel MR, Kim A, Sarfehnia A, et al. Experimental evaluation of a GPU-based monte carlo dose calculation algorithm in the Monaco treatment planning system. *J Appl Clin Med Phys*. 2016; 17(6):230–241. https://doi.org/10.1120/jacmp.v17i6.6455.

[4] Mackie TR, Scrimger JW, Battista JJ. *A convolution method of calculating dose for 15 MV x rays*. *Med Phys*. 1985; 12(2):188–196. https://doi.org/10.1118/1.595774.

[5] Mackie TR, Bielajew AF, Rogers DWO, Battista JJ. Generation of photon energy deposition kernels using the EGS Monte Carlo code. *Phys Med Biol*. 1988; 33(1):1–20. https://doi.org/10.1088/0031-9155/33/1/001.

[6] Löf V. The Difference Between a Collapsed Cone Based and a Monte Carlo Based Dose Calculation Algorithm. 2015;

[7] Philips Medical Systems. *Pinnacle3 Physics Reference Guide, Release 9.10*. 2014;

[8] Starkschall G, Steadham RE, Popple RA, Ahmad S, Rosen II. Beam-commissioning methodology for a three-dimensional convolution/superposition photon dose algorithm. *J Appl Clin Med Phys*. 2000; 1(1):8–27. https://doi.org/10.1120/jacmp.v1i1.2651.

[9] Fippel M. Fast Monte Carlo dose calculation for photon beams based on the VMC electron algorithm. *Med Phys*. 1999; 26(8):1466–1475. https://doi.org/10.1118/1.598676.

[10] Fippel M. Monte Carlo Treatment Planning, in *Shaped Beam Radiosurgery*, edited by A. De Salles (Springer-Verlag, 2011), pp. 47–59.

[11] Chetty IJ, Curran B, Cygler JE, et al. Report of the AAPM Task Group No. 105: Issues associated with clinical implementation of Monte Carlo-based photon and electron external beam treatment planning. *Med Phys*. 2007; 34(12):4818–4853. https://doi.org/10.1118/1.2795842.

[12] Fogliata A, Cozzi L. Dose calculation algorithm accuracy for small fields in non-homogeneous media: The lung SBRT case. *Phys Medica*. 2017; 44:157–162. https://doi.org/10.1016/j.ejmp.2016.11.104.

[13] Haga A, Magome T, Takenaka S, et al. Independent absorbed-dose calculation using the Monte Carlo algorithm in volumetric modulated arc therapy. *Radiat Oncol*. 2014; 9(1):1–9. https://doi.org/10.1186/1748-717X-9-75.

[14] Lee YK, Munawar I, Mashouf S, Sahgal A, Ruschin M. Dosimetric comparison of two treatment planning systems for spine SBRT. *Med Dosim*. 2020; 45(1):77–84. https://doi.org/10.1016/j.meddos.2019.07.001.

[15] Saenz DL, Crownover R, Stathakis S, Papanikolaou N. A dosimetric analysis of a spine SBRT specific treatment planning system. *J Appl Clin Med Phys*. 2019; 20(1):154–159. https://doi.org/10.1002/acm2.12499.

[16] Halvorsen PH, Cirino E, Das IJ, et al. AAPM-RSS Medical Physics Practice Guideline 9.a. for SRS-SBRT. *J Appl Clin Med Phys*. 2017; 18(5):10–21. https://doi.org/10.1002/acm2.12146.

[17] Kry SF, Jones J, Childress NL. Implementation and evaluation of an end-to-end IGRT test. *J Appl Clin Med Phys*. 2012; 13(5):46–53. https://doi.org/10.1120/jacmp.v13i5.3939.

[18] Sutton MW, Fontenot JD, Matthews KL, et al. Accuracy and precision of cone-beam computed tomography guided intensity modulated radiation therapy. *Pract Radiat Oncol*. 2014; 4(1) https://doi.org/10.1016/j.prro.2013.02.006.

[19] Alderson SW, Lanzl LH, Rollins M, Spira J. An instrumented phantom system for analog computation of treatment plans. *Am J Roentgenol Radium Ther Nucl Med*. 1962; 87:185–195.

[20] Cox BW, Spratt DE, Lovelock M, et al. International spine radiosurgery consortium consensus guidelines for target volume definition in spinal stereotactic radiosurgery. *Int J Radiat Oncol Biol Phys*. 2012; 83(5):e597–e605. https://doi.org/10.1016/j.ijrobp.2012.03.009.

[21] Ryu S, Gerszten P, Yin F-F, et al. *Radiation Therapy Oncology Group RTOG 0631 Phase II / III Study of Image-Guided Radiosurgery/SBRT for Localized Spine Metastasis*. 2010;

[22] Philips Medical Systems. *P3IMRT Instructions for Use, Release 9.10*. 2014;

[23] Butts JR, Foster AE. Comparison of commercially available three-dimensional treatment planning algorithms for monitor unit calculations in the presence of heterogeneities. *J Appl Clin Med Phys*. 2001; 2(1):32. https://doi.org/10.1120/1.1336496.

[24] Elekta. *Monaco IMRT/VMAT Treatment Planning Training Module*. 2020;

[25] Elekta. *Monaco Physics Training Module*. 2019;

[26] Ezzell GA, Burmeister JW, Dogan N, et al. IMRT commissioning: Multiple institution planning and dosimetry comparisons, a report from AAPM Task Group 119. *Med Phys*. 2009; 36(11):5359–5373. https://doi.org/10.1118/1.3238104.

[27] *Test Suite by Task Group 119*. 2009; https://www.aapm.org/pubs/tg119/default.asp.

[28] Niroomand-Rad A, Chiu-Tsao ST, Grams MP, et al. Report of AAPM Task Group 235 Radiochromic Film Dosimetry: An Update to TG-55. *Med Phys*. 2020; 47(12):5986–6025. https://doi.org/10.1002/mp.14497.

[29] Lewis DF, Chan MF. Technical Note: On GAFChromic EBT-XD film and the lateral response artifact. *Med Phys*. 2016; 43(2):643–649. https://doi.org/10.1118/1.4939226.

[30] Khachonkham S, Dreindl R, Heilemann G, et al. Characteristic of EBT-XD and EBT3 radiochromic film dosimetry for photon and proton beams. *Phys Med Biol*. 2018; 63(6) https://doi.org/10.1088/1361-6560/aab1ee.

[31] Miura H, Ozawa S, Hosono F, et al. Gafchromic EBT-XD film: Dosimetry characterization in high-dose, volumetric-modulated arc therapy. *J Appl Clin Med Phys*. 2016; 17(6):312–322. https://doi.org/10.1120/jacmp.v17i6.6281.

[32] Radiological Imaging Technology Inc. *RIT Family of Products Technical Manual Version 6.0*. 2012;

[33] Fitzpatrick JM, West JB, Maurer CR. Predicting error in rigid-body point-based registration. *IEEE Trans Med Imaging*. 1998; 17(5):694–702. https://doi.org/10.1109/42.736021.

[34] Royston P. Remark AS R94: A Remark on Algorithm AS 181: The W-test for Normality. *J R Stat Soc Ser C (Applied Stat*. 1995; 44(4):547–551.

[35] Chaikh A, Giraud JY, Perrin E, Bresciani JP, Balosso J. The choice of statistical methods for comparisons of dosimetric data in radiotherapy. *Radiat Oncol*. 2014; 9(1):1–11. https://doi.org/10.1186/1748-717X-9-205.

[36] Ju T, Simpson T, Deasy JO, Low DA. Geometric interpretation of the γ dose distribution comparison technique: Interpolation-free calculation. *Med Phys*. 2008; 35(3):879–887. https://doi.org/10.1118/1.2836952.

[37] Paddick I. A simple scoring ratio to index the conformity of radiosurgical treatment plans. Technical note. *J Neurosurg*. 2000; 93(SUPPL. 3):219–222. https://doi.org/10.3171/jns.2000.93.supplement_3.0219.

[38] Goodall SK, Ebert MA. Recommended dose voxel size and statistical uncertainty parameters for precision of Monte Carlo dose calculation in stereotactic radiotherapy. *J Appl Clin Med Phys*. 2020; 21(12):120–130. https://doi.org/10.1002/acm2.13077.

[39] Miften M, Olch A, Mihailidis D, et al. Tolerance limits and methodologies for IMRT measurement-based verification QA: Recommendations of AAPM Task Group No. 218. *Med Phys*. 2018; 45(4):e53–e83. https://doi.org/10.1002/mp.12810.

[40] Wang Y, Chen L, Zhu F, Guo W, Zhang D, Sun W. A study of minimum segment width parameter on VMAT plan quality, delivery accuracy, and efficiency for cervical cancer using Monaco TPS. *J Appl Clin Med Phys*. 2018; 19(5):609–615. https://doi.org/10.1002/acm2.12422.

[41] Yang K, Yan D, Tyagi N. Sensitivity analysis of physics and planning SmartArc parameters for single and partial arc VMAT planning. *J Appl Clin Med Phys*. 2012; 13(6):34–45. https://doi.org/10.1120/jacmp.v13i6.3760.

[42] Paelinck L, De Neve W, De Wagter C. Precautions and strategies in using a commercial flatbed scanner for radiochromic film dosimetry. *Phys Med Biol*. 2007; 52(1):231–242. https://doi.org/10.1088/0031-9155/52/1/015.

[43] Ferreira BC, Lopes MC, Capela M. Evaluation of an Epson flatbed scanner to read Gafchromic EBT films for radiation dosimetry. *Phys Med Biol*. 2009; 54(4):1073–1085. https://doi.org/10.1088/0031-9155/54/4/017.

[44] Poppinga D, Schoenfeld AA, Doerner KJ, Blanck O, Harder D, Poppe B. A new correction method serving to eliminate the parabola effect of flatbed scanners used in radiochromic film dosimetry. *Med Phys*. 2014; 41(2):021707. https://doi.org/10.1118/1.4861098.

[45] Lewis D, Chan MF. Correcting lateral response artifacts from flatbed scanners for radiochromic film dosimetry. *Med Phys*. 2015; 42(1):416–429. https://doi.org/10.1118/1.4903758.

[46] Micke A, Lewis DF, Yu X. Multichannel film dosimetry with nonuniformity correction. *Med Phys*. 2011; 38(5):2523–2534. https://doi.org/10.1118/1.3576105.

[47] Mayer RR, Ma F, Chen Y, et al. Enhanced dosimetry procedures and assessment for EBT2 radiochromic film. *Med Phys*. 2012; 39(4):2147–2155. https://doi.org/10.1118/1.3694100.

Vita

Michael James Taylor was born in Fort Walton Beach, Florida, in 1996, to Doina and Curtis Taylor. He graduated from Pace High School in 2015 and attended the University of West Florida until he earned his Bachelor of Science in Physics-Engineering in 2019, minoring in both Mathematics and Computer Science. He was introduced to the field of medical physics during a visit at Louisiana State University in 2017, ultimately applying and matriculating into their Medical Physics and Health Physics program. He anticipates graduating from the program with a Master of Science in the summer of 2022, beginning residency shortly afterwards at UPMC Hillman Cancer Center in Pittsburgh, Pennsylvania.